2022

Time-Resolved Method for Spectral Analysis based on Linear Predictive Coding, with Application to EEG Analysis

Jin Xu
Technological University Dublin, xujin@outlook.ie

Time-Resolved Method for Spectral Analysis based on Linear Predictive Coding, with Application to EEG Analysis

by

Jin Xu

A thesis is submitted to the Technological University Dublin

for the degree of *Doctor of Philosophy*

Supervisor: Prof. Mark Davis and Dr. Ruairí de Fréin

School of Electrical and Electronic Engineering

September 2022

Declaration

I certify that this thesis which I now submit for examination for the award of Doctor of Philosophy, is entirely my own work and has not been taken from the work of others, save and to the extent that such work has been cited and acknowledged within the text of my work.

This thesis was prepared according to the regulations for graduate study by research of the Technological University Dublin and has not been submitted in whole or in part for another award in any other third level institution.

The work reported on in this thesis conforms to the principles and requirements of the TU Dublin's guidelines for ethics in research.

TU Dublin has permission to keep, lend or copy this thesis in whole or in part, on condition that any such use of the material of the thesis be duly acknowledged.

Signature _____ Date _____

Jin Xu

September 2022

Acknowledgements

This thesis would not exist without the support from my supervisors, family and friends, etc. I am very happy to take this opportunity to give my appreciation to those people who helped and guided me during my graduate career.

First and foremost I would like to acknowledge my supervisors Prof. Mark Davis and Dr. Ruairí de Fréin for their invaluable advice, continuous support, and patience during my PhD study. Prof. Mark Davis is open-minded, supportive and caring. I thoroughly enjoyed my PhD study under his supervision. He generously shared with me his wealth of knowledge in research, academic skills and Irish culture. He gives me the confidence to help me to turn dreams into reality. Dr. Ruairí de Fréin is brilliant and he has a very admirable professional academic ability. His insightful feedback pushed me to sharpen my thinking and brought my work to a higher level. I owe them a great many heartfelt thanks.

Very special thanks to Prof. Mary McNamara, she help me gain the scholarship and the opportunity of studying at TU Dublin. I also would like to express my sincere gratitude to the Higher Education Authority Government of Ireland International Education Scholarship for letting me has the opportunity to study in Ireland.

During my lifetime in Ireland, friendship has always supported me. I would like to mention their names here: Miss Chu Yuan, Mrs. Dan Zhang (Maggie), Mr. Zhenchao Zhang, Mrs. Shu Wan (Cindy), Mr. Wufeng Chen, Mr. Limin Zhang, Mr. Chen Liang, Dr. Ting Bi, Dr. Fan Zhang, Mr. Jiajia Liu, Dr. Ali Malik, Dr. Obinna Izima, Dr. Miroslaw Narbutt, Mr. Yang Yu, Mr. Shaoqin Hou (Sean), Mr. Hongtao Zhao and Mr. Ziran Xu.

I would like to give high respect to my fantastic girlfriend Luhan Wang who has always loved, encourage and supported me since we met four years ago. Without her love, supports and sacrifices, this work would have never come to fruition. I would like to thank Luhan Wang for sharing these years and for brightening my life. I would like to thank my parents Mr. Yongqin Xu and Mrs. Liping Jing for their wise counsel and sympathetic ear. You are always there for me. I also would like to thank my little brother Jinxuan Xu for telling me that I am awesome and I am his role model.

Thank you all for the strength you gave me. I love you all!

Abstract

EEG (Electroencephalogram) signal is a biological signal in BCI (Brain-Computer Interface) systems to realise the information exchange between the brain and the external environment. It is characterised by a poor signal-to-noise ratio, is time-varying, is intermittent and contains multiple frequency components. This research work has developed a new parameterised time-frequency method called the Linear Predictive Coding Pole Processing (LPCPP) method which can be used for identifying and tracking the dominant frequency components of an EEG signal. The LPCPP method further processes LPC (Linear Predictive Coding) poles to produce a series of reduced-order filter transfer functions to estimate the dominant frequencies. It is suited for processing high-noise multi-component signals and can directly give the corresponding frequency estimates unlike transform-based methods. Furthermore, a new EEG spectral analysis framework involving the LPCPP method is proposed to describe the EEG spectral activity. The EEG signal has been divided into different frequency bands (i.e. Delta, Theta, Alpha, Beta and Gamma). However, there is no consensus on the definitions of these band boundaries. A series of EEG centre frequencies are proposed in this thesis instead of fixed frequency boundaries, as they are better suited to describe the dominant EEG spectral activity.

Table of contents

List of figures

List of tables

List of abbreviations

EEG	Electroencephalography
BCI	Brain-Computer Interface
SNR	Signal-to-Noise Ratio
MI	Motor Imagery
GAL	Grasp-and-Lift
STFT	Short-Time Fourier Transform
CWT	Continuous Wavelet Transform
LPC	Linear Predictive Coding
LPCPP	Linear Predictive Coding Pole Processing
AWGN	Additive White Gaussian Noise
RFEP	Relative Frequency Error Percentage
RFDP	Relative Frequency Distance Percentage
EPDF	Error Probability Density Function
TBP	Time-Bandwidth Product
DPDF	Discrete Probability Density Function
PRVF	Pseudo-Randomly Varying Frequency
LCFM	Linearly Chirped Frequency Modulation

AEP	Average Error Percentage
IFP	Identification Frequency Percentage
VEP	Valid Estimate Percentage
IEP	Ideal Experiment Percentage

List of symbols

t	Time
f	Frequency
Δf	Frequency resolution
Δt	Time resolution
$g(t)$	Window function
$G(f)$	Fourier transform of the window function
$s(n)$	Discrete-time signal
P	Filter order
a	Constant coefficient
α	Linear predictor cofficient
$e(n)$	LPC prediction error
E	Mean-squared prediction error
$S(z)$	Z-transform of a discrete-time signal
$H(z)$	All-poles transform function
$\tilde{s}(n)$	Prediction signal
$A(z)$	All-roots transform function

$\dot{f}$	LPC frequency estiamte
T	Sample period
f_s	Sampling frequency
p	LPC pole
$D(m)$	LPCPP discriminating enhancement function
m_i	The magnitude of each LPC pole
β	LPCPP parameter for the identification of the dominant pole
λ	LPCPP parameter for the identification of the associated pole
$\tilde{H}$	LPCPP reduced-order transform function
$\tilde{f}$	LPCPP frequency estimate
μ	The bias of the EPDF
σ	The standard deviation of the EPDF
e	Error between the frequency estimate and signal frequency
ν	Frequency percentage for the performance metric
κ	Frequency change rate of a LCFM signal

Chapter 1

Introduction

1.1 Problem Statement

Brain-Computer Interfaces (BCI) based on the electroencephalogram (EEG) signal can facilitate information exchange between the brain and the external environment. The EEG signal is a high-complexity time series bioelectric signal that is characterized by a poor signal-to-noise ratio. In addition, EEG signals are time-varying and intermittent and they contain multiple frequency components. Specifically, the acquisition of an EEG signal is always accompanied by noise. The spectral components of EEG signals are intermittent because the appearance and disappearance of some brain activities are dynamic. EEG signal is a multi-component signal where the frequency components reflect various brain electrical activities. A robust and time-resolved spectral analysis method for EEG signals is required for its use in BCI systems. In addition, many biomedical researchers are interested in establishing significant levels of electrical activity across defined frequency bands. They have divided the EEG spectrum into a number of fixed frequency bands

(i.e. Delta, Theta, Alpha, Beta and Gamma) to investigate the various brain functions. However, there is little consensus among researchers in terms of the frequency ranges of these bands. Different publications have used different definitions for the boundaries of these frequency bands. The spectral activity of the EEG depends on the activity being performed by the subject and is not restricted to a series of fixed frequency bands.

1.2 Objective and Contributions

The objective of the thesis is to improve the analysis of continuous EEG signals. The method pursued involved the development of a new method called the Linear Predictive Coding Pole Processing (LPCPP) method which is a new parameterised time-frequency method. The LPCPP method is based on the Linear Predictive Coding (LPC) method. The standard LPC method suffers from a sensitivity to the choice of filter order and has a poor tolerance of high noise environments. The LPCPP method further processes the LPC poles to produce a series of reduced-order filter transform functions to perform dominant frequency estimation. The LPCPP method can identify the dominant spectral features and it can directly provide the corresponding frequency estimates instead of spectral waveforms. Waveform time-frequency methods can tell whether a certain frequency component exists or not at any given time interval. However, a challenge in analysing multi-component signals is to separate the spectrum components when they are overlapped in the time-frequency plane. The LPCPP method is a parameterised time-frequency method that can produce numerical dominant frequency estimates and it is suitable for multi-component signal processing (i.e. EEG signals). Furthermore, it significantly improves

the performance in terms of a robustness in the presence of noise when compared to the LPC method. The LPCPP method has a higher spectral resolution than that of the LPC method and it has a reduced time-bandwidth product. The LPCPP method can be used to track the dynamics of the dominant frequency of time-varying signals. Therefore, it is particularly suitable for EEG spectral analysis. The LPCPP method can help us observe the spectral changes of EEG signals in real-time. In this thesis, there are three public EEG datasets used for the EEG spectral analysis. The three datasets comprise EEG signals collected from 173 subjects and the total EEG acquisition duration exceeds 100 hours. A new EEG spectral analysis framework that involves the LPCPP method will be developed for the analysis of the EEG signals based upon nominal centre frequencies. Instead of fixed EEG frequency boundaries, the EEG waves are classified in terms of nominal band centre frequencies to describe the dominant EEG spectral activity. They have the following advantages:

1. Instead of artificially fixed wave frequency boundaries, the distribution of the dominant EEG spectral activity in the full frequency domain can be described by the normal centre frequency rather than a specific frequency band.

2. Better suited to describe the dynamic and variable EEG frequencies. Because of the individual differences, gender, age etc., there is still no consensus on the classification of EEG bands and there exist undefined gaps between the different bands. The central frequencies are more suited expression of this dynamic variable EEG spectral activity and there are no gaps between bands.

3. Three common central frequencies (i.e. 1.75 Hz, 6.75 Hz and 10.75 Hz) are identified on three different EEG datasets corresponding to EEG spectral activity in the Delta, Theta, and Alpha bands of the EEG.

In addition, since the LPCPP method can be incorporated into a machine learning or AI system, the LPCPP method will be of significant benefit in the development of BCI applications to help in pushing BCI techniques out of the laboratory and into addressing real-world problems.

1.3 Publications

As a result of the research work in this thesis, there were 5 academic papers published. Specifically, two of these papers were published in the prestigious journal IET Electronic Letters and one of the papers was selected as the "Featured Paper" in the May 2021 issue. The Publications arising from this thesis are as follows:

1. **Jin Xu**, Mark Davis, and Ruairí de Fréin. "An LPC Pole Processing Method for Enhancing the Identification of Dominant Spectral Features." Electronics Letters (2021).

   $*$ This paper was selected as a "**Featured Paper**" in the issue of Electronics Letters.

2. **Jin Xu**, Mark Davis, and Ruairí de Fréin. "A Linear Predictive Coding Filtering Method for the Time-resolved Morphology of EEG Activity." 32nd Irish Signals and Systems Conference. IEEE, 2021.

3. **Jin Xu**, Mark Davis, and Ruairí de Fréin. “Dominant Frequency Component Tracking of Noisy Time-varying Signals using the Linear Predictive Coding Pole Processing Method." Electronics Letters (2022).

4. **Jin Xu**, Mark Davis, and Ruairí de Fréin. “New Robust LPC-Based Method for Time-resolved Morphology of High-noise Multiple Frequency Signals." 31st Irish Signals and Systems Conference. IEEE, 2020.

5. **Jin Xu**, Mark Davis, and Ruairí de Fréin. “A Robust LPC Filtering Method for Time-Resolved Morphology of EEG Activity Analysis." 26th Annual Conference of the Section of Bioengineering of the Royal Academy of Medicine in Ireland (2020).

6. **Jin Xu**, Mark Davis, and Ruairí de Fréin. “An Uncertainty Principle Analysis for Parameterisation Time-frequency Method." IEEE Transactions on Signal Processing (In Preparation, 2022).

7. **Jin Xu**, Mark Davis, and Ruairí de Fréin. “Analysis of the Estimation Bias and Time-Bandwidth Product for a Linear Predictive Coding Pole Processing Algorithm" IEEE/ACM Transactions on Computational Biology and Bioinformatics (In Preparation, 2022).

8. **Jin Xu**, Mark Davis, and Ruairí de Fréin. “ EEG Centre Frequency Analysis using Linear Predictive Coding Pole Processing Method" IEEE Transactions on Biomedical Circuits and Systems (In Preparation, 2022).

1.4 Organisation

This thesis is organised as follows:

Chapter 2 describes the main technologies that are used through the course of this research by introducing the general technical background regarding the spectral analysis of the EEG signals. First, an overview of EEG signals is presented, including EEG acquisition, EEG artifacts and definitions of EEG frequency bands. In addition, the three public EEG datasets used in this thesis are described in detail. Second, the time-frequency analysis method and the Heisenberg-Gabor uncertainty principle are introduced. Finally, the LPC method is introduced in detail, including the mathematical derivation of the LPC method and some of its limitations are discussed.

Chapter 3 describes the design and the development of the LPCPP method. The first section presents a fundamental analysis of the LPC poles and the LPC spectra under the different parameters, i.e. filter order, signal duration, sampling frequency, signal noise and window function. The definitions of the dominant pole and non-dominant pole are proposed and defined. The second section analyses the relationship between the dominant pole and non-dominant pole in a series of second-order transform functions. The definition of the associated pole is proposed to determine the final location of the spectral peak. Finally, the details of the LPCPP method are presented.

Chapter 4 presents the experimental results of the analysis of the LPCPP method. The first section shows that the LPCPP method can achieve the enhancement of frequency estimation when compared to the LPC method. The second section demonstrates that the LPCPP method can track the change of dominant frequency in real-time and it can

significantly reduce the invalid frequency estimates of the LPC method. The third section presents the time-bandwidth product analysis of the LPCPP method and shows that the LPCPP method can significantly improve the spectral resolution compared to the LPC method. The LPCPP method is well suited for processing poor signal-to-noise ratio, time-varying, intermittent and multi-component signals. It is suited for the analysis of EEG signals.

Chapter 5 presents a new EEG spectral analysis framework involving the LPCPP method. The LPCPP method can realise real-time tracking of the dominant frequencies of EEG signals. Furthermore, a series of EEG centre frequencies are proposed in place of the fixed frequency bands to describe dominant EEG spectral activities. Compared to fixed EEG bands, the EEG centre frequencies can be better suited to describe the dynamic changes of the dominant spectrum components in the EEG signal.

Chapter 6 provides the summary of the main findings and conclusions from the research work carried out in this thesis. Furthermore, it also gives some suggestions for future research in the area. Finally, the skills acquired during this research work are summarised.

Chapter 2

Technical Background

In this chapter, the technical background of this thesis will be presented. The first section will present the properties of EEG signals. The core component of the Brain-Computer Interface (BCI) system is to translate the subject's EEG signals into control commands or instructions for external devices. However, the EEG signal is a high-complexity bioelectric signal, typically characterized by a poor signal-to-noise ratio whose frequency is time-varying, intermittent and contains multiple frequency components. Therefore, a robust and time-resolved spectral analysis method for EEG signals is required for its use in BCI systems. The second section discusses popular time-frequency methods and the limitations imposed by the Heisenberg-Gabor uncertainty principle on time-frequency analysis methods. The time-frequency methods give a view of a signal represented over both time and frequency. Furthermore, many time-frequency methods are waveform methods and are useful for demonstrating whether a certain frequency component exists or not by showing how the energy of the signal is distributed across the time-frequency domain. Linear Predictive Coding (LPC) provides a parameterised time-frequency method that

can directly provide the signal frequencies in the form of numerical frequency estimates. These numerical frequency estimates are well suited to frequency estimation and frequency tracking of multi-component signals (e.g. EEG signals). The third section will present the details of the foundation of the basis of the LPC method. Furthermore, the shortcomings of the LPC method are also analysed. Finally, the last section is the summary of the chapter.

2.1 Electroencephalography

EEG signal can record the electrical activity of the brain to reflect the states of the brain in real-time which can support its use in BCI applications. In this section, the first part introduces the development of the EEG signals and the international EEG acquisition standard. The second part presents the EEG artifacts which are divided into biological noise and environmental noise. The third part presents the different definitions of EEG frequency bands (i.e. Delta, Theta, Alpha, Beta and Gamma) introduced by different researchers. The fourth part introduces the details of the three EEG public datasets that will be used in this thesis. Finally, a summary of this section is presented.

2.1.1 Introduction to EEG

The BCI system can convert the subject's EEG signals into control commands or instructions for external devices [1, 2, 3, 4, 5, 6]. EEG signals are an efficient means to acquire brain signals corresponding to various electrical activities on the scalp surface area. It was first recorded by Richard Caton from an animal brain in 1875. In 1924, the first human

EEG was recorded by a German psychiatrist Hans Berger [7, 8]. EEG records electrical activity arising from the human brain. The average human brain has about 100 billion neurons and ten times more glial cells and the communication between them is the key brain activity [9]. The EEG signal provides a view of the evaluation of dynamic cerebral functioning. The continuous EEG signal is used to monitor and track the state of a patient's brain, for example it has been used in ICU units to track a patient's response to treatment for seizures and status epilepticus [10].

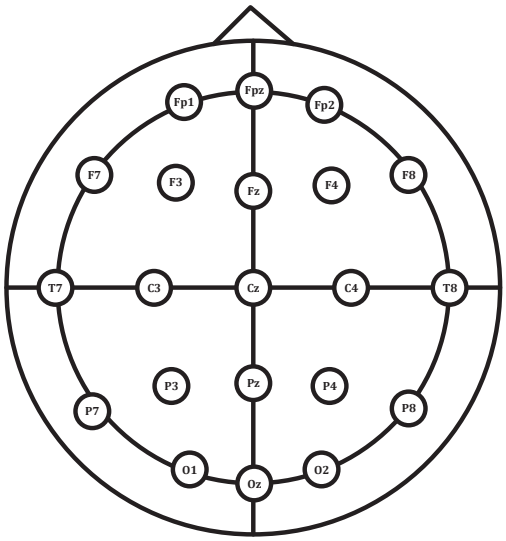

Fig. 2.1 EEG international 10-20 system.

EEG signals are acquired by electrodes placed on the scalp surface. There are some internationally recognised methods to specify the location of scalp electrodes in the EEG collection [11, 12, 13, 14, 15, 16, 17]. In 1958, Jasper defined the international 10-20 electrode system to provide a standardised EEG electrode placement [11]. The 10-20 system provides a reproducible method to maintain a standardized testing method ensuring that different studies could be reproduced and effectively analysed and compared. The inter-

national 10-20 system is shown in Fig. 2.1. The “10” and “20” denote the fact that the actual distance between adjacent electrodes is either 10% or 20% of the total front-back or right-left distance of the skull, typically the number of the electrodes in the 10-20 system is 21. With the development of hardware and the demands posed by researchers, there was an increased need for extending the 10-20 system to higher density electrode settings. Chatrian et al. proposed the 10-10 system based on the 10-20 system with supplementary electrodes applied midway between leads of the 10-20 system or electrodes in turn situated between 10-20 leads [12, 13, 14]. Oostenveld et al. further proposed the high-resolution 10-5 system which has 345 electrode locations [15]. In the work of Jurcak et al., they revisited the 10-20, 10-10 and 10-5 systems and analysed the validity as a relative head-surface-based positioning system, they found the 10-10 positions could be well separated on a scalp without overlapping [16, 17]. Therefore, all EEG datasets in this thesis use the 10-10 system to acquire EEG signals and the details about the topographic of these datasets will be introduced in Section 2.1.4.

2.1.2 EEG Artifacts

An unfortunate reality of EEG is that cerebral activity may be overwhelmed by other electrical activity generated by the body or in the environment. The noise in an EEG signal can be divided into biological noise and environmental noise often termed artifacts. The most common types of biological artifacts include a cardiac signal (ECG), movement artifacts caused by muscle (EMG) and eye signals caused by eyeball movement (EOG). ECG artifacts are quite common and are unavoidable in recorded EEG signals, but it has the smallest impact [18]. EMG and EOG can be avoided or reduced by asking the subjects

to close their eyes and to stay relaxed when they are doing EEG collection. There are some works that try to remove the artifacts from EEG signals, these methods include blind source separation, empirical-mode decomposition, wavelet transform and independent component analysis [19, 20, 21, 22, 23]. The other sources of the noise come from the outside of the body, they include the steps of collecting and processing EEG signals. The most common source of environmental noise is the local power system's frequency, either 50 Hz or 60 Hz (according to which country you are in) [24, 25, 26]. When the electrode contact is poor, the collected EEG signal cannot reflect genuine brain activity. In addition, some of these differences are due to the hardware configuration which applies different filtering to the signal during the EEG preprocessing, such as the notch filters are often applied at 50 Hz or 60 Hz to filter out AC line noise [26]. As a result of the artifacts on the EEG records, a robust signal processing method is required for processing noisy EEG signals.

EEG signals have a low SNR and their recordings are always accompanied by a variety of noise. There is a considerable part of the EEG dataset that is invalid data corrupted by noise contamination. In the work of Cho et al., they collected EEG datasets from 52 subjects for motor imagery brain-computer interface, but only 73% of datasets (38 subjects) included reasonably discriminative information [27]. The artifacts are to be detected and removed in order to improve the interpretation of EEG signals. There are some de-noising methods for EEG signals. Majmudar Charvi et al. proposed a hybrid method to detect and remove artifacts from single-channel EEG signal [28]. Asaduzzaman et al. applied the discrete wavelet transform for removing noise from the raw EEG signals of healthy patients [29]. Zhou Weidong et al. used a combination of wavelet

threshold de-noising and independent component analysis to remove the EMG and ECG artifacts in EEG signals[19]. Rohál'ová Martina et al. proposed an extended Kalman filter approach and a neural network instead of the autoregressive model for the detection of EEG artifacts [30]. Therefore, the EEG signal is a high-noise signal and data cleaning is required for EEG signal analysis. In this thesis, the autocorrelation method will be used to clean the EEG datasets and the specific experiment analysis will be shown in section 5.2.

2.1.3 EEG Frequency Bands

The spectrum of EEG has been divided into a number of fixed frequency bands by many biomedical researchers to investigate the corresponding brain functions. However, different researchers have defined different frequencies for these bands with little consensus between them which has significant consequences for EEG interpretation. These EEG frequency bands are based on their frequency range using Greek letters which are Delta, Theta, Alpha, Beta and Gamma. For the different EEG waves, their corresponding brain activities have also been analysed. Specifically,

- The Delta wave is a type of high amplitude brain wave with a frequency of oscillation. It is physiologically seen in deep sleep and is prominent in the frontocentral head regions [31, 32, 33]. Tinguely et al. described fundamental aspects in relation to the functional significance of Delta oscillations in cognitive processing, their work showed that the power of the Delta oscillations increases during mental tasks and has the role of inhibiting all the interferences that may affect the performance of the task [32].

- The Theta waves were first reported by Walter and Dovey in 1944, who observed their occurrence in cases of sub-cortical tumour [34]. Different functional relationships were observed between Theta-activity and attention as well as memory processes [35, 36].

- The Alpha wave was discovered by the German neurologist Hans Berger, the inventor of the EEG itself. The best-known and most extensively studied rhythm of the human brain is the normal Alpha rhythm. Alpha activity is induced by closing the eyes and by relaxation [37, 38].

- The Sigma wave is seen most prominently in the frontocentral head regions and its activity includes brief but powerful bursts of synchronous neuronal firing during the second stage of sleep in mammals [39]. It is also a slow-wave activity were positively correlated with the pre–post-sleep consolidation of declarative (word list) and procedural (mirror-tracing) memories [40].

- The Beta wave is the most frequently seen rhythm in normal adults and children. It is most prominent in the frontal and central head regions and attenuates as it extends posteriorly. The studies of Beta activity are mostly in relation to sensorimotor behavior [41, 42].

- The Gamma wave is a fast oscillation and is usually found during conscious perception. The Gamma activity has also been detected and studied across parietal, temporal and frontal cortical regions [43]. The work from Li Mu and Lu Bao-Liang investigates emotion classification based on Gamma waves, their work shows that the Gamma band is suited for EEG-based emotion classification [44].

However, the definitions of EEG waves (i.e. Delta, Theta, Alpha, Beta and Gamma) vary between different publications. Specifically, Deuschl et al. defined four EEG bands: Delta (0-4 Hz), Theta (4-8 Hz), Alpha (8-14 Hz) and Beta ($\geq$14 Hz) [45]. Adeli et al. decomposed EEG into five EEG bands: Delta (0-4 Hz), Theta (4-8 Hz), Alpha (8-12 Hz), Beta (13-30 Hz) and Gamma (30-60 Hz) [46]. Ferri et al. separated the EEG signal into five bands in their work: Delta (0.25-2.5 Hz), Theta (4.0-7.0 Hz), Alpha (7.0-11.0 Hz), Sigma (11.0-15.0 Hz) and Beta (15.0-30.0 Hz) [47]. de Munck et al. defined the EEG bands as: Delta (0.1-4 Hz), Theta (4.5-8 Hz), Alpha (8.5-12 Hz), Beta (12.5-36 Hz) and Gamma (36.5-100 Hz) [48]. Zheng et al. used the five EEG bands as Delta (1-3 Hz), Theta (4-7 Hz), Alpha (8-13 Hz), Beta (14-30 Hz) and Gamma (31-50 Hz) [49]. Abo-Zahhad et al. used the EEG frequency bands are that Delta (0.5-4 Hz), Theta (4-8 Hz), Alpha (8-14 Hz), Beta (14-30 Hz) and Gamma (>30 Hz) [50]. Fig. 2.2 summarises the

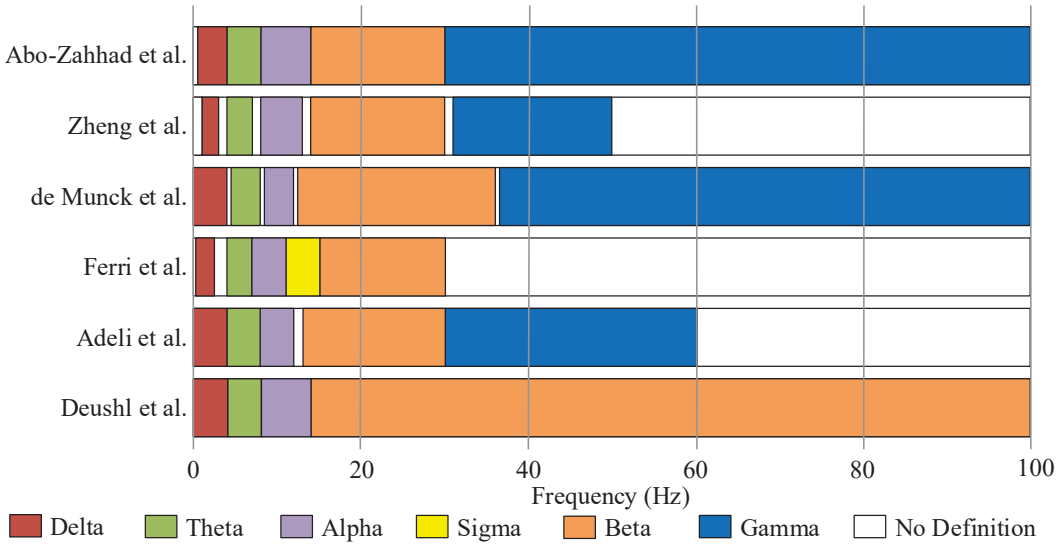

Fig. 2.2 The different EEG band definitions used by various researchers.

different frequency band definitions of the EEG bands. As shown there are many different definitions used for the different EEG frequency bands and the researchers have not yet

reached a unified approach. Many definitions have gaps between frequency bands and these gaps represent undefined frequency segment. Furthermore, Table 2.1 demonstrates

Table 2.1 Summary of frequency band parameters.

EEG band	% of Publications	Typical range (Hz)	Minimum start value (Hz)	Maximum end value (Hz)
Delta	70	1.3-3.5	0	6
Theta	84	4-7.5	2.5	8
Alpha	85	8-13	6	14
Beta	80	12.5-30	12	50
Gamma	18	30-40	20	100

the work of Newson et al. who investigated the differences in EEG frequency bands in the resting state condition from 184 EEG studies [26]. There is no consensus among researchers regarding the frequency boundaries. There are a number of factors that may cause this lack of a unified consensus on the classification of EEG bands, such as

1. Some EEG characteristics are unique between individuals. EEG signals still vary between individuals [51] and these different characteristics have been successfully used for authentication [52, 53].

2. The effect of differences in clinical equipment on EEG acquisition. The acquisition of EEG signals can be affected by the hardware and software of the acquisition equipment, such as sensor accuracy, contact with the brain (i.e. poor contact or good contact), parameter settings (sampling frequency, electrode position, filter selection etc.), acquisition software (Natus, ANT Neuro etc.).

3. The effect of gender differences on EEG. Gender-related EEG studies have shown that the brain's EEG activity is related to gender differences, for example, men have

less Theta band EEG activity and more Alpha band EEG activity than women and there is a developmental lag in EEG in females compared to males [54].

4. The effect of age differences on EEG. The activity of the EEG varies with age, for example, the coherence of the theta and alpha bands decreases significantly with age, while the coherence with the beta band continues to increase [55]. Furthermore, in a study of EEG development from 5 months to 4 years of age a significant developmental change in the frequency of peak power spectra in the 6-9 Hz range was found in infants and the relative amplitude of the central rhythm peaked in the second year of life when significant changes in motor behavior were occurring [56].

Therefore, there is a great deal of variability and difference in opinion as to the specific frequency range that defines each band. A new spectral analysis tool will be proposed in this thesis that can analyse spectral information in different EEG bands and is not limited to fixed boundaries. In addition, instead of fixed band boundaries, a series of EEG centre frequencies will be proposed to describe the dominant spectral activity of the EEG. These EEG centre frequencies can describe the spectral activity of EEG without being restricted by boundaries and the specific experimental analysis will be presented in Section 5.4.

2.1.4 EEG Datasets

Three public EEG datasets were used in this thesis and their acquisitions are all based on the international 10-10 system. Fig. 2.3(a) demonstrates the topographic map of international 10-10 system. The three EEG datasets are called BCI109, MI52 and GAL12 and they are public datasets. Furthermore, they were published in 2004, 2017 and 2014,

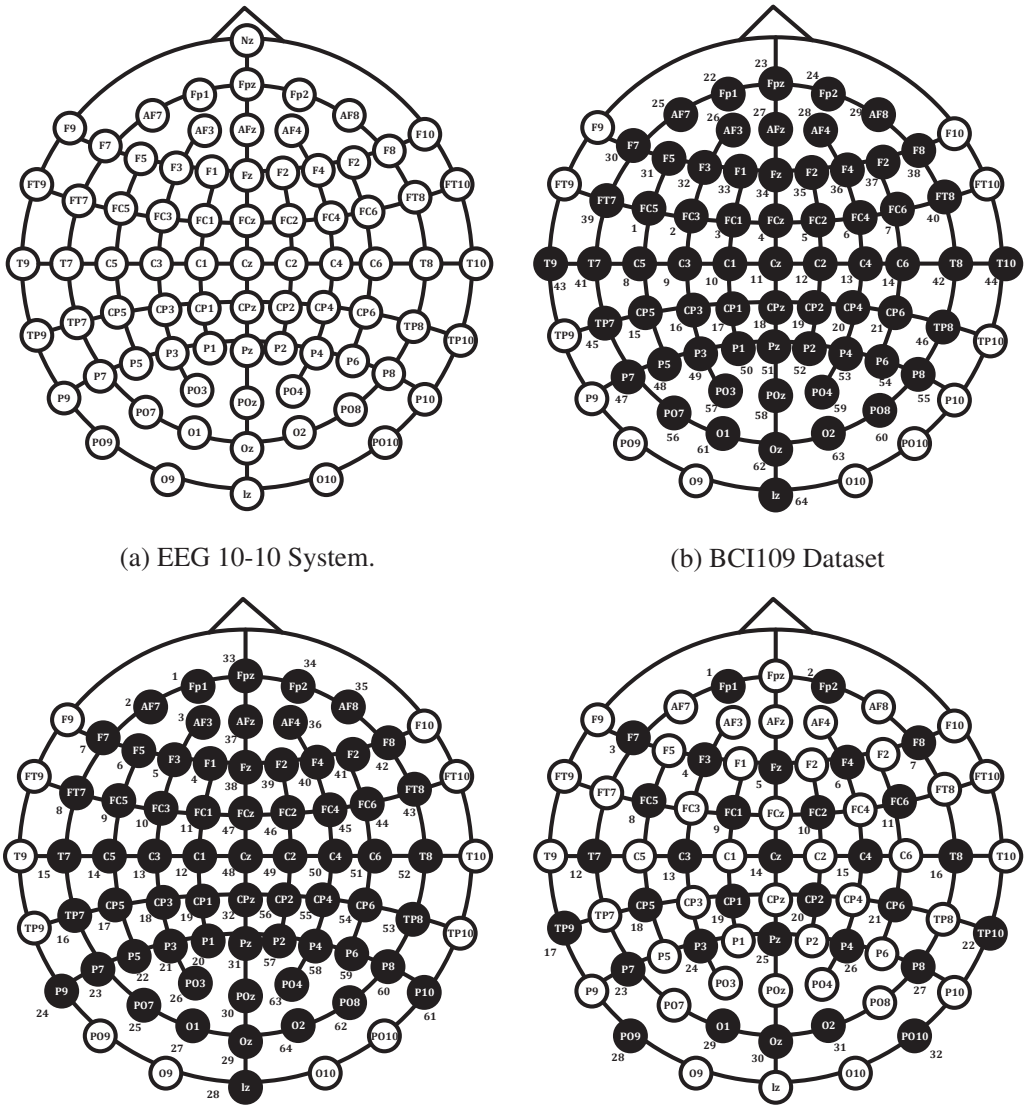

(a) EEG 10-10 System.

(b) BCI109 Dataset

(c) MI52 Dataset

(d) GAL12 Dataset

Fig. 2.3 Topographic maps of different EEG datasets.

respectively. Fig. 2.3(b), Fig. 2.3(c) and Fig. 2.3(d) respectively show the topographic maps of the three datasets. Each sampling point is represented by a solid circle.

The first dataset is called BCI109 from PhysioNet [57]. The dataset was created by the developers of the BCI2000 instrumentation system [2]. The BCI109 dataset contains 109 subjects from 64 electrodes and its topographic map is shown in Fig. 2.3(b). Each subject

Table 2.2 The details of BCI109 Dataset.

Task Number	Task Content	Collection Times	Collection Duration (s)
T_{b1}	Resting state (eyes open)	1	60
T_{b2}	Resting state (eyes closed)	1	60
T_{b3}	Open and close left or right fist	3	120
T_{b4}	Imagine opening and closing left or right fist	3	120
T_{b5}	Open and close both fists or both feet	3	120
T_{b6}	Imagine opening and closing both fists or both feet	3	120

performed 14 experimental runs, the sampling frequency is 160 Hz and the details of the BCI109 dataset are in Table 2.2.

Table 2.3 The details of MI52 Dataset.

Task Number	Task Content	Collection times	Collection Duration (s)
T_{m1}	Resting state (eyes open)	1	60
T_{m2}	Movement of left hand	1	140
T_{m3}	Movement of right hand	1	140
T_{m4}	Imagery of left hand	1	700
T_{m5}	Imagery of right hand	1	700

The second dataset was collected through the Motor Imagery (MI) based brain-computer interface and is called MI52 [27]. The MI52 dataset was recorded from 52 subjects using 64 electrodes and the topographic map of the MI52 is shown in Fig. 2.3(c). Each subject performed 5 experimental runs, the sampling frequency is 512 Hz and the details of the dataset are in Table 2.3.

The third dataset was used to detect Grasp-and-Lift (GAL) ability and is called GAL12 [58]. The GAL12 dataset contains 12 subjects using 32 electrodes to record EEG signals and the topographic map of GAL12 is shown in Fig. 2.3(d). The GAL12 collection method is different for the first two datasets, each collection has 6 events (hand start, first

digit touch, both start load phase, lift off, replace and both released). These events always occur in the same order, the number of trials varies for each collection. Each subject performed 10 collection experiments and the sampling frequency is 500 Hz.

2.1.5 Conclusions

In this section, the relevant background of EEG signals is presented. The EEG signal is a high-complexity bioelectric signal, typically characterized by a poor signal-to-noise ratio whose frequency is time-varying, intermittent and contains multiple frequency components. Furthermore, analysis of the EEG spectrum is divided into a series of fixed frequency bands (Delta, Theta, Alpha, Beta and Gamma). However, there is no consensus among researchers regarding the boundaries of these bands. Furthermore, the EEG frequency features should not be restricted by an arbitrary classification. Finally, the three EEG datasets that will be used in this thesis are introduced in detail. In the next section, the time-frequency methods will be introduced which provide a way to estimate the signal frequency components and reveal their time-varying features.

2.2 Time-frequency Analysis Method

The EEG signal records fast-changing neuronal signaling and communication and thus can offer a understanding of cognitive processes. The ability to track the dominant frequency changes in real-time is important for studying EEG signals to observe the dynamics of brain activities. Time-frequency methods provide a way to analyse the frequency dynamics in EEG signals [59, 60, 61, 62, 63, 64]. The first part of this section

presents an overview of time-frequency methods. Specifically, the Short-Time Fourier Transform (STFT) is introduced which is a typical waveform time-frequency method [65, 66, 67, 68, 69, 70]. The second part presents the Heisenberg-Gabor uncertainty principle which highlights that the time-frequency methods need to consider the balance between the time and frequency resolution and there is a trade-off between the time and frequency resolution.

2.2.1 Introduction to Time-frequency Analysis

For the time-frequency analysis, the motivation is that the time t or the frequency f descriptions of a signal alone cannot provide comprehensive information for feature extraction and classification. Each representation of the signal is non-localized, i.e. the frequency representation is essentially averaged over time. In other words, it shows what frequencies are present in the signal but it gives no information regarding at what time these spectral components appear. The time-frequency method provides a solution to seek a representation of the signal in a two-dimensional (t, f) space. The time-frequency analysis can depict how the spectra of the signal changes with time.

Any signal can be described as a function of time $s(t)$ and any signal can be represented in the frequency domain by its Fourier transform $S(f)$, given by

$$S(f) = \int_{-\infty}^{\infty} s(t) \cdot e^{-2j\pi ft} dt \tag{2.1}$$

The representation $S(f)$ is a function of frequency only with time having been "integrated out". The inverse Fourier transform of $S(f)$ is

$$s(t) = \int_{-\infty}^{\infty} S(f) \cdot e^{2j\pi ft} df \tag{2.2}$$

In practice, many signals have a time-varying frequency and here the frequency has been averaged out. In the Eq. 2.1, the information provided by the integral, corresponds to all-time instances, since the integration is from minus infinity to plus infinity over time. In other words, the Fourier transform tells whether a certain frequency component exists or not, it gives no information about the time for which the frequency component exists. However, some portion of a non-stationary signal can be assumed to be stationary. The Fourier transform can provide information about the frequency components occurring in a given time window. Shifting this window to a new location in order to get the spectral content of the signal changes with time. This method is a typical time-frequency analysis method known as the STFT. The basic goal of time-frequency methods is to provide a distribution that represents the energy or intensity of a signal simultaneously in time and frequency.

The traditional methods of calculating the time-frequency relationship for a signal are based on the Fourier transform. The Fourier transform can give the spectral content of the signal. The Fourier transform may be applied to a short time interval (or window) of the signal resulting in an estimate of the frequency content of the signal over that time interval. In this case, a signal $s(t)$ originally measured in the time domain can be converted into a signal in the frequency domain. The STFT for signal $s(t)$ windowed by a fixed-length

function $w(\tau - t)$ at time t where τ is a time variable.

$$STFT_s(t,f) = \int_{-\infty}^{+\infty} s(\tau)w(\tau - t)exp(-j2\pi f\tau)d\tau \tag{2.3}$$

The STFT power is defined as the modulus squared of the STFT,

$$P_s(t,f)_{STFT} = |STFT_s(t,f)|^2 \tag{2.4}$$

In general, the time and frequency resolutions are determined by the width of the analysis window. In Fig. 2.4(a), each box represents a value in the time-frequency plane, the size of the box is fixed due to the time and frequency resolutions of STFT being constant. The STFT requires a trade-off between frequency and temporal resolution. Short windows improve temporal resolution but reduce frequency resolution. The STFT gives a fixed resolution at all times whereas the wavelet transform gives a variable resolution which is why researchers have proposed the wavelet transform.

The Continuous Wavelet Transform (CWT) method allows the length of the wavelet to vary, the temporal and spectral resolution is no longer fixed but is matched to the spectral components of the signal. The illustration in Fig. 2.4(b) is commonly used to explain how time and frequency resolutions should be interpreted. It can be seen that each box represents an equal portion of the time-frequency plane, but gives different proportions to time and frequency. At low frequencies, the heights of the boxes decrease (i.e. the frequency resolution gets better), but their widths increase (i.e. the time resolution gets poorer). At high frequencies, the widths of the boxes decrease, (i.e. the time resolution gets better) and the heights of the boxes increase (i.e. the frequency resolution gets poorer). Regard-

less of the dimensions of the boxes, the areas of all boxes also are the same as determined by the Heisenberg-Gabor uncertainty principle [71, 72, 73, 74, 75, 76]. In this thesis, the STFT method will be used as a benchmark waveform time-frequency method in the experimental analysis.

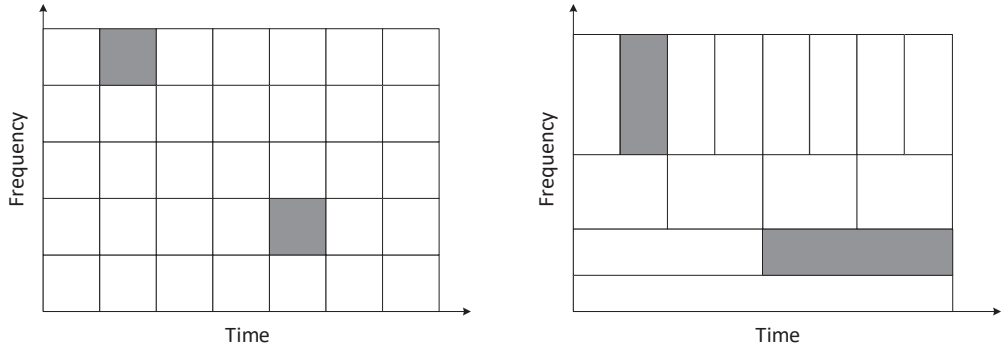

(a) STFT (b) CWT

Fig. 2.4 Time-frequency plane of STFT and CWT.

2.2.2 Heisenberg-Gabor Uncertainty Principle

The Heisenberg-Gabor uncertainty principle theory was proposed by Gabor in 1946 [71, 77, 78, 79, 80]. The principle describes how the product of the uncertainties in frequency and time are lower bounded. With the time-frequency method, it is not possible to have arbitrary time and frequency resolution. Consequently, the accuracy with which one of them can be measured limits the accuracy with which the other can be measured. Given f and t, the uncertainty principle refers to a product of errors in determining simultaneously f and t.

$$\Delta f \Delta t = K \tag{2.5}$$

where Δt is a measure of the time resolution, Δf is a measure of the frequency resolution and K is a constant.

Here is a demonstration of how to calculate the Time-bandwidth Product (TBP) of the STFT which can be used to measure the ability of the STFT to discriminate between two sinusoids [77, 78, 79, 80, 81, 82]. The Δf of the filter as

$$\Delta f = \sqrt{\frac{\int f^2 |G(f)|^2 df}{\int |G(f)|^2 df}} \tag{2.6}$$

where $g(t)$ represent a window function and $G(f)$ represents its corresponding Fourier transform. The frequency resolution of the STFT is given by Δf. The spread in time is given by Δt as

$$\Delta t = \sqrt{\frac{\int t^2 |g(t)|^2 dt}{\int |g(t)|^2 dt}} \tag{2.7}$$

Since the time resolution Δt and the frequency resolution Δf cannot be arbitrarily small, their product is lower bounded:

$$\text{TBP} = \triangle t \triangle f \geq \frac{1}{4\pi} \tag{2.8}$$

The implications of the Heisenberg-Gabor principle are easier to understand by looking at it in the time-frequency plane in Fig. 2.4(a). The time and frequency resolutions are determined by the width of the analysis window which is selected once for the entire analysis, i.e. both time and frequency resolutions are constant. Furthermore, Gaussian windows are often used since they satisfy the bound with equality where $\triangle t \triangle f = (4\pi)^{-1}$. They provide a good compromise between time resolution and frequency resolution of the

signal [77, 78, 79, 80, 81, 82]. It should be noted that wavelet functions are subject to the same uncertainty principle applicable to STFT windows. Furthermore, the resolution is fixed for each window function (STFT) or mother wavelet (CWT), they are all subject to the Heisenberg-Gabor uncertainty principle. However, since the LPC-based method (i.e. LPCPP or LPC) directly gives us the numerical frequency estimates, a new definition of the TBP for the LPC-based method will be presented and the experiments show that the Heisenberg-Gabor uncertainty principle still applies to the LPC and LPCPP methods.

2.2.3 Conclusions

In this section, an overview of time-frequency analysis methods was presented. The time-frequency methods give a view of a signal represented over both time and frequency and many time-frequency methods are waveform (not parameterised) methods that indicate how the energy of the signal is distributed over the two-dimensional time-frequency plane. However, it is still a challenge in analysing multi-component signals (i.e. EEG signals) to realise the separation of the spectrum components when they are overlapped in the time-frequency plane. Furthermore, these time-frequency methods need to balance the relationship between the time and frequency resolution subject to the Heisenberg-Gabor uncertainty principle. Time-frequency analysis methods with a higher spectral resolution are necessary to observe the dominant spectra of dynamic EEG in real-time. In the next section, a parameterised time-frequency method (i.e. the LPC method) will be presented which can directly give us numerical estimation frequency results.

2.3 Linear Predictive Coding Method

The LPC method is a parameterised time-frequency method that can be used to observe the change of spectral information of dynamic signals over time. In this section, the details of the LPC method are introduced. The first part introduces the development of the LPC method and its applications. The second part introduces the mathematical derivation of the LPC method. The third part describes the solutions of the LPC coefficients. The fourth part describes how to obtain the frequency estimates from the LPC method. Finally, some limitations of the LPC method are discussed.

2.3.1 Introduction to LPC Method

The LPC method was initially proposed for speech coding and audio compression. It has been influential in the field of speech coding for the past 40 years [83, 84, 85, 86, 87, 88, 89, 90, 91]. The origin of LPC began in the 1970s with the development of the first LPC method [88]. The LPC method is defined as a method for encoding an analog signal in which a particular value is predicted by a linear function of the past values of the signal. There are many variants of the basic scheme: In 1974, Magill and Chong-Kwan proposed the residual excited LPC, the method has a relatively low bit rate and the method is simple for hardware implementation [83]. In 1982, Tremain and Thomas proposed the LPC-10 method, the method based on the 10th order lattice filter to create the prediction parameters [84]. In 1985, Schroeder and Atal proposed the code excited linear predictive method, the vocoder used a codebook to obtain the best matches for the LPC residual signal and it provided significantly better quality than LPC vocoder [85]. In

1994, a low-delay code excited linear prediction method was proposed. The method used backward linear prediction instead of forwarding prediction used in LPC and can produce good quality of speech at 8kb/s [86]. In 1995, McCree et al. proposed mixed excitation linear prediction. The method is based on the traditional LPC vocoder with either a periodic impulse train or white noise. It can produce high-quality speech at low bit rates [87]. In 2001, Harma proposed an LPC method with modified filter structures. The method is based on modified inverse filters and synthesis filters. It significantly increases the number of free parameters [92]. In short, the early studies of the LPC method are mainly used in speech coding and audio compression. It is the basis of the speech encoder used in the digital 2G GSM mobile phone standard [93]. However, the LPC method is a parameterised method that generates a numerical estimate of the dominant frequency components and is therefore ideally suited to its integration into machine learning-based systems. The LPC method has been applied to some applications of pattern recognition and biological signal processing. For example, Min and Tewfik realised the automatic detection of behavioral patterns of patients with autism using the LPC method and the clusters of the LPC poles locations are used for behavioral classification [94]. Javier and Kim used the LPC method to achieve the human activity classification based on micro-Doppler signatures and the LPC method is used to represent the frequency characteristic of the Doppler signal and the resulting classification accuracy is found to be over 85% [95]. Anjum et al. used the LPC method to distinguish spectral EEG features of Parkinson's disease and the LPC method enables real-time encoding of EEG time series into features that can detect Parkinson's disease [96]. Although the LPC method has already had some applications in EEG research, the LPC method still has some limitations that can be improved. In

this thesis, a modification to the LPC method will make it more suitable for EEG signal processing.

2.3.2 Mathematical Derivation of LPC Method

The basic idea of the linear predictive coding is that the current signal sample $s(n)$ can be closely approximated as a linear combination of past samples, i.e.

$$s(n) \approx a_1 s(n-1) + a_2 s(n-2) + \cdots + a_P s(n-P) \tag{2.9}$$

where P is the LPC filter order and $a_1, \cdots, a_P$ are the constant coefficients. The above equation can be transformed, by including an excitation term $Gu(n)$

$$s(n) = \sum_{k=1}^{P} a_k s(n-k) + Gu(n) \tag{2.10}$$

where G is the gain and $u(n)$ is the normalised excitation. Transforming Eq. 2.10 into the z-plane we have

$$S(z) = \sum_{k=1}^{P} a_k z^{-k} S(z) + GU(z) \tag{2.11}$$

and consequently, the transform function $H(z)$ becomes

$$H(z) = \frac{S(z)}{GU(z)} = \frac{1}{1 - \sum_{k=1}^{P} a_k z^{-k}} = \frac{1}{A(z)} \tag{2.12}$$

This corresponds to the transfer function of a digital time-varying filter. An estimate of the signal value $s(n)$ at time index n, is denoted as $\tilde{s}(n)$. This estimate is computed using

$$\tilde{s}(n) = \sum_{k=1}^{P} \alpha_k s(n-k) \tag{2.13}$$

where α_k are the coefficients of the predictor. The prediction error $e(n)$ is defined as

$$e(n) = s(n) - \tilde{s}(n) = s(n) - \sum_{k=1}^{P} \alpha_k s(n-k) \tag{2.14}$$

which is the output of the system with the transfer function

$$A(z) = 1 - \sum_{k=1}^{P} \alpha_k z^{-k} \tag{2.15}$$

if the signal $s(n)$ obeys the prediction model exactly and if $a_k = \alpha_k, 1 \leq k \leq P$, then

$$H(z) = \frac{1}{A(z)} \tag{2.16}$$

The basic problem of linear prediction analysis is to determine the set of predictor coefficients α_k that minimises the square of the prediction error from a short segment of a signal. The resulting α_k is assumed to be the actual a_k in the prediction model. The short-time average prediction squared-error is defined as

$$\begin{aligned} E_{\hat{n}} &= \sum_m e_{\hat{n}}^2(m) = \sum_m [s_{\hat{n}}(m) - \tilde{s}_{\hat{n}}(m)] \\ &= \sum_m [s_{\hat{n}}(m) - \sum_{k=1}^{P} \alpha_k s_{\hat{n}}(m-k)]^2 \end{aligned} \tag{2.17}$$

where $s_{\hat{n}}(m)$ is a segment of a signal $s_{\hat{n}}(m) = s(m+\hat{n})$ in the vicinity of sample $\hat{n}$. The coefficients α_k can be obtained that minimise $E_{\hat{n}}$ by setting

$$\frac{\partial E_{\hat{n}}}{\partial \alpha_i} = 0, \quad i = 1,2,\cdots,P \tag{2.18}$$

giving the set of equations

$$\sum_m s_{\hat{n}}(m-i)s_{\hat{n}}(m-k) = \sum_{k=1}^{P} \hat{\alpha}_k \sum_m s_{\hat{n}}(m-i)s_{\hat{n}}(m-k), \quad 1 \leq i \leq P \tag{2.19}$$

where $\hat{\alpha}_k$ are the values of α_k that minimise $E_{\hat{n}}$. Defining

$$\phi_{\hat{n}}(i,k) = \Sigma_m s_{\hat{n}}(m-i)s_{\hat{n}}(m-k) \tag{2.20}$$

then, get

$$\Sigma_{k=1}^{p} \alpha_k \phi_{\hat{n}}(i,k) = \phi_{\hat{n}}(i,0), \quad i = 1,2,\cdots,P \tag{2.21}$$

leading to a set of P equations in P unknowns that can be solved in an efficient manner for the α_k. Minimum mean-squared prediction error has the form

$$E_{\hat{n}} = \Sigma_m s_{\hat{n}}^2(m) - \Sigma_{k=1}^{P} \alpha_k \sum_m s_{\hat{n}}(m)s_{\hat{n}}(m-k) \tag{2.22}$$

which can be written in the form

$$E_{\hat{n}} = \phi_{\hat{n}}(0,0) - \sum_{k=1}^{P} \alpha_k \phi_{\hat{n}}(0,k) \tag{2.23}$$

Now, the values $\phi_{\hat{n}}(i,k)$ have to be obtained for $1 \leq i \leq P$ and $1 \leq k \leq P$ and the α_k coefficients are obtained by solving Eq. 2.21. The following describes in detail how to calculate the LPC coefficients.

2.3.3 Solving for the LPC Coefficients

The basic problem of the linear prediction analysis is to determine the set of predictor coefficients [92, 97, 98, 99]. There are two main ways of solving for the LPC coefficients α_k namely the autocorrelation method and the covariance method. For the autocorrelation method, it requires a window that will suppress the side lobes, the window shape affects the values of the predictor coefficients obtained and the appearance of the spectrum envelop. For the covariance method, it is a slightly misleading term as it is not a covariance in the usual probability sense here and it has the benefit that every point in the time series makes an equal contribution to the predictors. The choice of method depends on the assumptions made about the input signal. The autocorrelation method has the additional useful practical advantage that the linear filters it produces are stable, while the covariance method may produce unstable filters. Furthermore, the autocorrelation method requires less computation than the covariance methods [98]. So for these reasons the autocorrelation method will be used to solve the LPC equation in this thesis.

The autocorrelation method considers the segment $s_{\hat{n}}(m)$ exits for $0 \leq n \leq L-1$ and is exactly zero everywhere else that can be expressed as

$$s_{\hat{n}}(m) = s(m+\hat{n})w(m), \quad 0 \leq m \leq L-1 \tag{2.24}$$

where $w(m)$ is a finite length window of length L samples. If $s_{\hat{n}}(m)$ is non-zero for $0 \leq m \leq L-1$ then the corresponding prediction error $e_{\hat{n}}(m)$ will be non-zero over the interval $0 \leq m \leq L-1+P$. Thus, for this case $E_{\hat{n}}$ giving

$$E_{\hat{n}} = \sum_{m=-\infty}^{\infty} e_{\hat{n}}^2(m) = \sum_{m=0}^{L-1+P} e_{\hat{n}}^2(m) \tag{2.25}$$

However, the prediction error $e_{\hat{n}}(m)$ is relatively large at the beginning and at the end of the interval. The reason is that when m near 0, $m = 0, 1, \cdots, P-1$, the prediction signal is obtained from zero-valued samples outside the window range, the $e_{\hat{n}}(m)$ will be relatively large. At same time, the m near L, $m = L, L+1, \cdots, P+L-1$, the zero-valued samples are predicted from non-zero samples, the $e_{\hat{n}}(m)$ also will be relatively large. Thus, one should normally use windows that taper the segment to zero (e.g. a Hamming window). Considering that $s_{\hat{n}}(m) = 0$ outside the range $0 \leq m \leq L-1$, then

$$\phi_{\hat{n}}(i,k) = \sum_{m=0}^{L-1+P} s_{\hat{n}}(m-i)s_{\hat{n}}(m-k), \quad 1 \leq i \leq P, 0 \leq k \leq P \tag{2.26}$$

which can be rewritten as

$$\phi_{\hat{n}}(i,k) = \sum_{m=0}^{L-1+(i-k)} s_{\hat{n}}(m)s_{\hat{n}}(n+i-k), \quad 1 \leq i \leq P, 0 \leq k \leq P \tag{2.27}$$

In this case, $\phi_{\hat{n}}(i,k)$ is related the short-time autocorrelation function valued for $i-k$ where

$$\phi_{\hat{n}}(i,k) = R_{\hat{n}}(i-k), \quad 1 \leq i \leq P, 0 \leq k \leq P \tag{2.28}$$

where

$$R_{\hat{n}}(k) = \sum_{m=0}^{L-1-k} s_{\hat{n}}(m)s_{\hat{n}}(m+k) \tag{2.29}$$

Therefore

$$\phi_{\hat{n}}(i,k) = R_{\hat{n}}(|i-k|), \quad 1 \leq i \leq P, 0 \leq k \leq P \tag{2.30}$$

Thus, the basic equation becomes

$$\begin{aligned} \sum_{k=1}^{P} \alpha_k \phi_{\hat{n}}(i-k) &= \phi_{\hat{n}}(i,0), \quad 1 \leq i \leq P \\ \sum_{k=1}^{P} \alpha_k R_{\hat{n}}(|i-k|) &= R_{\hat{n}}(i), \quad 1 \leq i \leq P \end{aligned} \tag{2.31}$$

with the minimum mean-squared prediction error of the from

$$\begin{aligned} E_{\hat{n}} &= \phi_{\hat{n}}(0,0) - \sum_{k=1}^{P} \alpha_k \phi_{\hat{n}}(0,k) \\ &= R_{\hat{n}}(0) - \sum_{k=1}^{P} \alpha_k R_{\hat{n}}(k) \end{aligned} \tag{2.32}$$

The system of equations can be expressed in the following matrix vector form

$$\begin{bmatrix} R_{\hat{n}}(0) & R_{\hat{n}}(1) & \cdots & R_{\hat{n}}(P-1) \\ R_{\hat{n}}(0) & R_{\hat{n}}(1) & \cdots & R_{\hat{n}}(P-1) \\ . & . & \cdots & . \\ . & . & \cdots & . \\ R_{\hat{n}}(0) & R_{\hat{n}}(1) & \cdots & R_{\hat{n}}(P-1) \end{bmatrix} \begin{bmatrix} \alpha_1 \\ \alpha_2 \\ . \\ . \\ \alpha_P \end{bmatrix} = \begin{bmatrix} R_{\hat{n}}(1) \\ R_{\hat{n}}(2) \\ . \\ . \\ R_{\hat{n}}(P) \end{bmatrix} \tag{2.33}$$

Furthermore, it can be simplified as

$$\Re\alpha = \mathbf{r} \tag{2.34}$$

The matrix $\Re$ is a $P \times P$ Toeplitz matrix which is symmetric with all diagonal elements equal. Finally, the LPC coefficients α_k can be obtain though a matrix inversion

$$\alpha = \Re^{-1}\mathbf{r} \tag{2.35}$$

In the next part, the calculation of the frequency estimation of LPC will be presented.

2.3.4 Frequency Estimation using the LPC Method

The LPC method gives a good point of departure for obtaining formant frequencies, the transfer function $|H(z)| = 1/|A(z)|$ is the envelope of the speech signal and its maxima correspond to the resonances of the vocal track, e.g. the formants [100]. The term "formant" is used for speech signal analysis, here the term "dominant frequency" will be used in the following description. Most researchers to date have used the poles of $H(z)$ to directly estimate the dominant frequencies of the response [101, 102, 103, 104, 105, 100]. The fundamental theorem of algebra tells us that $H(z)$ has P complex poles which are the values of z for which $H(z) = \infty$. Therefore the poles of $H(z)$ can be expressed as

$$z_k = \gamma_k e^{j\omega_k} \tag{2.36}$$

where

$$\omega_k = \tan^{-1}[\mathrm{Im}(z_k)/\mathrm{Re}(z_k)] \tag{2.37}$$

is the angle corresponding to the pole. The magnitude of the pole is represented as $m_k = |z_k|$ and the corresponding pole frequency is represented as

$$\dot{f}_k = \omega_k/(2\pi T) \tag{2.38}$$

where T is the sample period. The poles occur in complex conjugate pairs which are mirrored in the real axis of the z-plane. Fig. 2.5 shows the LPC poles of a pure sinusoidal

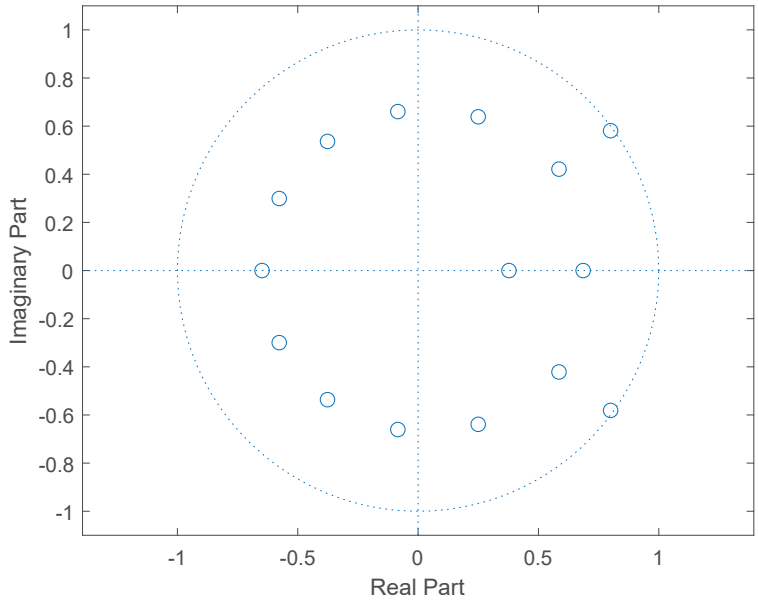

Fig. 2.5 LPC poles/roots of the z-plane.

signal in the z-plane. The parameters are the sampling frequency $f_s = 100$ Hz, the signal duration $t = 1$ s, the LPC filter order $P = 15$ and the sinusoid frequency is 10 Hz. Here, the poles with non-negative imaginary parts $\mathrm{Im}(z_i) \geq 0$ are considered as the outputs of the LPC method. The frequencies estimated by LPC are $\{\dot{f}_1, \dot{f}_2, \cdots\}$.

2.3.5 The Limitations of the LPC Method for Frequency Estimation

There are some limitations of the LPC method discussed here. The first one is that the LPC method suffers from a sensitivity to the filter order and the number of the frequency estimates depends on the number of the filter order. Furthermore, the LPC method exhibits a poor tolerance of high noise environments.

The LPC method requires a model whose filter order P must correspond to the signal for best results [101, 106, 88, 107, 108]. The choice of the filter order for the LPC method is a compromise between spectral accuracy, the length of signal and the sampling frequency. In the speech signal analysis, the choice of LPC order P depends on the analysis bandwidth which in turn depends on the sampling frequency f_s. The rule of thumb is

$$P = \frac{f_s}{1000} + K \tag{2.39}$$

The K is a constant, empirically determined and is typically between 2 and 3 [101]. However, the rule only applies to speech signals, not to other signals and it is essentially just a rule of thumb. Furthermore, this rule does not apply to the selection of filter order for other types of signals. In addition, the different LPC filter orders will have different effects on the LPC spectrum. Models which are of too low an order tend to provide poor spectral separation in the frequency domain whereas too high an order causes deterioration of the noise immunity of the spectral estimator by creating a profusion of candidate peaks in the estimated vocal tract frequency response [106]. The filter orders P correspond to the length of the inverse filter which is used to model the LPC spectrum. Furthermore, the number of the frequency estimates of the LPC method depends on the filter order rather

than the real number of frequencies of the signal. Typically, the number of frequency estimates is half the filter order. Therefore, the LPC method is sensitive to the choice of LPC order.

Another restriction is the LPC method has poor tolerance of high noise environments and the outputs of LPC coefficients are sensitive due to noise [101, 109, 110, 111, 112, 113, 114]. When the signal is corrupted by noise, the assumptions of the all-pole model have been violated and its accuracy in modeling the signal suffers. Low signal-to-noise ratios (e.g. below 5 to 10 dB) can cause serious distortion of the model spectral density [101]. Furthermore, a small quantization error also may cause an unstable synthesis filter [109, 110]. There have been numerous methods proposed to investigate this problem, such as Kay Steven discussed a large LPC order model to combat the effects of the noise [110]. However, this technique cannot guarantee the stability of the AR filter. Joseph Tierney increased the LPC filter order to model both speech and noise spectral features [111]. Unfortunately, the LPC spectral overestimates the underlying speech spectrum when the filter order increases. Shimamura Tetsuya et al. proposed a method to improve the performance of the LPC method, in which the autocorrelation function of the noisy speech is transformed into its noiseless autocorrelation function [112]. However, the method cannot guarantee the stability of the all-pole filter. Liu Liqing et al. proposed a noise compensation LPC method to attenuate the influence of the noise by an a priori estimate of the noise [114]. However, this method is only constrained to its use in white noise environments. In summary, the LPC method suffers from sensitivity to the choice of model order and it has poor tolerance of high noise environments.

2.3.6 Conclusions

In this section, the details of the LPC method are introduced. First, the origin and development of LPC are introduced. Furthermore, the details of the mathematical expression of the LPC method are also introduced. Finally, some limitations of the LPC method are also discussed. The LPC method was initially proposed for speech coding and audio compression. Since the LPC method is a parameterised time-frequency method, a new modified LPC method that overcomes the shortcomings of the LPC method will be proposed in the next chapter and it will be used for the processing of EEG signals.

2.4 Chapter Summary

In this chapter, the details of the technical background were presented. The first section introduced the details of the EEG signals. First of all, EEG collection is always accompanied by a variety of noise corruption. The EEG signal may be overwhelmed by other electrical activity generated by the body or in the environment. Furthermore, EEG is a dynamic signal response to human brain activity (emotion, cognitive, etc.), these activities change over time and are not continuous. In addition, EEG signals often have multiple frequency components. The spectrum of EEG has been divided into a number of fixed frequency bands by many biomedical researchers to investigate the corresponding brain functions However, different researchers have defined different frequencies for these bands with little consensus between them which has significant consequences for EEG interpretation. The second section presented an overview of time-frequency analysis methods that provide a way to analyse the frequency dynamics in EEG signals. Many

time-frequency methods are spectral waveform (not parameterised) methods, they can tell whether a certain frequency component exists or not at any given time interval. However, it is still a challenge in analysing multi-component signals to realise the separation of the spectrum components when they are overlapped in the time-frequency plane. Furthermore, the Heisenberg-Gabor Uncertainty Principle indicates that there is a trade-off relationship between time resolution and frequency resolution. When the time-frequency analysis method has a smaller TBP value, it can provide a higher frequency resolution at the same time duration (i.e. time resolution). Similarly, it can provide a higher time resolution at the same frequency resolution. In summary, some requirements for time-frequency analysis methods for EEG signal analysis need to be considered:

- The method should be a parameterised method. The parameterised time-frequency method can produce numerical dominant frequency estimates and it is well suited to multi-components signal processing (i.e. EEG signals).

- The method should provide higher spectral resolution and enable real-time observation of dynamic EEG dominant spectra. The time-frequency analysis methods with a smaller TBP value are required for real-time analysis of dynamic EEG frequencies.

- The method requires a high tolerance for noise. It needs to have a robust performance in high noise environments.

Finally, the LPC method was presented which is a parameterised time-frequency method. However, the LPC method suffers from a sensitivity to the filter order and it has poor tolerance to noisy environments. In the next chapter, a detailed analysis of the LPC method

will be presented and a new modified LPC method called the LPCPP method will be introduced which will be better suited to the spectral analysis of EEG.

Chapter 3

Technical Detail of the LPCPP Method

In this chapter, the full technical details of the LPCPP method are presented. The proposed LPCPP method will be applied to EEG signal processing. The first section presents an analysis of the LPC poles and the LPC spectra. The definitions of the dominant pole and the non-dominant pole are first proposed. Furthermore, the effect of different experimental parameters (i.e. the filter order, the signal duration, the sampling frequency, the signal noise and the different window functions) are analysed for distinguishing the dominant and non-dominant poles. The second section demonstrates the effect of the relationship between the dominant pole and non-dominant pole on the spectrum. Furthermore, the associated pole is first proposed and introduced. The third section introduces the technical details of the proposed LPCPP method. It has three steps to realise the frequency estimation. The first step classifies the LPC poles into dominant and non-dominant poles. The second step identifies the associated poles corresponding to each dominant pole. Finally, the dominant poles and their corresponding associated pole(s) form a series of reduced-

order transfer functions to obtain the frequency estimates. The last section is the summary of the chapter.

3.1 The Fundamental Analysis of the LPC Method

In this section, the definitions of the dominant pole and non-dominant pole are introduced to classify the LPC poles. These definitions were originally introduced in [115, 116, 117, 118]. Furthermore, the effects of different experimental parameters on distinguishing the dominant pole and the non-dominant pole are analysed. These experimental parameters include filter order, signal duration, sampling frequency, signal noise and different window functions. At the same time, the effect of these parameters on the LPC spectral peaks is also analysed.

3.1.1 The Classification of the LPC Poles

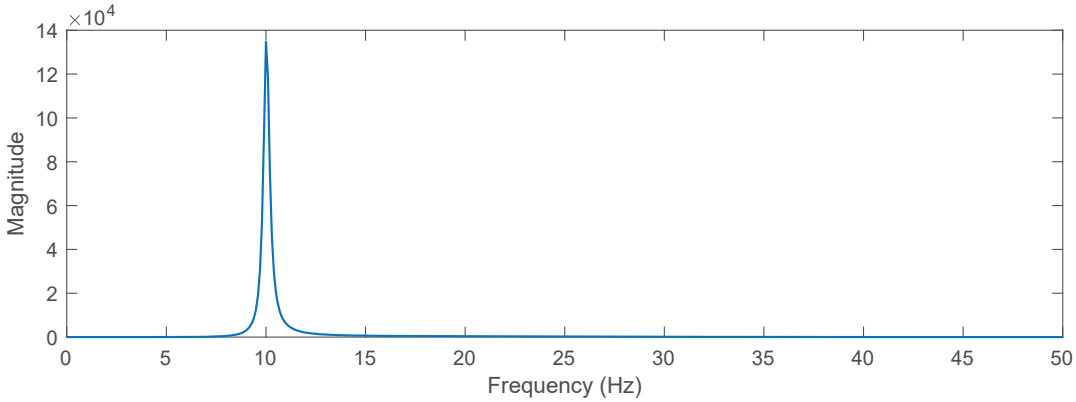

Fig. 3.1 LPC spectrum of all-pole model.

The LPC all-pole models are most often used in practical applications. The LPC all-pole model is given by

$$H(z) = \frac{1}{1 - \sum_{k=1}^{P} \alpha_k z^{-k}} = \frac{1}{\prod_{k=1}^{P} (1 - p_k z^{-1})} \tag{3.1}$$

where P is the LPC filter order. Fig. 3.1 shows the LPC spectrum of an all-pole model. The experimental parameters in this figure are the same as those in Fig. 2.5. The LPC poles occur in the filter as complex conjugate pole pairs and the LPC poles have mirror symmetry in the real axis of the z-plane. Again, only poles with positive imaginary parts $Im(z_i) > 0$ are considered. For example, the Fig. 3.2 shows the LPC poles $\{p_1, p_2, \cdots, p_6\}$ in the positive part of the z-domain and the LPC poles in the frequency domain respectively. The magnitude of the pole in the frequency domain corresponds to its distance from the origin in the z-domain. In the following analysis, only the LPC poles in the frequency domain will be shown.

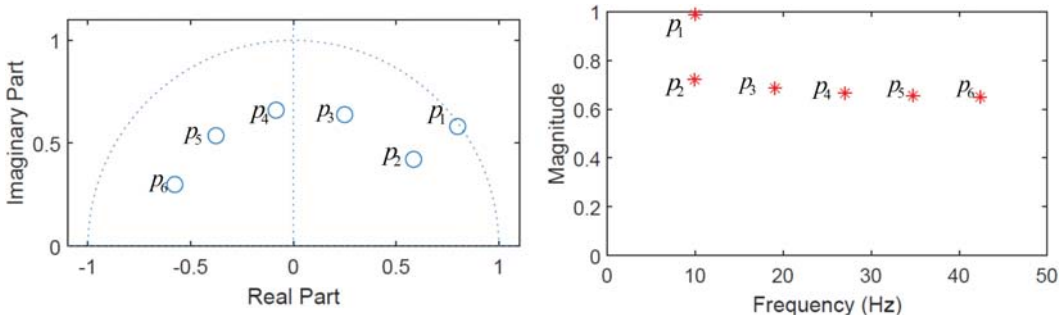

(a) LPC poles in the z-domain.

(b) LPC poles in the frequency domain.

Fig. 3.2 LPC poles in the frequency domain.

The signal analysed here is a noise-free single-component sinusoidal signal. The signal frequency is 10 Hz, the sampling frequency is $f_s = 100$ Hz, the signal duration is $t = 1$ s and the filter order is $P = 15$. Fig. 3.2 shows that not all the LPC poles correspond to

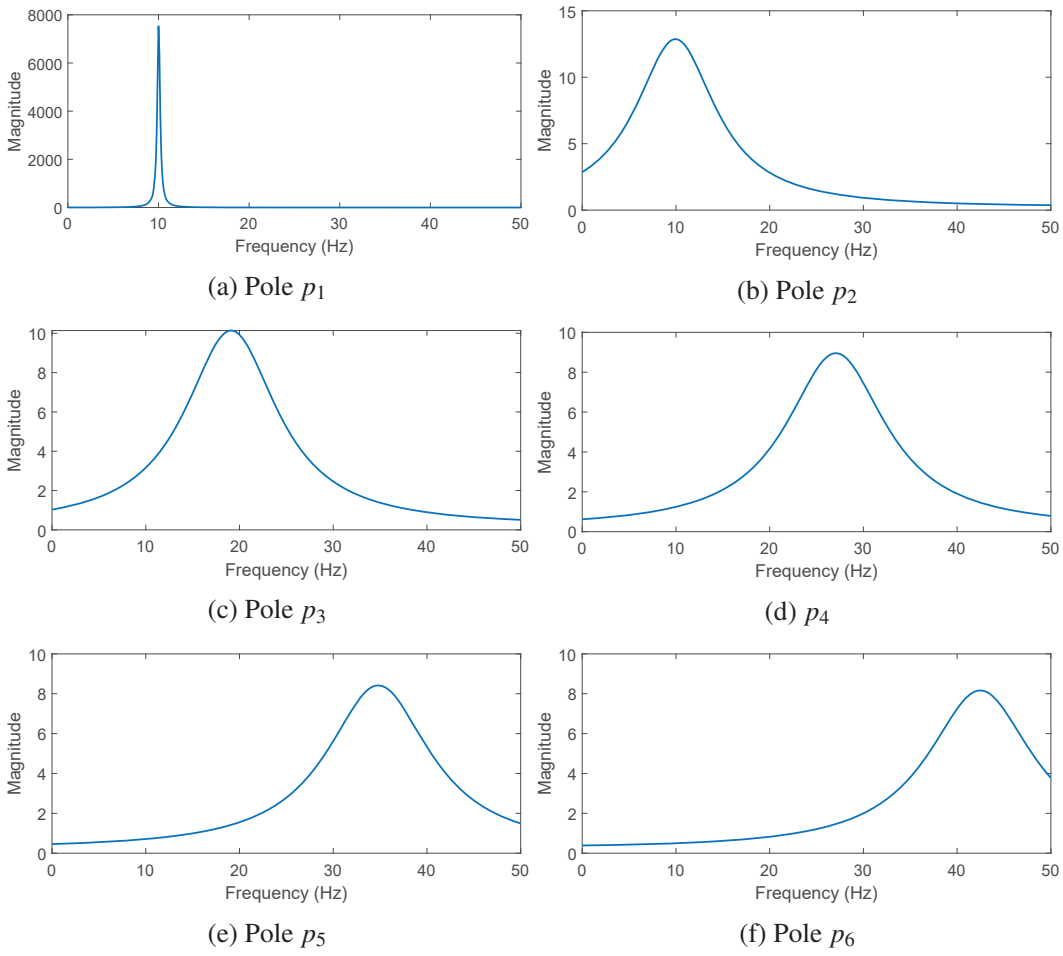

(a) Pole p_1 (b) Pole p_2

(c) Pole p_3 (d) p_4

(e) Pole p_5 (f) Pole p_6

Fig. 3.3 LPC spectra of each single-pole model.

a signal frequency. Only the pole whose magnitude is close to 1 (i.e. the radius in the z domain closest to the unit circle) p_1 can correspond to the dominant frequency component of 10 Hz. It can be observed that the magnitude of the LPC pole is an important feature to find the pole which can correspond to a signal component. Furthermore, the pole p_1 is termed the dominant pole and the other poles are termed non-dominant poles. The dominant pole has a higher magnitude than that of the non-dominant pole and it can represent the dominant frequency component of the signal. The reason is that the magnitude of the pole can be used as an indicator of the size of the spectral peak in the classical filter

analysis. Therefore, each single pole at $z = p_i$ can be represented by

$$\hat{H}_i(z) = \frac{1}{1 - p_i z^{-1}}. \tag{3.2}$$

Fig. 3.3(a)-(f) show the LPC spectra of each single-pole model which correspond to the poles $\{p_1, p_2, \cdots, p_6\}$ respectively. It is easy to see only the LPC spectral peak of pole p_1 in Fig. 3.3a has the narrowest and highest LPC spectral peak and the peak can correspond to the signal's dominant frequency component at 10 Hz. The higher spectral peak means that the associated frequency component has a higher amplitude. On the other hand, Fig. 3.2 shows that the dominant pole p_1 has the highest magnitude in the frequency domain. The magnitude of the pole can be used as an indicator of the size of the spectral peak. Furthermore, Fig. 3.3(a) shows the single-pole model of the dominant pole and it is termed the dominant spectrum. Otherwise, the magnitude of the non-dominant poles is much lower than that of the dominant pole and they cannot represent the dominant frequency component of the signal. Figs. 3.3(b)-(f) show a series of the single-pole models of the non-dominant poles and they are termed non-dominant spectra. The magnitudes of these non-dominant spectra are lower than that of the dominant spectra and their spectral widths are wider than that of the dominant spectra.

The signal analysed above is a single component signal, but these categories of LPC poles are also applicable to multiple components signal analysis. For example, Fig. 3.4(a) and (b) show the analysis of two multi-component signals. The first one is a two-component signal whose signal frequencies are 10 Hz and 35 Hz. The second one is a three-component signal whose signal frequencies are 10 Hz, 20 Hz and 35 Hz. The other

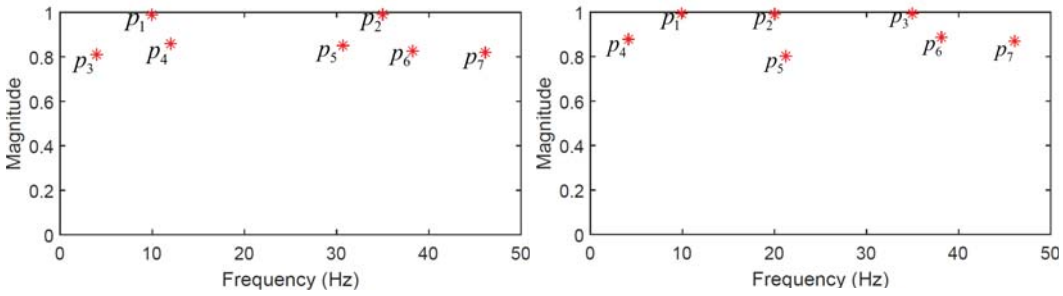

(a) LPC poles of a two-component signal. (b) LPC poles of a three-component signal.

Fig. 3.4 LPC poles of multiple components signals in the frequency domain.

parameters are the same as the above single component signal analysis. The poles p_1 and p_2 in Fig. 3.4(a) are dominant poles for the two-component signal and the others are non-dominant poles. The poles p_1, p_2 and p_3 in Fig. 3.4(b) are dominant poles for three-component signal and the other poles are non-dominant poles. It can be observed that the magnitude of the pole still can be used as an indicator to distinguish between the dominant pole and the non-dominant pole. In the following analysis, the LPC poles under the different parameters are analysed. In order to facilitate the analysis of the performance of the LPC method under different parameters, the following analysis will use a simple scenario where the single-component signals are analysed.

3.1.2 Filter Order Analysis of LPC

The first experiment is to analyse the effect of the filter order on the LPC pole. A sinusoidal signal with a frequency of 10 Hz is used here, the sampling frequency of the signal is $f_s = 100$ Hz and the signal duration is $t = 1$ s. The filter order P is increased from 5 to 20 in steps of 5. Fig. 3.5 shows that the LPC poles in the frequency domain under different filter orders. It can be seen that the dominant pole represents the signal frequency component at 10 Hz under different filter orders. The number of non-dominant poles is increased

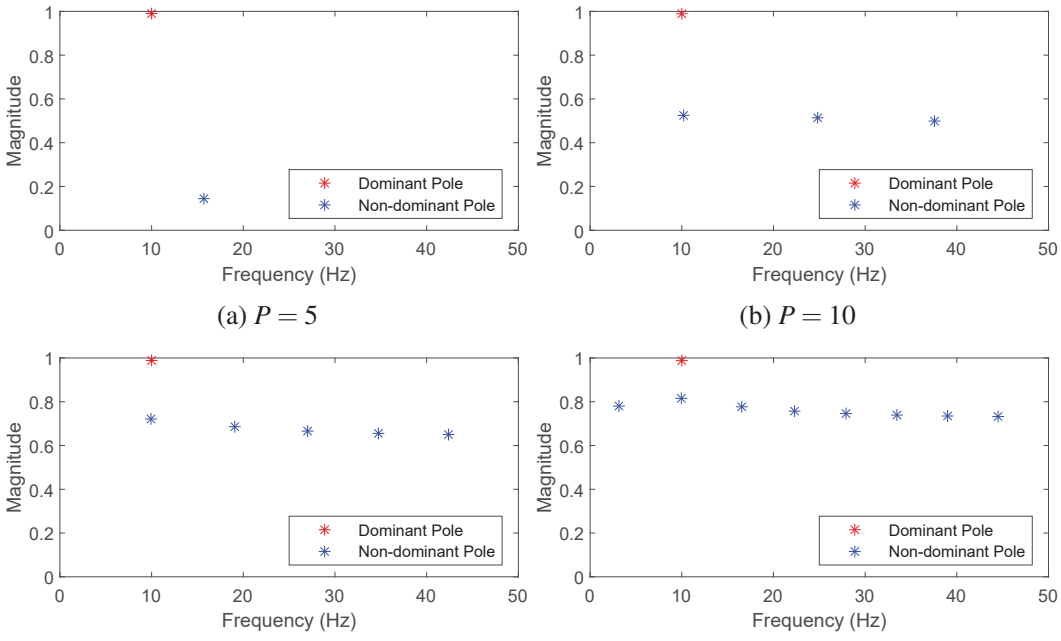

(a) $P = 5$ (b) $P = 10$

(c) $P = 15$ (d) $P = 20$

Fig. 3.5 LPC poles of LPC method with different filter orders.

with the increase of the filter order. For the magnitude of LPC poles, the dominant pole has the highest magnitude and its magnitude is closest to 1. For the non-dominant poles, their magnitudes are increased with the increase in the filter order. Furthermore, the change of filter order cannot increase the number of dominant poles but will increase the number of non-dominant poles. When the filter order is 5, the magnitude difference between the dominant and non-dominant poles is the most obvious and the number of non-dominant poles is the least. Therefore, the number of the non-dominant poles is sensitive to the choice of filter order.

The LPC spectra under the different filter orders are shown in Fig. 3.6. These LPC spectra are normalised to the range of 0 to 1 and the frequency axis is fixed from 9 to 11 Hz to zoom in on the LPC spectra to make it easier to observe the difference between these LPC spectra. Furthermore, these LPC spectral peak does not change under the different filter

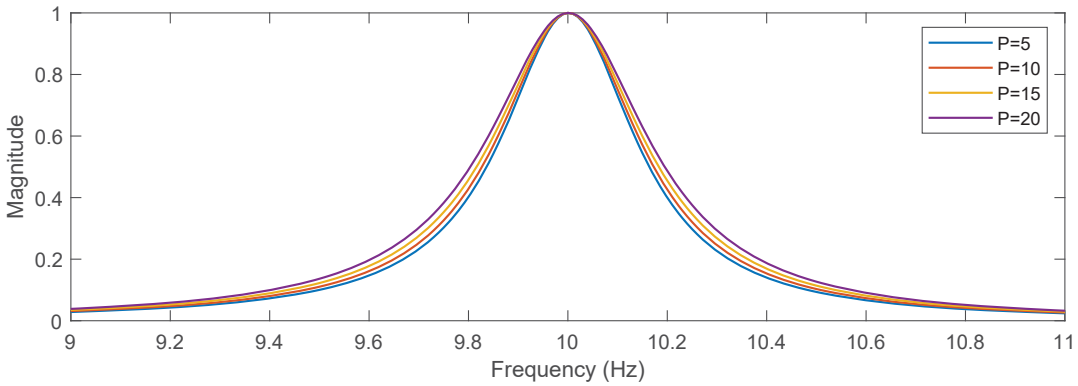

Fig. 3.6 LPC spectra for different filter orders.

orders. However, the width of the spectral increases as the filter order increases. The reason is that the dominant pole and non-dominant pole jointly determine the position and width of the LPC spectrum peak. When the filter order increases, the number of non-dominant poles also increases while these non-dominant poles cannot correspond to the dominant signal frequency component of 10 Hz. This is the reason why when the filter order is 5, the LPC spectra provide the narrowest spectral peak.

In summary, the number of the LPC poles depends on the choice of the filter order. However, not all of the LPC poles can correspond to the dominant frequency component of the signal. Furthermore, when the filter order increases, the number of dominant poles will not change, while the number of non-dominant poles will increase. Moreover, the width of the spectral peak is affected by the number of non-dominant poles. Therefore, the performance of the LPC method is sensitive to the choice of the filter order.

3.1.3 Signal Duration Analysis of LPC

Here, the effects of different duration signals on the LPC method are analysed. The experimental signal is a noise-free sinusoidal signal of 10 Hz. The sampling frequency is

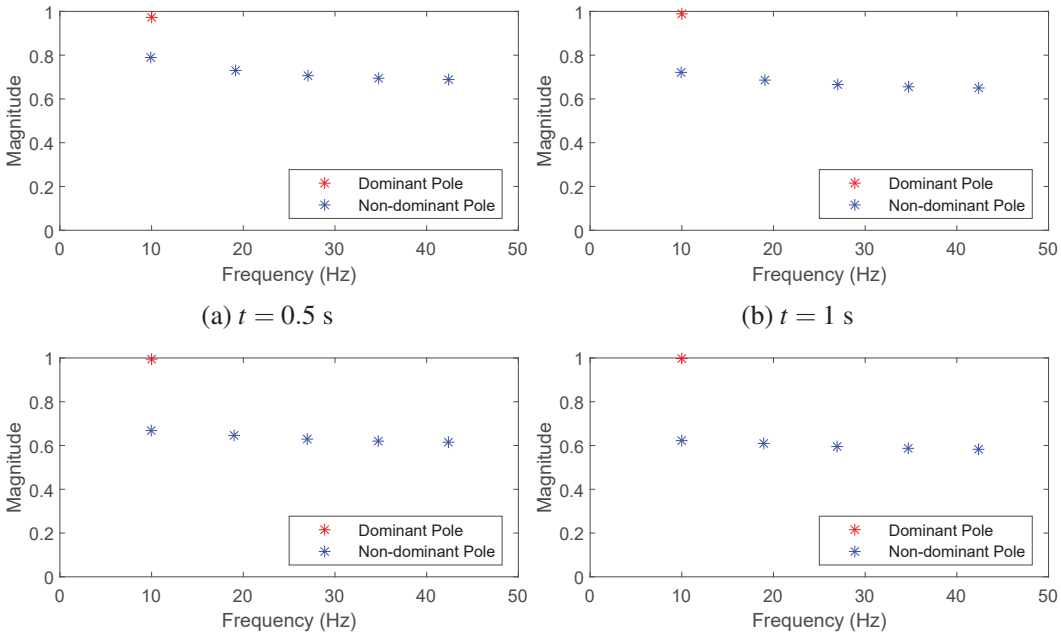

(a) $t = 0.5$ s (b) $t = 1$ s

(c) $t = 2$ s (d) $t = 4$ s

Fig. 3.7 LPC poles for signals of different durations.

$f_s = 100$ Hz and the filter order is $P = 15$. The signal duration is 0.5 s, 1 s, 2 s and 4 s. Fig. 3.7 shows the LPC poles under the different signal lengths. The length of the pure sinusoidal signal has little effect on the positions of the LPC poles on the frequency axis. However, the signal length affects the magnitude of non-dominant poles. The magnitude of the non-dominant poles in the frequency domain decreases as the signal length increases. The magnitude of the dominant pole is always closest to 1 and correctly corresponds to the signal frequency component under the different signal lengths. Therefore, increasing the length of the signal can increase the magnitude difference between the dominant pole and the non-dominant poles to better distinguish between them.

The LPC spectra under different signal lengths are shown in Fig. 3.8. These LPC spectra are normalized to the range of 0 to 1 and the frequency axis is fixed from 9 to 11 Hz to zoom in on the LPC spectra. It can be seen that as the signal length increases, the

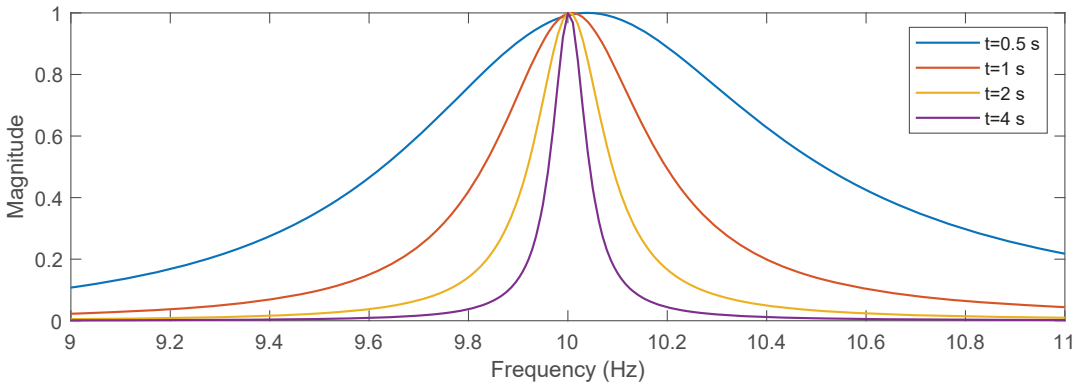

Fig. 3.8 LPC spectra for different signal durations.

LPC spectra can provide a narrower spectral peak for spectral separation of frequencies. This result is a consequence of the Heisenberg-Gabor uncertainty principle. Long signals reduce the temporal resolution but improve the frequency resolution. In addition, as the signal length increases, the LPC spectra have a narrower spectral peak to correspond to the signal frequency component. In Fig. 3.8, when the signal length is 4 s, the spectral peak provides the narrowest spectral peak which is identified accurately at 10 Hz.

This result has shown that increasing the signal duration can reduce the magnitude of the non-dominant poles, so as to better distinguish between the dominant pole and the non-dominant pole. Moreover, the increase in signal duration can provide richer spectral information and produce narrower LPC spectral peaks. However, increasing the signal duration will cause a decrease in temporal resolution, this is a trade-off relationship between the temporal resolution and spectral resolution.

3.1.4 Signal Sampling Frequency Analysis of LPC

The effects of different sampling frequencies are analysed here. Furthermore, this part will have two scenarios to consider: the first one is that the number of samples of the

signal is fixed and the second one is that the length of duration of the signal is fixed. Furthermore, the sampling frequency is changed from 50 Hz to 400 Hz in steps of 50 Hz.

The signals with the fixed number of samples

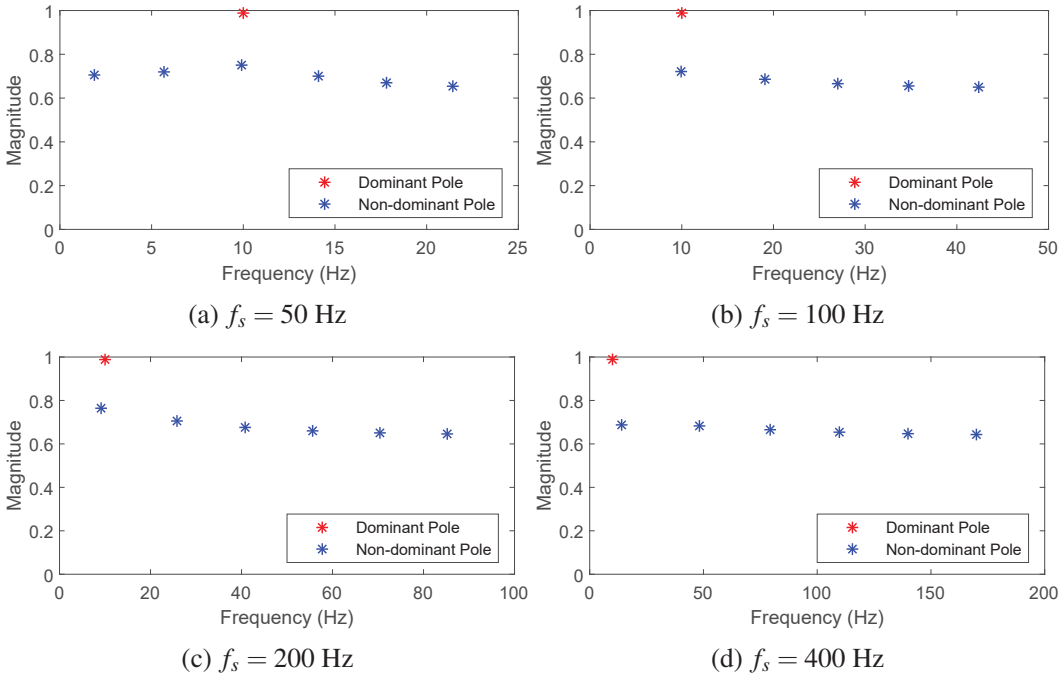

(a) $f_s = 50$ Hz (b) $f_s = 100$ Hz

(c) $f_s = 200$ Hz (d) $f_s = 400$ Hz

Fig. 3.9 LPC poles at different sampling frequencies for a signal with a fixed number of samples.

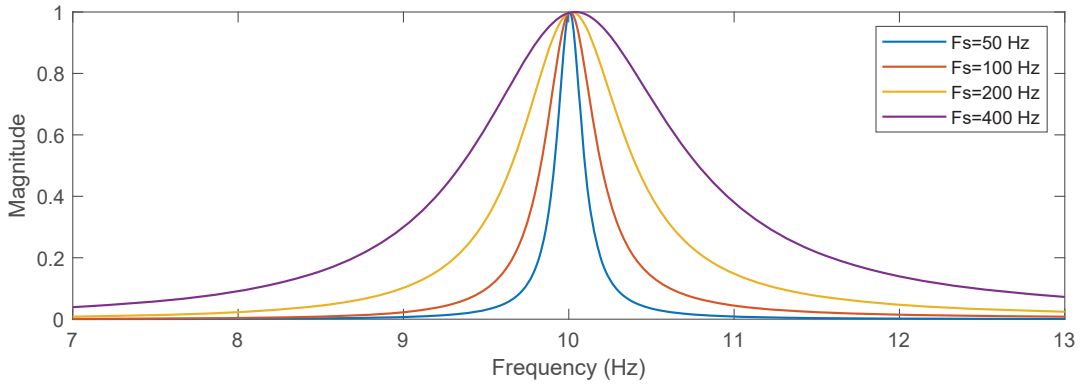

Fig. 3.10 LPC spectra at different sampling frequencies for a signal with a fixed number of samples.

The first experiment of this part shows the LPC poles at a fixed 100 signal samples at different sampling frequencies in Fig. 3.9. The signal is a noise-free 10 Hz sinusoidal signal and the filter order is $P = 15$. It can be seen that there is still a dominant pole that can represent the dominant frequency component of 10 Hz at different sampling frequencies. However, the non-dominant poles are scattered across the frequency domain. And as the sampling frequency increases, the non-dominant poles are further spaced out in the frequency domain. Furthermore, under the same number of samples of the signal, the increase of the sampling frequency has little effect on distinguishing the dominant pole and the non-dominant pole by magnitude. Fig. 3.10 shows the LPC spectra for the different sampling frequencies at the signals that have the same number of samples. These LPC spectra are normalised to the range of 0 to 1 and the frequency axis only shows the frequency domain from 7 to 13 Hz. It can be seen the LPC spectra with the sampling frequency of 50 Hz have the narrowest spectral peak to correspond to the dominant frequency. The reason is that under the same number of signal samples, the signal with the 50 Hz sampling frequency has the longest duration of 2 s. Longer signal duration results in narrower spectral peaks.

The signals with the fixed duration

The second experiment shows the LPC poles at different sampling frequencies for a fixed duration signal of 1 s in Fig. 3.9. The signal is a noise-free 10 Hz sinusoidal signal and the filter order is $P = 10$. As can be seen, increasing the sampling frequency can more significantly distinguish dominant and non-dominant poles from amplitude when the signal duration is fixed. Furthermore, as the sampling frequency increases, the magni-

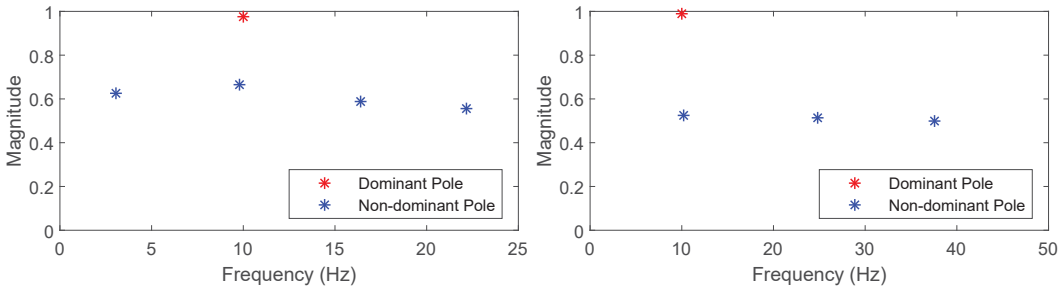

(a) $f_s = 50$ Hz (b) $f_s = 100$ Hz

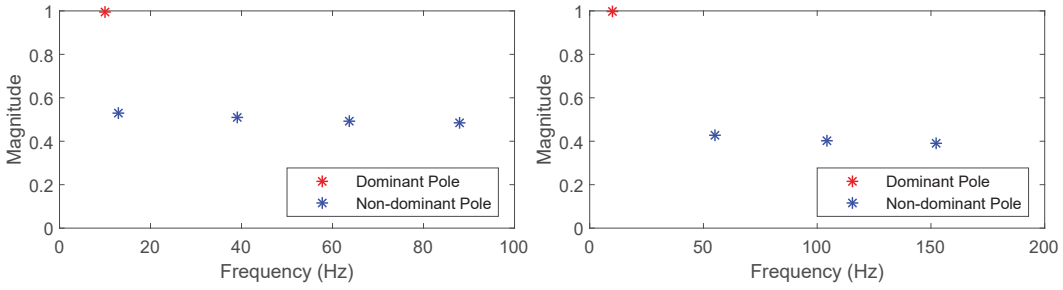

(c) $f_s = 200$ Hz (d) $f_s = 400$ Hz

Fig. 3.11 LPC poles at different sampling frequencies for a signal with a fixed duration.

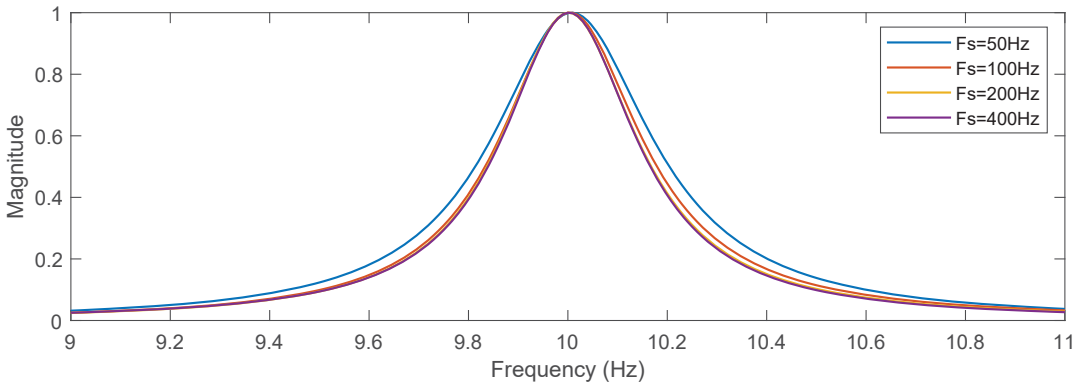

Fig. 3.12 LPC spectra at different sampling frequencies for a signal with a fixed duration.

tude of the non-dominant poles decreases. The reason is that when the signal duration is fixed, the increase in the sampling frequency will increase the number of samples of the signal. Increasing the number of samples can more significantly identify dominant and non-dominant poles. Fig. 3.10 shows the LPC spectra for the different sampling frequencies at the signals that have the same duration. These LPC spectra are still normalised to the range of 0 to 1 and the frequency axis only shows the frequency domain from 9 to

11 Hz to better observe the LPC spectra. It can be seen that these positions of the LPC spectral peak have little difference under the different sampling frequencies. The reason is that the signal duration at different sampling frequencies is fixed and the time resolution is constant, the LPC spectra are still limited by the Heisenberg-Gabor uncertainty principle, so different sampling frequencies have little effect on the width of the spectral peak.

The effect of different sampling frequencies on the LPC method is analysed here. It can be seen that under a fixed number of signal samples, different sampling frequencies have little effect on distinguishing the dominant and non-dominant poles. However, the increase in sampling frequency will shorten the duration of the signal, thus resulting in a wider spectral peak. At a fixed signal duration, the increase of the signal sampling frequency can effectively reduce the amplitude of the non-dominant pole which will significantly distinguish the dominant pole from the non-dominant poles. In summary, factors that affect the LPC method come from the signal duration and the number of signal samples. Specifically, longer signal durations can result in narrower spectral peaks. Furthermore, a larger number of signal samples can better identify the dominant pole.

3.1.5 Signal Noise Analysis of LPC

The influence of different levels of noise on the LPC method is analysed here. Additive White Gaussian Noise (AWGN) is used to corrupt the pure sinusoidal signal and the power spectral density of AWGN is uniform across all frequencies. The Signal-to-Noise Ratio (SNR) is expressed in dB.

$$SNR(dB) = 10\log_{10}(\frac{\tilde{P}_{signal}}{\tilde{P}_{noise}}) \tag{3.3}$$

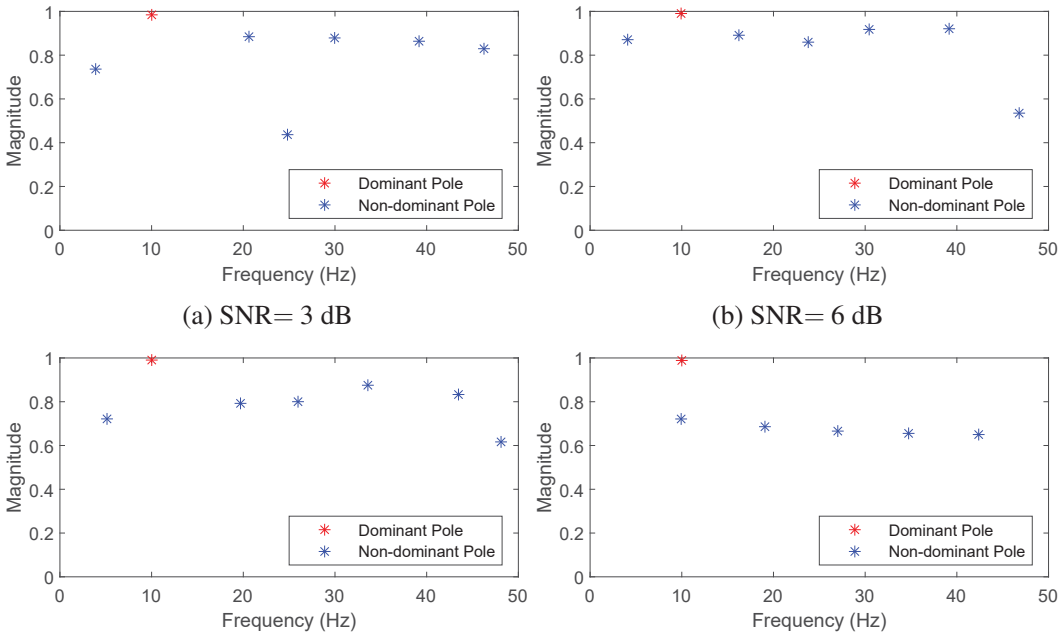

(a) SNR= 3 dB (b) SNR= 6 dB

(c) SNR= 9 dB (d) No Noise

Fig. 3.13 LPC poles of signal with different noise levels.

where $\tilde{P}$ is the average power. The noise of this experiment has four cases: 3 dB, 6 dB, 9 dB and no noise. The signal duration here is 1 s and the other parameters of this experiment are the same as the above experiment. Fig. 3.13 shows the LPC poles of the signal with different noise levels in the frequency domain. It can be seen that the dominant pole still has the highest magnitude and it can correspond to a dominant signal frequency component of 10 Hz. In addition, the noise causes a change in the positions of the non-dominant poles and the magnitudes of non-dominant poles are increased when the signal is corrupted by noise. Noise is not conducive to distinguishing between dominant pole and non-dominant poles from an analysis of their magnitudes.

The LPC spectra under different noise levels are shown in Fig. 3.14 and they are normalised to the range of 0 to 1. The shapes of these LPC spectra are similar, the LPC spectral peak of the noise-free signal can correspond to a signal frequency component of 10 Hz.

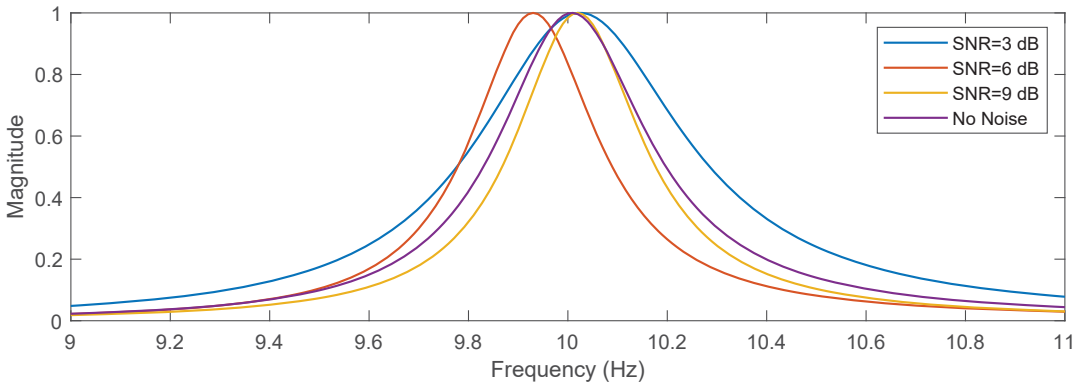

Fig. 3.14 LPC spectra of signal under different noise levels.

However, the spectral peaks of the signal corrupted by noise are all slightly shifted around 10 Hz. The reason is that the dominant pole has a dominant effect on the position of the LPC spectral peak, but the non-dominant pole also affects the position of the LPC spectral peak, especially when the non-dominant pole is closer to the dominant pole. The effect of the dominant pole and non-dominant pole on the LPC spectra will be analysed in detail in the section 3.2. Therefore, the spectral peaks of the corresponding dominant signal component under different noise levels have different deviations and these deviations will not increase with the increase of the noise level. Specifically, the maximum deviation of the spectral peak in the Fig. 3.14 is in the case of a SNR=6 dB, not in the case of a SNR=3 dB where the noise level is higher.

In summary, the signal corruption by noise will be reflected in the changes in the position of the LPC poles and the position of the LPC poles is sensitive to noise. In addition, the noise can cause the magnitudes of the non-dominant pole to increase. For the LPC spectra analysis, the ability of the LPC spectral peak to correspond to the signal frequency is still related to the position of the dominant pole and non-dominant poles. Therefore, the LPC method is sensitive to noise and has poor tolerance to a noise environment.

3.1.6 Window Function Analysis

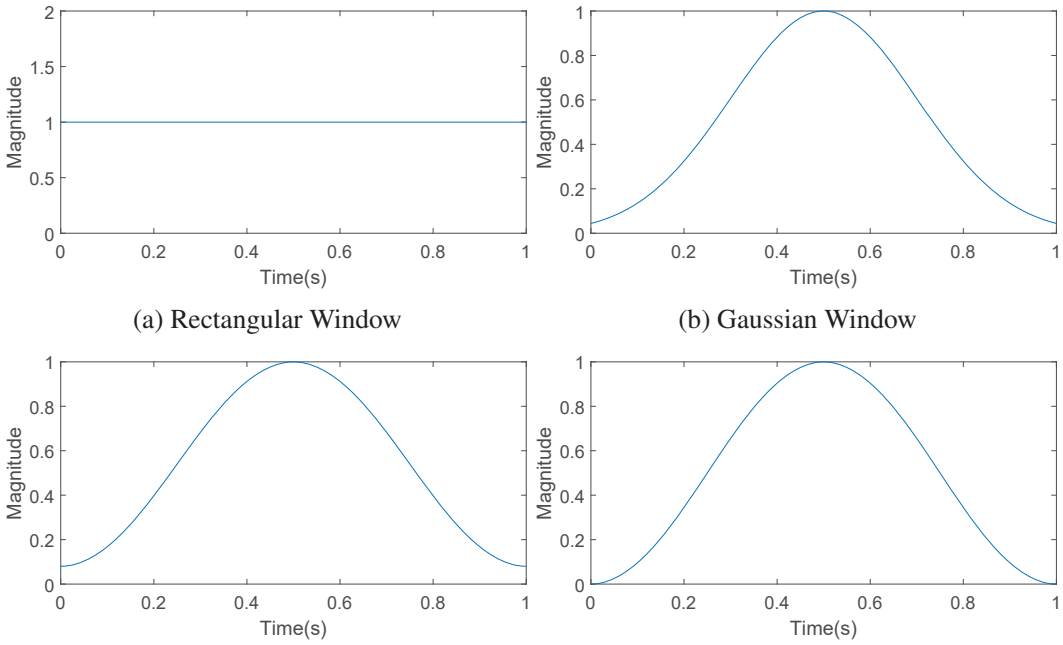

(a) Rectangular Window (b) Gaussian Window

(c) Hamming Window (d) Hann Window

Fig. 3.15 Four window functions.

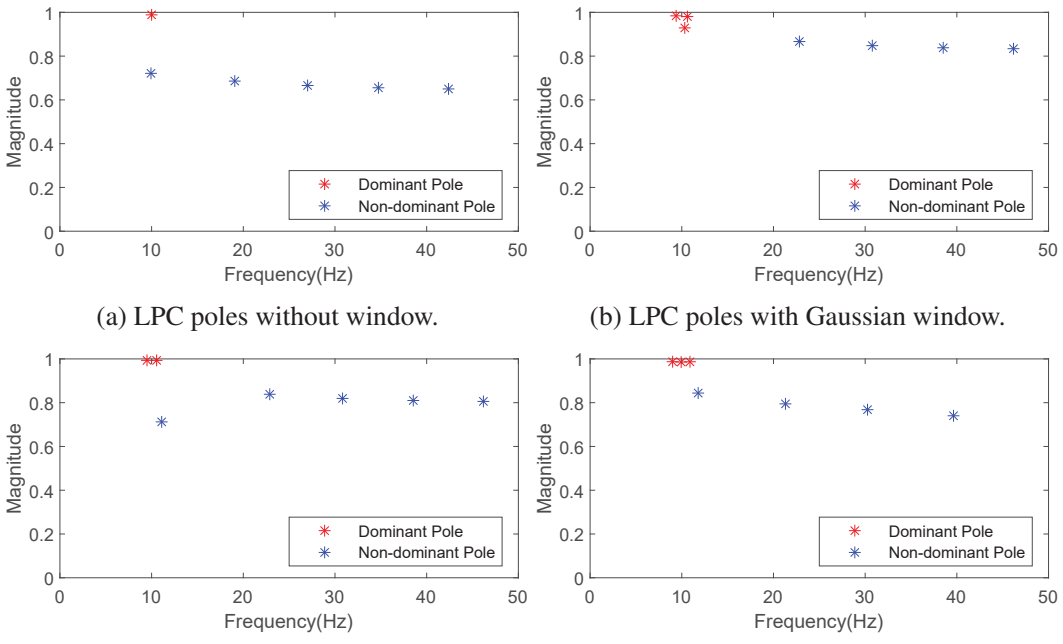

(a) LPC poles without window. (b) LPC poles with Gaussian window.

(c) LPC poles with Hamming window. (d) LPC poles with Hann window.

Fig. 3.16 LPC poles of no noise signal using different window functions.

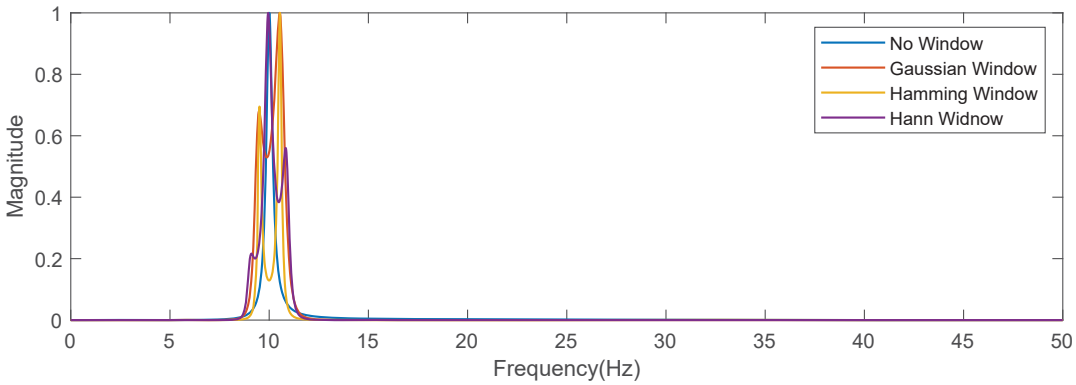

Fig. 3.17 LPC spectra of no noise signals using different window functions.

A window function that tapers the signal segment to zero is required for the autocorrelation method to solve for the LPC coefficients. In this section, three typical window functions for the LPC method are analysed: Gaussian window, Hamming window and Hann window. A rectangular window is used as a benchmark case which means that it is a non-windowed signal. These window functions are shown in Fig. 3.15. It should be noted that the term window functions refers to the last three window functions in Fig. 3.15 (i.e. Gaussian window, Hamming window and Hann window) except the rectangular window in the following description. In this section, there are two conditions to demonstrate the effect of window functions: noise-free environment and noise environment. The first experimental signal is a pure $f = 10$ Hz sinusoidal signal without noise. The sampling frequency $f_s = 100$ Hz, the filter order is $P = 15$ and the duration of the signal is $t = 1$ s. Fig. 3.16 shows the LPC poles in the frequency domain. In this noise-free environment, the number of the dominant poles under the different window functions is increased compared to the case of a non-windowed signal. The magnitude of the dominant poles is close to 1. However, the magnitude of the non-dominant poles is increased when the signal is windowed by the window functions. In addition, Fig. 3.17 demon-

strates the LPC spectra in the frequency domain. These LPC spectra are normalised to the range of 0 to 1. The LPC spectra that use window functions have more than one peak around 10 Hz. Only the LPC spectra without the window functions can produce one peak that correctly corresponds to the signal frequency component of 10 Hz. The reason is that the number of the dominant poles is increased when the signal is windowed. Furthermore, the dominant poles cause the LPC spectra to generate more than one peak around the position of the signal frequency component at around 10 Hz.

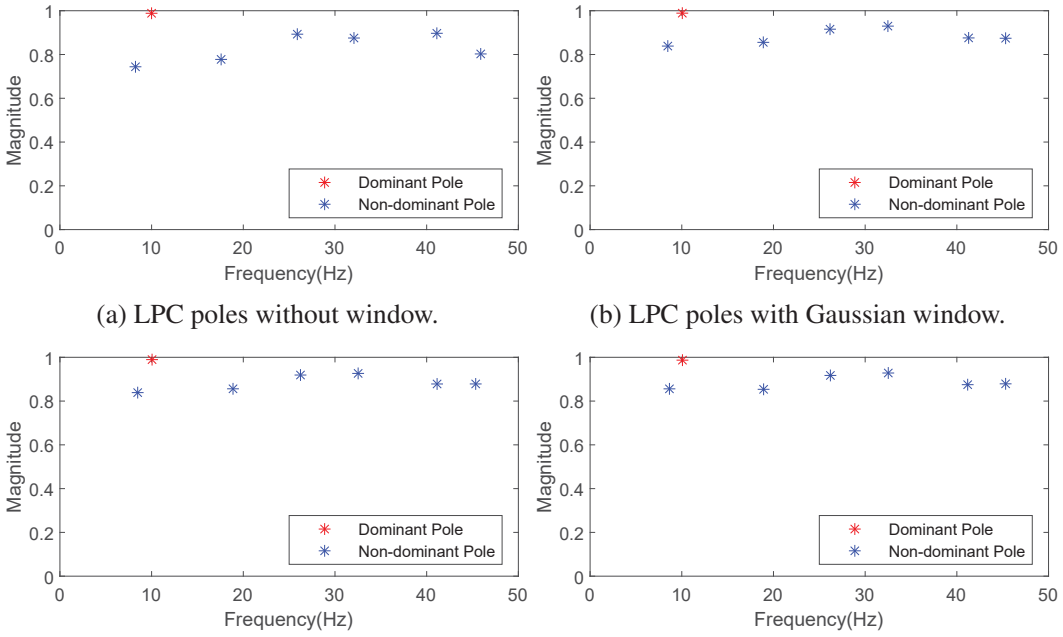

(a) LPC poles without window.

(b) LPC poles with Gaussian window.

(c) LPC poles with Hamming window.

(d) LPC poles with Hann window.

Fig. 3.18 LPC poles of noise signal using different window functions.

The above experiment is conducted in a noise-free environment. Here, a noise environment is also considered for the analysis of the effect of the window functions. The SNR under AWGN is 10 dB and the other parameters are the same as in the above experiment. Fig. 3.18 shows the LPC poles under this noisy environment in the frequency domain. It can be seen that the window functions have little effect on the position of LPC poles. The

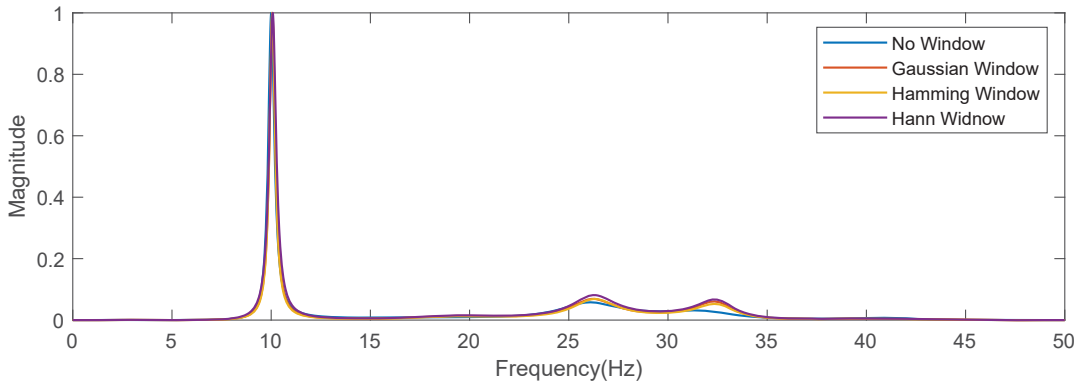

Fig. 3.19 LPC spectra of noise signals using different window functions.

magnitudes of the non-dominant pole are slightly higher under different window functions than that of the non-window function. Fig. 3.19 shows the LPC spectra in this noise environment and they are normalised to the range of 0 to 1. The LPC spectra with different window functions have a single peak at 10 Hz with little difference between the spectral peaks.

This section demonstrates the effect of window functions on the LPC pole and LPC spectra. For the noise-free environment, the number of dominant poles is increased when the signal is windowed and the dominant poles can represent the dominant frequency components. However, the increase in the number of the dominant poles will cause the LPC spectra to have more than one peak which is not conducive to identifying the signal frequency component. Furthermore, the magnitude of non-dominant poles is increased when the signal is windowed which makes the magnitude difference between the dominant pole and non-dominant pole less obvious. For a noisy environment, the window functions have little effect on the position of LPC poles and the LPC spectra. Considering that the scenario used in this thesis is EEG signal processing which is characterised by the

presence of high noise, therefore, the window function is not used for the LPC method in the following analysis.

3.1.7 Conclusions

In this section, the concept of the definition of the dominant pole and non-dominant poles were introduced. The magnitude of the LPC poles can be used to classify them into dominant poles and non-dominant poles. Furthermore, the experimental parameters (i.e. filter order, signal duration, noise level and the window functions) of the LPC method are analysed. The effects of these parameters on the LPC poles and LPC spectra are summarised as follows:

- The analysis of filter order further verified that the LPC method is sensitive to it. The number of LPC poles depends on the filter order. The increase in filter order is not conducive to distinguishing between dominant poles and non-dominant poles. Furthermore, the dominant pole is used in conjunction with the non-dominant poles to determine the final position of the spectral peak.

- The analysis of the signal duration shows that the LPC method is still subject to the Heisenberg-Gabor uncertainty principle. Increasing the signal duration can better distinguish between the dominant pole and non-dominant pole. In addition, the increase in signal duration can provide richer spectral information and produce narrower LPC spectral peaks.

- The analysis of the sampling frequency shows that the signal duration and the number of signal samples can affect the LPC method. Specifically, longer signal

durations result in narrower spectral peaks. Furthermore, a larger number of signal samples can better identify the dominant pole.

- The LPC poles are sensitive to noise. A noisy environment is not conducive to distinguishing between the dominant pole and the non-dominant pole. The noise will give a wider spectral peak than a noise-free environment.

- The analysis of different window functions shows that the impact of window functions on the LPC method is limited. In a noise-free environment, the window function is not conducive to the peak selection of LPC spectra and it is not conducive to distinguishing between the dominant pole and non-dominant poles. In a noisy environment, the window functions have little effect on the position of LPC poles and LPC spectral peak.

In the next section, the effects of dominant and non-dominant poles on spectral peaks are analysed. Furthermore, the associated poles from non-dominant poles will be defined.

3.2 Analysis of the Impact of the Poles on the Spectra

The previous section presented the analysis of the effects of different parameters on the LPC poles and the LPC spectra. It can be observed that the dominant pole and non-dominant poles serve to define the bandwidth of the signal component in the LPC spectra. The magnitude of the poles can be used as an indicator of the size of the spectral peak. The magnitude of the dominant pole is higher than that of the non-dominant pole. Thus, the dominant pole has a major effect on the LPC spectra. However, the non-dominant pole still can affect the final position of the peak in the LPC spectra and the bandwidth of

the LPC spectra. In this section, the effect of the dominant pole and non-dominant poles on the spectra through a simulation experiment will be introduced. Furthermore, a new definition of the associated pole will be proposed which together with the dominant pole can determine the final location of the spectral peak.

Table 3.1 Mathematical notation of the dominant pole and non-dominant pole.

Poles Categories	**Dominant Pole**	**Non-dominant Pole**
Pole	$\tilde{p}$	$\bar{p}_j$
Magnitude	$\tilde{m}$	$\bar{m}_j$
Frequency	$\tilde{f}$	$\bar{f}_j$

The simulation experiment will generate a series of artificial poles and these poles still have two categories: dominant poles and non-dominant poles. The effect of the poles on the spectra will be investigated by fixing the dominant pole and changing the non-dominant poles (i.e. the magnitude and frequency of the LPC pole). Thus, there is one dominant pole $\tilde{p}$ and a series of the non-dominant poles $\{\bar{p}_1, \bar{p}_2, \cdots\}$ in the artificial simulation experiments. The dominant pole $\tilde{p}$ will form a series of second-order transform functions $\tilde{H}_j$ with each individual non-dominant pole $\bar{p}_j$ where j is the index of the non-dominant pole. The $\tilde{H}_j$ is given by

$$\tilde{H}_j(z) = \frac{1}{(1-\hat{p}z^{-1})} \times \frac{1}{(1-\bar{p}_j z^{-1})} \tag{3.4}$$

It should be noted that all the poles here only consider the poles with non-negative imaginary parts. Furthermore, the details of the mathematical representation of the dominant pole and non-dominant pole are given in Table 3.1. The following experiments are all second-order transfer functions that have one dominant pole and one non-dominant pole. These second-order functions will only produce one spectra peak which is expressed as

$\acute{f}$. In order to measure the effectiveness of the poles on the spectra, the frequency error between the peak of the single-pole model of the dominant pole $\tilde{f}$ and the peak of the second-order model spectra $\acute{f}$ is measured using the Relative Frequency Error Percentage (RFEP):

$$RFEP = \frac{|\acute{f} - \tilde{f}|}{\tilde{f}} \times 100\% \tag{3.5}$$

The RFEP value is used to analyse the effect of the relationship between the dominant pole and non-dominant pole on the second-order spectra. In the following analysis, an artificial simulation experiment is designed. The effect of the magnitude of the artificial poles on the second-order spectra and the effect of the frequency separation between the artificial dominant pole and non-dominant pole on the second-order spectra is demonstrated.

3.2.1 Analysis of the Pole Magnitude on the Spectra

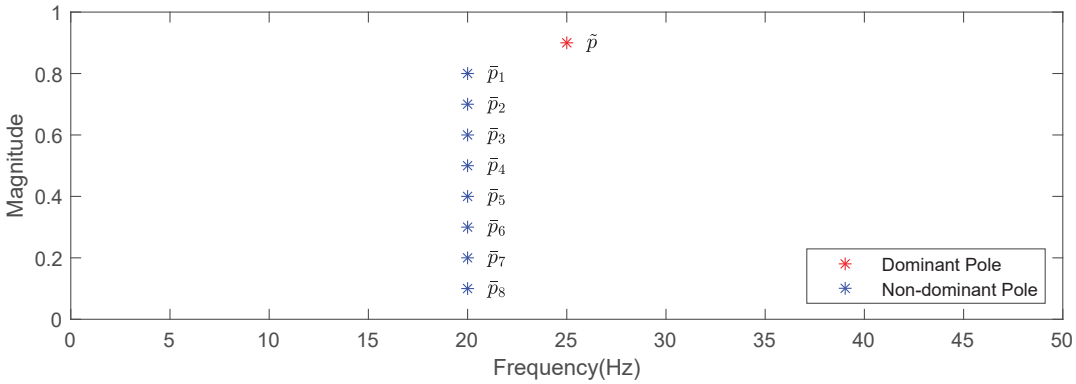

Fig. 3.20 The artificial poles where the non-dominant poles have different magnitudes.

In this part, the effect of the magnitude of the dominant pole and non-dominant pole on the spectra is analysed in a simulation experiment. The sampling frequency of the experimental signal is chosen as 100 Hz and the signal duration is 1 s. The dominant pole is fixed, the magnitude of the dominant pole is 0.9 and its frequency is 25 Hz. For the non-

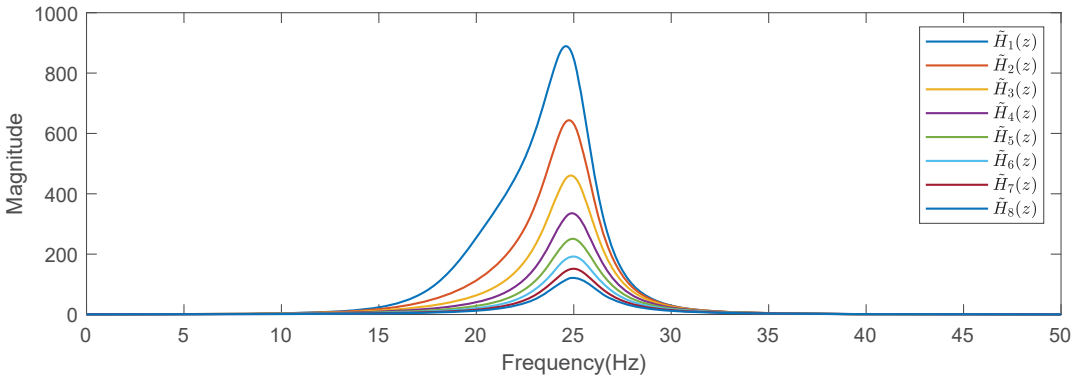

Fig. 3.21 The second-pole model spectra with the different magnitude non-dominant poles.

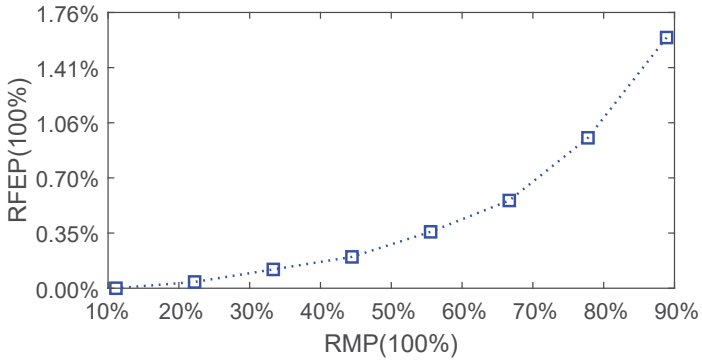

Fig. 3.22 The RFEP values under the different magnitude non-dominant poles.

dominant poles, their frequencies are all 20 Hz and their magnitudes change from 0.8 to 0.1 and the step is -0.1. Fig. 3.20 shows the artificial dominant pole $\tilde{p}$ and non-dominant poles $\{\bar{p}_1, \bar{p}_2, \cdots, \bar{p}_8\}$. The dominant pole will form a series of second-order transform functions with every single non-dominant pole. These second-order transform functions are $\{\tilde{H}_1(z), \tilde{H}_2(z), \cdots, \tilde{H}_8(z)\}$ which are shown in Fig. 3.21. It can be seen that the spectra of $\tilde{H}_1(z)$ which is composed of a non-dominant pole $\bar{p}_1$ and dominant pole $\tilde{p}$ have the highest magnitude than others. The reason is that the $\bar{p}_1$ has the highest magnitude among all non-dominant poles. Furthermore, the RFEP value is analysed in Fig. 3.22. The y-axis is the RFEP value and the x-axis represents the ratio of the magnitude of each non-dominant pole $\bar{m}_j$ to the magnitude of the dominant pole $\tilde{m}$ which was called Relative

Magnitude Percentage (RMP) and it is expressed as

$$\mathrm{RMP} = \frac{\bar{m}_j}{\tilde{m}} \times 100\% \tag{3.6}$$

As can be seen, the RFEP value will increase as the magnitude of the non-dominant pole increases. In other words, as the magnitude of the non-dominant pole increases, the deviation between the spectral peak and the dominant pole will also increase. On the other hand, the magnitude is an important indicator that distinguishes the dominant pole and the non-dominant pole. The dominant pole determines the approximate position of the spectral peak, while the non-dominant pole can further adjust the position and bandwidth of the spectral peak.

3.2.2 Analysis of the Pole Frequency Separation on the Spectra

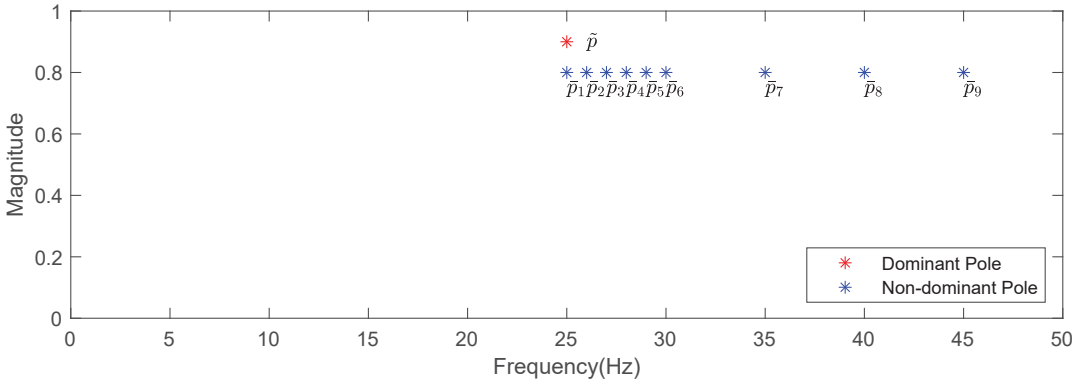

Fig. 3.23 The artificial poles where the non-dominant poles have different frequency separations from the dominant pole.

In this part, the effect of the frequency separation between the dominant pole and non-dominant pole on the spectra is analysed. This experiment is still a simulation experiment. The signal is 100 Hz sampling rate and 1 s signal duration. The artificial dominant pole

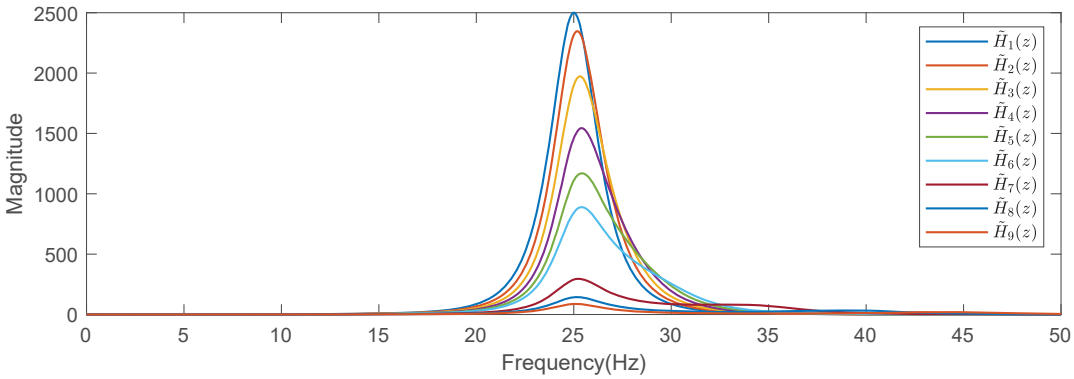

Fig. 3.24 The second-order model spectra where the non-dominant poles have different frequency separation from the dominant pole.

is 25 Hz and its magnitude is 0.9. The magnitudes of the non-dominant poles all are 0.8. In order to be able to see more details about the impact of non-dominant poles near the dominant pole on the spectra, the step size of the non-dominant poles from 25 Hz to 30 Hz is 1 Hz and the step size from 30 Hz to 45 Hz is 5 Hz. As shown in Fig. 3.23, the dominant pole is represented as $\tilde{p}$ and non-dominant poles are $\{\bar{p}_1, \bar{p}_2, \cdots, \bar{p}_9\}$. Fig. 3.24 shows the second-order transform functions $\{\tilde{H}_1(z), \tilde{H}_2(z), \cdots, \tilde{H}_9(z)\}$. Each second-order transform function is composed of a dominant pole and a non-dominant pole. It can be seen that the spectra $\tilde{H}_1(z)$ has the highest magnitude which is composed of the dominant pole $\tilde{p}$ and the non-dominant pole $\bar{p}_1$. The two poles are in the same frequency position 25 Hz and their separation is 0. As the separation between the dominant pole and non-dominant pole increases, the magnitude of their corresponding spectra will decrease. In order to analyse the shift of the spectral peak corresponding to each second-order transform function under different non-dominant poles, the RFEP value is still used. Here a new metric Relative Frequency Distance Percentage (RFDP) is proposed to represent the ratio of the frequency separation between the dominant pole and non-dominant pole

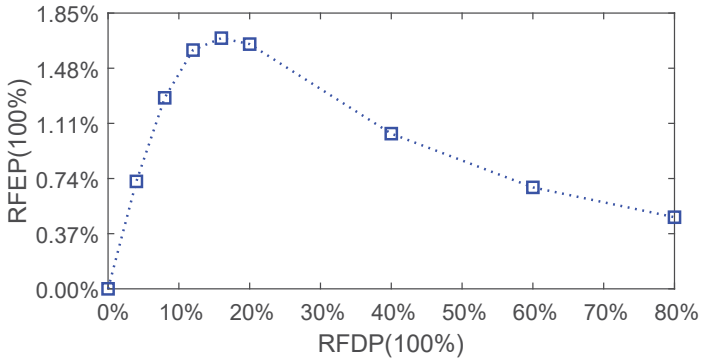

Fig. 3.25 The RFEP values under the different frequency separation between the dominant pole and non-dominant pole.

relative to the frequency of the dominant pole $\hat{f}$ which is defined as

$$\text{RFDP} = \frac{\bar{f}_j - \tilde{f}}{\tilde{f}} \times 100\% \tag{3.7}$$

Fig. 3.25 shows the results of REFP value under the different frequency distances between the dominant pole and non-dominant pole. It can be seen that the RFEP value first increases rapidly and then decreases slowly with the increase of RFDP. The highest RFEP value is a critical point. The RFEP before the critical point increases as the RFDP increase. In other words, the frequency separation between the spectral peak and the dominant pole increase as the frequency separation between the non-dominant pole and the dominant pole increases. However, when RFDP exceeds the critical point, the RFEP decreases as the RFDP increases. In other words, the frequency separation between the spectral peak and the dominant pole gradually decreases as the frequency separation between the non-dominant pole and the dominant pole increases. However, this case is only applicable when the magnitude of the dominant pole is 0.9 and the magnitude of the non-dominant pole is 0.8. The location of the critical point will change with the magnitude of the domi-

nant pole and non-dominant pole change. Therefore, the effect of artificial non-dominant poles of different magnitudes on spectral peaks will be analysed in the next part.

3.2.3 Analysis of the Poles Magnitude and Separation on the Spectra

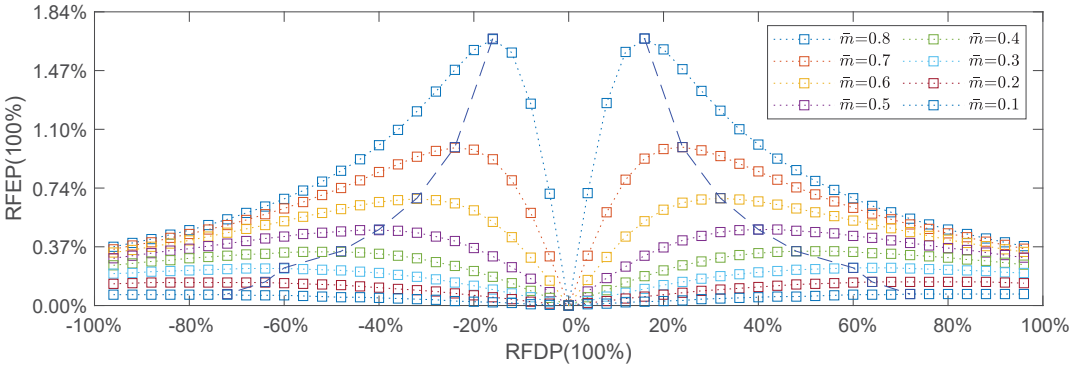

Fig. 3.26 The second-order model spectra where the non-dominant poles have different frequency distances from the dominant pole.

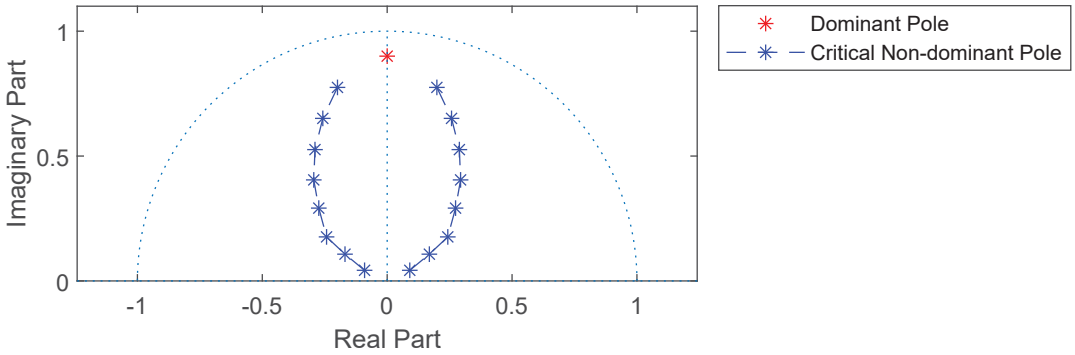

Fig. 3.27 The second-order model spectra where the non-dominant poles have different frequency distances from the dominant pole.

The artificial dominant pole frequency for Fig. 3.26 still is 25 Hz and its magnitude is 0.9. The artificial non-dominant poles are divided into 8 groups according to their magnitude and the magnitude $\bar{m}$ of each group is from 0.1 to 0.8 and the step size is 0.1. Furthermore, the frequency of each group of non-dominant poles are varied from 1 Hz to 49 Hz and the step size is 1 Hz. In Fig. 3.26, the square point lines of different colors represent

the REFP values generated by the second-order model spectra with different magnitudes of non-dominant poles. The blue dashed line indicates the change of the critical point (i.e. the highest RFEP value for each square point line) under different non-dominant pole magnitudes and the non-dominant poles corresponding to these critical points are shown in Fig. 3.27. It can be seen that these critical points in Fig. 3.26 are symmetrical about the position where RFDP is 0% and their corresponding non-dominant poles are also symmetrical about the position of the dominant pole in Fig. 3.26. Furthermore, the absolute value of RFDP of the critical points will increase as the magnitude of the non-dominant pole decreases in Fig. 3.26. Although these poles are artificially simulated, some rules about the effect of the dominant pole and non-dominant pole on the second-order model spectra can still be summarised:

- When the magnitude of the dominant pole and non-dominant pole is fixed, RFEP first increases and then decreases with the increase of the absolute value of RFDP and here has a critical point.

- The frequency separation between the non-dominant pole and the dominant pole and their magnitude together determine the value of RFEP.

Although the simulation scenario here (the amplitude of the dominant pole is 0.9) does not cover all scenarios (i.e. the dominant and non-dominant poles at different amplitudes). It still can be observed that the position of the spectral peak is more sensitive to the non-dominant poles around its corresponding dominant pole. Therefore, the non-dominant poles around the dominant poles in the LPC method are defined as associated poles. The associated pole and dominant pole together determine the final position of a spectral peak.

3.2.4 Conclusions

In this section, a series of second-order transform functions composed of artificial dominant poles and non-dominant poles were analysed. As the magnitude of non-dominant increases, the RFEP value will increase (i.e. the deviation between the spectral peak and the dominant pole will increase). For the frequency separation between the dominant pole and non-dominant pole analysis, there is a critical point here (i.e. the highest RFEP value). The position of the spectral peak is more sensitive to the non-dominant poles around its corresponding dominant pole. Therefore, a new term was proposed called associated poles. The associated poles come from the non-dominant poles close to the dominant poles. The dominant pole and its corresponding associated poles can determine the final position of the spectral peak. In the next section, the details of the proposed LPCPP method will be introduced. The new method will further process the LPC poles to produce several reduced-order transform functions to estimate the dominant frequencies. Each reduced-order transform function consists of one dominant pole and a series of associated poles.

3.3 LPC Pole Processing Method

In this section, the details of the LPCPP method will be presented. The LPCPP method is proposed to further process LPC poles to form a series of reduced-order transform functions. Specifically, each reduced-order transform function consists of one dominant pole and a series of associated poles. Furthermore, the reduced-order transform function has a lower order and it has fewer local maxima which makes it easier to find the peak as

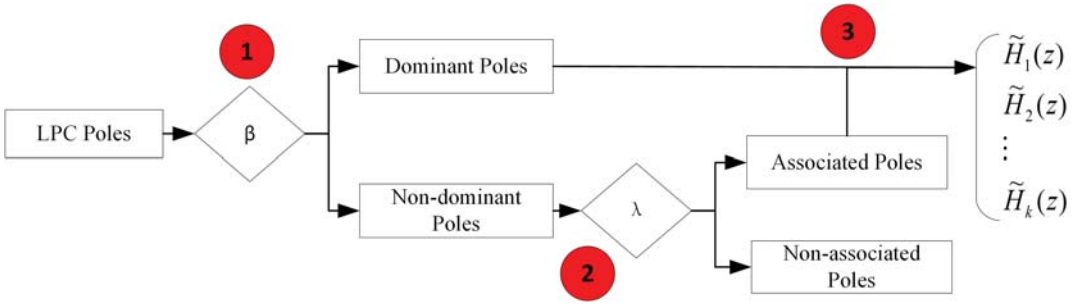

Fig. 3.28 The diagram of LPC poles processing of the LPCPP method.

the dominant frequency estimation. The method can be summarised as comprising three steps:

1. Categorise LPC poles into dominant poles and non-dominant poles.

2. Identify the associated poles of each dominant pole from non-dominant poles.

3. The dominant poles and their corresponding associated non-dominant pole(s) are used to form a series of reduced-order transform functions.

The diagram of LPC poles processing of the LPCPP method is shown in Fig. 3.28. However, there are two questions that need to be considered: the first is how to identify dominant and non-dominant poles and the second is how to classify non-dominant poles as associated poles corresponding to the dominant pole? Therefore, the LPCPP method will propose corresponding solutions and the details of each step will be described in the rest of this section.

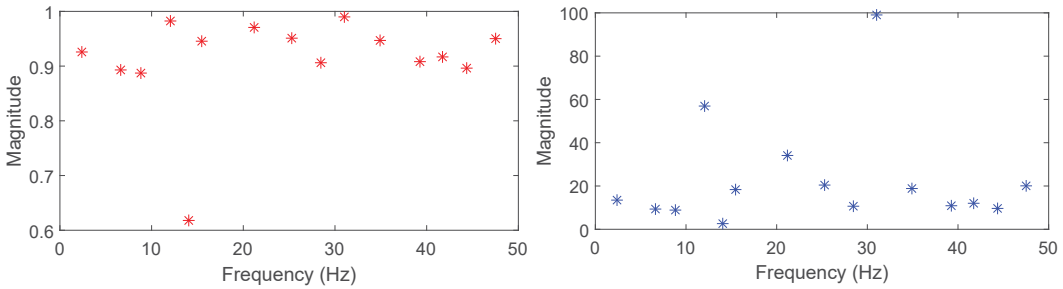

(a) The original LPC poles. (b) LPC poles with enhanced magnitude.

Fig. 3.29 The processing of LPC poles by the enhanced function.

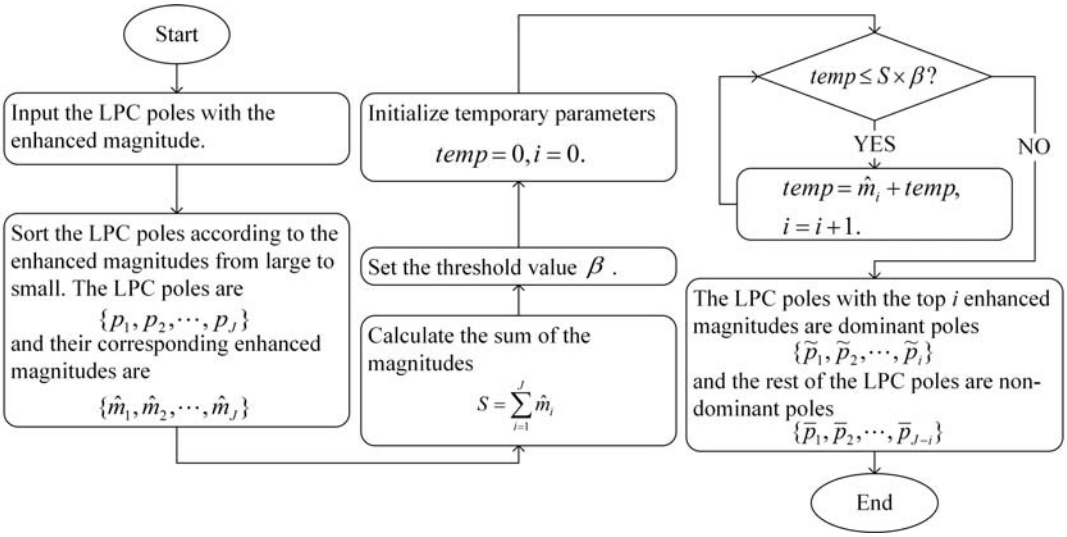

Fig. 3.30 Flow chart of the method used to identify the dominant poles and non-dominant poles.

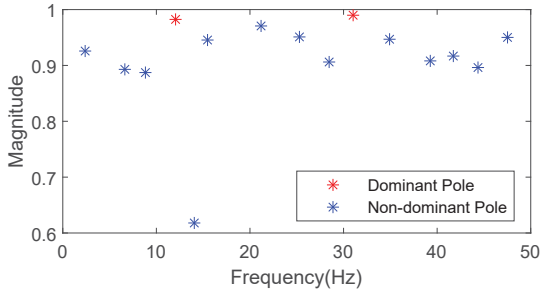

Fig. 3.31 Identifying dominant poles and non-dominant poles

3.3.1 First step: Categorise LPC poles into the dominant pole and non-dominant poles

The LPC poles are first categorised into dominant poles and non-dominant poles. The LPC poles here still only consider the poles with non-negative imaginary parts $\mathrm{Im}(z_i) > 0$. Since the magnitude of the LPC poles is an important feature to indicate the size of the spectral peak in the classical filter analysis, the magnitude of the LPC poles will be used to distinguish between the dominant pole and non-dominant poles. However, the previous section 3.1 shows that in some cases the difference between the magnitude of the dominant pole and the non-dominant pole is not obvious, such as in a high-noise environment, a short sampling time or the number of the LPC filter order is inappropriate. Therefore, a new discriminating enhancement function $D(m)$ is proposed to increase the difference in magnitude of LPC poles which is given by

$$\hat{m}_i = D(m_i) = \frac{1}{1-m_i} \tag{3.8}$$

where m_i is the magnitude of the i_{th} LPC poles and the $\hat{m}_i$ is the enhanced magnitude results. Fig. 3.29a shows the original LPC poles and Fig. 3.29b shows the LPC poles with enhanced magnitude. The input signal of the demonstration experiment in Fig. 3.29 is composed of two sinusoidal signals with frequencies $f_1 = 12$ Hz, $f_2 = 31$ Hz, the sampling frequency is $f_s = 100$ Hz, the signal duration is 1 s and the signal is corrupted with AWGN where the SNR= 3 dB and the filter order is $P = 30$. Then, the LPC poles with enhanced magnitude are used as the input in Fig. 3.30 to identify dominant and non-dominant poles. It should be noted that the enhanced magnitude of the LPC poles is only

used to identify the dominant pole and non-dominant pole and does not participate in the next process of the algorithm. The parameter β is a threshold value that has a range from 0 to 1.0, the details for choosing β will be discussed in chapter 4. The dominant poles are represented as $\{\tilde{p}_1, \tilde{p}_2, \cdots\}$ and the non-dominant poles are represented as $\{\bar{p}_1, \bar{p}_2, \cdots\}$. An example is shown in Fig. 3.31 and the β in here is 0.5.

3.3.2 Second step: Identify the associated poles of each dominant pole from non-dominant poles

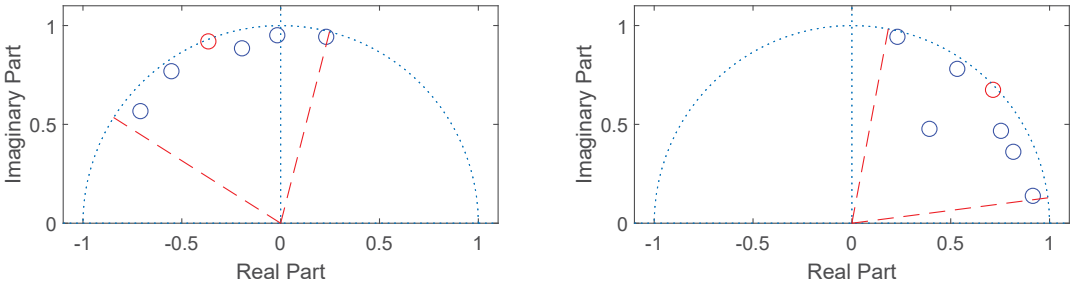

Fig. 3.32 The dominant poles with their corresponding associated poles.

The second step is to identify the associated poles from the non-dominant poles for each dominant pole. The non-dominant poles located around the dominant poles will determine the location of the spectral peaks and these poles are called associated poles. The associated poles are selected from the non-dominant poles and they depend on the distance (frequency separation) between the non-dominant poles and the dominant pole. A frequency threshold parameter λ is defined. When a non-dominant pole whose frequency distance from a dominant pole is less than λ, it is considered an associated pole $\breve{p}_{kj}$, $j = \{1, 2, \cdots, L_k\}$ of the k^{th} dominant pole $\tilde{p}_k$ where L_k is the number of local poles for the k^{th} dominant pole. When the sampling frequency and filter order are fixed, increasing

λ, more non-dominant poles will be considered as associated poles. It should be noted that the different dominant poles may share common associated poles. In Fig. 3.32, the value of λ is 10 Hz where the red lines represent the frequency range 2λ = 20 Hz around each dominant pole where the associated poles of this dominant pole can be identified. The red circles represent the dominant poles and the blue circles represent the associated poles of each dominant pole.

3.3.3 Third step: Form a series of reduced-order transfer functions and output the frequency estimates

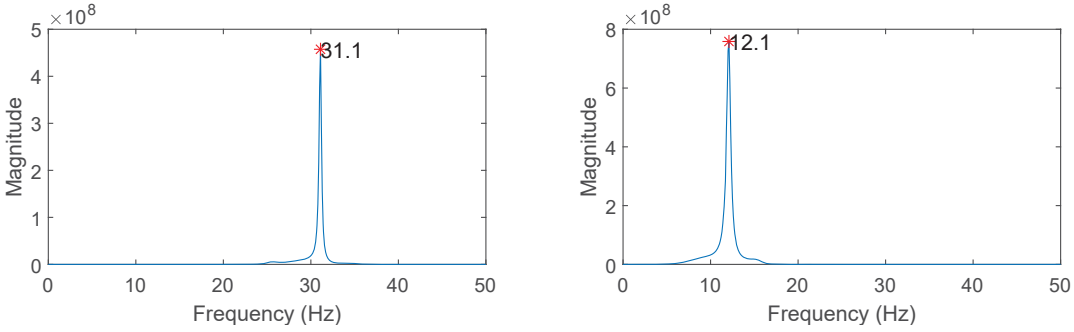

Fig. 3.33 The spectral peak of each reduced-order transform function.

Finally, the dominant poles and their corresponding associated pole(s) are used to form a series of reduced order transfer functions $\tilde{H}_k$ given by

$$\tilde{H}_k(z) = \frac{1}{(1-\tilde{p}_k z^{-1})} \times \frac{1}{\prod_{j=1}^{L_k}(1-\check{p}_{kj} z^{-1})} \tag{3.9}$$

As the new filter transfer function $\tilde{H}_k$ has a lower order and a single dominant pole, it is easier to determine the spectral peak. The frequency response is

$$\tilde{H}_k(e^{j\omega}) = \frac{1}{(1-\tilde{p}_k e^{-j\omega})} \times \frac{1}{\prod_{j=1}^{L_k}(1-\check{p}_{kj}e^{-j\omega})} = \frac{1}{\tilde{A}_k(e^{j\omega})} \tag{3.10}$$

where $\tilde{A}_k(e^{j\omega})$ is an inverse filter for $\tilde{H}_k(e^{j\omega})$. The spectra calculation of the reduced order transfer function in MATLAB by performing a series of the inverse of the FFT (Fast Fourier Transform) spectra and the pseudo-code is as follows:

1: This program calculates the spectra of the reduced order transfer function $\tilde{H}_k$.
2: function $fft\ (x)$ {
3: Perform the Discrete Fourier Transform (DFT) analysis of x using the FFT method.
4: return FFT spectra.
5: end
6: }
7: {
8: In the main function, calculate the spectra of $\tilde{H}_k$.
9: $\tilde{H}_k = 1./fft([1,-\tilde{p}_k]) \times 1./fft([1,-\check{p}_{k1}]) \cdots \times 1./fft([1,-\check{p}_{kj}])$
10: }

For detailed implementation code please see Section A.3. The maximum spectral peak $\tilde{f}_k$ of the $\tilde{H}_k(z)$ is the k^{th} dominant frequency estimation from LPCPP method. The $max()$ function in MATLAB is used here to find the maximum spectral peak. So the frequency

estimation results of the LPCPP method are $\{\tilde{f}_1, \tilde{f}_2, \cdots\}$. The results of this process are shown in Fig. 3.33.

3.3.4 Conclusions

In this section, the details of the LPCPP method were presented. The LPCPP method is based upon further processing of the LPC poles in order to produce a series of reduced-order filter transfer functions to estimate the dominant frequencies. Here two new parameters β and λ were proposed to identify the dominant pole and associated pole respectively. The LPCPP method is a new parameterised time-frequency analysis method and its detailed experimental comparative analysis will be presented in the next chapter.

3.4 Chapter Summary

This chapter introduced the technical details of the new proposed LPCPP method in this thesis. The proposed LPCPP method will further process LPC poles to achieve a spectral estimation of EEG signals. The first section presented the analysis of the LPC poles and the LPC spectra under the different parameters (i.e. filter order, signal duration, sampling frequency, signal noise and window function). The definitions of the dominant pole and non-dominant pole were then proposed. Furthermore, it can be observed that the magnitude of the pole still can be used as an indicator to distinguish between the dominant pole and the non-dominant pole. The second section further analysed the relationship between the dominant pole and non-dominant pole in a series of second-order transform functions. It can be observed that the dominant pole and the non-dominant pole jointly determine the

final position of the second-order spectral peak. Furthermore, the second-order spectral peak is more sensitive to non-dominant poles around the domain pole. The non-dominant poles near the dominant pole are defined as the associated poles and these associated poles can be used to assist the dominant pole to determine the final location of the spectral peak. The third section presented the details of the LPCPP method. Furthermore, the two parameters β and λ of the LPCPP method are used to identify the dominant pole and associated pole respectively. The LPCPP method produces a series of reduced-order filter transfer functions to realise the identification of the dominant frequencies. In the next chapter, a series of experiments will show that LPCPP can overcome the shortcomings of LPC methods including sensitivity to filter order and low tolerance to noise. Furthermore, the LPCPP method can satisfy the spectral processing of EEG signals, enabling the tracking and analysis of the spectral components.

Chapter 4

Simulation Analysis of the LPCPP Method

In this chapter, some representative analytical results of the LPCPP method are presented which show that the LPCPP method can overcome the shortcomings of the LPC method and is well suited for processing poor signal-to-noise ratio, time-varying, intermittent and multi-component signals (i.e. EEG signals). The first section analyses the ability of the LPCPP method to identify the dominant frequency components. A new simulation signal and a series of new metrics for analysing LPCPP methods are proposed. Furthermore, this section will analyse the LPCPP method under the different experimental parameters (i.e. filter order and signal noise). Moreover, the tuning parameters β and λ of the LPCPP will be analysed. The second section presents the ability of the LPCPP method to track the dominant frequency in real-time for a signal whose frequency is varying. The third section presents the analysis of the time-bandwidth product of the LPCPP method. Furthermore,

the bias of the frequency estimation of the LPCPP method is analysed. The last section is the summary of the chapter.

4.1 Dominant Frequency Identification of LPCPP

In this section, the ability of the LPCPP method to identify the dominant frequency will be analysed. A Pseudo-Randomly Varying Frequency (PRVF) signal is used for the experimental analysis and four metrics are used to analyse the performance of the LPCPP method to identify the dominant frequencies. The LPC method is used as a benchmark method. Furthermore, the different experimental parameters for the LPCPP method are analysed. Specifically, the first experiment shows the effect of different filter orders on the LPCPP method. The second experiment analyses the noise tolerance of the LPCPP method. Finally, the selection of the two tuning parameters β and λ is analysed from the perspective of the performance of the LPCPP method.

4.1.1 Experimental Metrics

The LPCPP method is a parameterised time-frequency method that can generate frequency estimates. However, most signals in the real world have unknown frequency components and it is difficult for these signals to determine whether the frequency estimate is correct. Therefore, an artifical signal (i.e. PRVF signal) with known frequency components is proposed here to assess the ability of the LPCPP method to correspond to the dominant frequency components. The PRVF signal is a sinusoidal signal where the frequencies are uniformly distributed in the range 0 to $f_s/2$ and they are evaluated using 10,000 Monte

Carlo trials. One important advantage of the simulation signals is that the frequency components of the signal are known. Furthermore, there is one question that needs to be considered for the frequency estimations of the parameterised time-frequency method: how to determine if these frequency estimations are valid or invalid? In this section, a new parameter ν is used to address this question. When the absolute frequency error e between the real signal frequency and the estimated frequency is less than a frequency threshold value $\nu \times f_s$, the estimated value is considered to be valid and the real signal frequency is considered to be correctly identified. It should be noted that the value of ν is not always fixed, the choice of its value needs to be considered according to its corresponding application scenario. The terms "valid estimate" and "invalid estimate" are used to describe the validity of the LPCPP method estimates. The terms "correctly identified signal frequency" and "incorrectly identified signal frequency" are used to describe whether the frequency of the signal is correctly identified. Moreover, there are four additional questions that need to be considered:

1. How to measure the frequency errors between the estimated frequencies and the real signal frequencies?

2. How many frequency components of the signals are identified?

3. How many frequency estimates from the LPC-based method (i.e. LPCPP method and LPC method) are valid?

4. How many ideal experiments are there in all frequency estimation experiments? (The term "ideal experiment" refers to situations when the LPCPP method can

correctly identify all the frequency components of the signal without producing redundant invalid estimates.)

Table 4.1 The mathematical symbols used in the analysis.

Parameters	Symbol
The total number of all frequency components in simulation signals	N_χ
The number of all estimated frequencies in the LPC-based method	N_ϕ
The number of correctly identified frequencies in simulation signals	N_ψ
The number of valid estimated frequencies	N_φ
The number of ideal experiments	N_τ

Therefore, four experimental metrics are proposed to address the four questions above. Furthermore, there are some mathematical symbols introduced in Table 4.1. The four metrics are as follows:

1. The Average Error Percentage (AEP) which represents the average of the relative errors across all the identified frequencies and their corresponding valid estimates. The relative error at time t is defined as $ADP_i = e_i/f(t)$ and the AEP is expressed as

$$AEP = \frac{\sum_{i=1}^{N_\psi} ADP_i}{N_\chi} \times 100\% \tag{4.1}$$

2. The Identification Frequency Percentage (IFP) which represents the percentage of the number of identified frequencies from all the number of the frequencies in the signal and the diagram is shown in Fig. 4.1(a). The mathematical expression for IFP is

$$IFP = \frac{N_\psi}{N_\chi} \times 100\% \tag{4.2}$$

3. The Valid Estimate Percentage (VEP) which represents the proportion of valid estimates from all the estimates and the diagram is shown in Fig. 4.1(b). The mathe-

matical expression for VEP is

$$VEP = \frac{N_{\varphi}}{N_{\phi}} \times 100\% \tag{4.3}$$

4. The Ideal Experiment Percentage (IEP) which represents the percentage of experiments that have no invalid estimates and is defined as

$$IEP = \frac{N_{\tau}}{N_{\chi}} \times 100\% \tag{4.4}$$

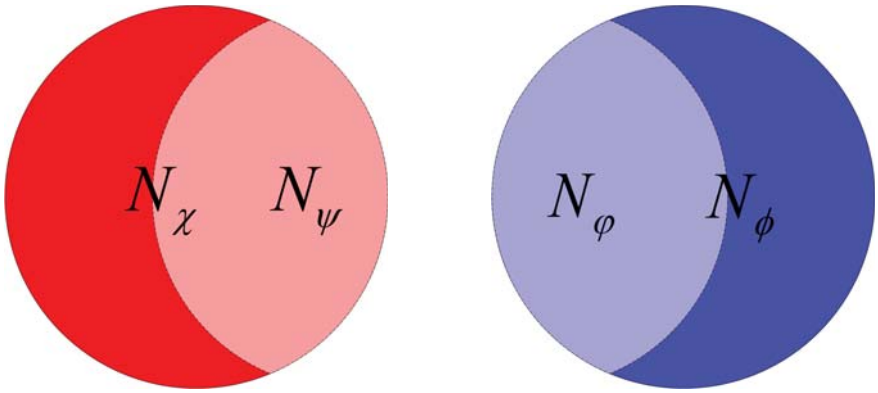

(a) IFP (b) VEP

Fig. 4.1 The diagram of two metrics. IFP is used to indicate how many frequencies in the signal are correctly identified and VEP is used to indicate how many of the LPCPP's frequency estimates are valid.

Specifically, the AEP value is used to measure the accuracy of the valid estimates of the LPCPP method (i.e. the error between all valid estimates and their corresponding real signal frequencies) The IFP value is used to measure the proportion of valid estimates among all LPCPP method estimates. The VEP value is used to measure the proportion of correctly identified frequencies out of the total signal frequencies. The IEP value is used to express the proportion of ideal experiments among all experiments.

4.1.2 Filter Order Analysis of LPCPP

This section has two parts to demonstrate the effect of the filter order of the LPC-based method on frequency identification. One is the single-component PRVF signal and the other is the multiple-component PRVF signal. The sampling frequency of the PRVF signal is $f_s = 100$ Hz and the duration of the PRVF signal for each Monte Carlo trial is $t = 1$ s. Furthermore, the value of ν used in this simulation experiment is 1% which means when the absolute frequency error e is less than 1 Hz, the frequency estimate is considered to be valid and the signal frequency is considered to be correctly identified. In order to simulate a high noise environment, the PRVF signal is corrupted by Additive White Gaussian Noise (AWGN) and the SNR is 3 dB. Finally, the filter order P is increased from 5 to 40 in steps of 5.

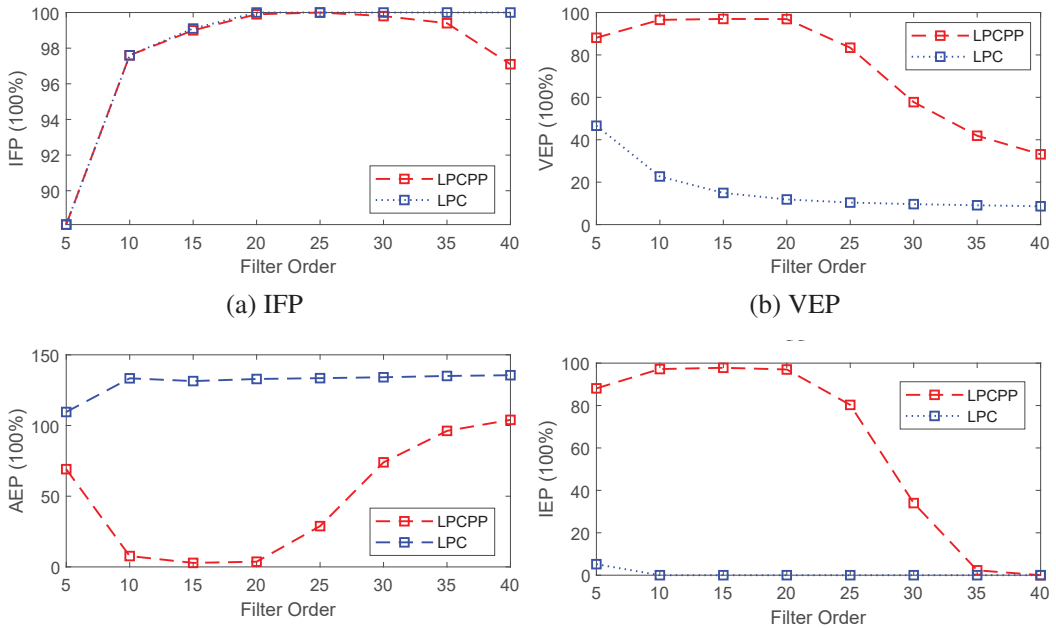

(a) IFP (b) VEP

(c) AEP (d) IEP

Fig. 4.2 Performance analysis for single-component PRVF signals for various filter orders.

The first experiment demonstrates the performance of both LPC-based methods on the single-component PRVF signals under the different filter orders. The parameters of the LPCPP method are $\beta = 0.3$ and $\lambda = 10$ Hz. Fig. 4.2 shows the results of the four metrics. For the different filter orders considered, the IFP values of the LPCPP method and the LPC method are all above 88%. Consequently, both methods can identify the dominant frequency component in most of the experiments. The VEP value of the LPCPP method is much greater than the VEP value of the LPC method for different filter orders. Furthermore, the VEP value of the LPCPP method initially increases and then decreases. The LPCPP method can achieve the highest VEP values when the filter order is $P = 20$ under $\beta = 0.3$. In addition, the VEP value of the LPC method decreases as the filter order increases. This is because as the filter order increases, the LPC method will produce many invalid frequency estimates which leads to a decrease in the value of VEP. For the AEP analysis, the value of the LPCPP method is less than that of the LPC method under different filter orders and the LPCPP method can give more accurate frequency estimates than that of the LPC method. Furthermore, the AEP value of the LPCPP method first decreases and then increases. The AEP value of the LPCPP method achieves the minimal AEP value when the filter order $P = 20$. For the IEP analysis, the value of the LPCPP method is much higher than that of the LPC method and the difference between the IEP of the two methods is up to 98.3% when $P = 20$. The IEP value still increases initially and then decreases and this result corresponds to the result of the IFP value of the LPCPP method. Furthermore, the IEP values of the LPC method are low (i.e. close to 0) for different filter orders. The LPCPP method can provide a higher IEP value than that of the LPC method when the filter order is in a specific interval (here from 5 to 35). The

reason is that the performance of the LPCPP method depends on the choice of the filter order and β. When the filter order is increased, the smaller β is required to filter out the non-dominant poles and to identify the dominant poles. However, the parameter β in this experiment is fixed. This is also the reason why the LPCPP method initially increases and then decreases in the analysis of IFP and VEP values. And it initially decreases and then increases in the analysis of AEP values. In short, the LPCPP method can reliably identify the dominant frequency in single-component PRVF signals.

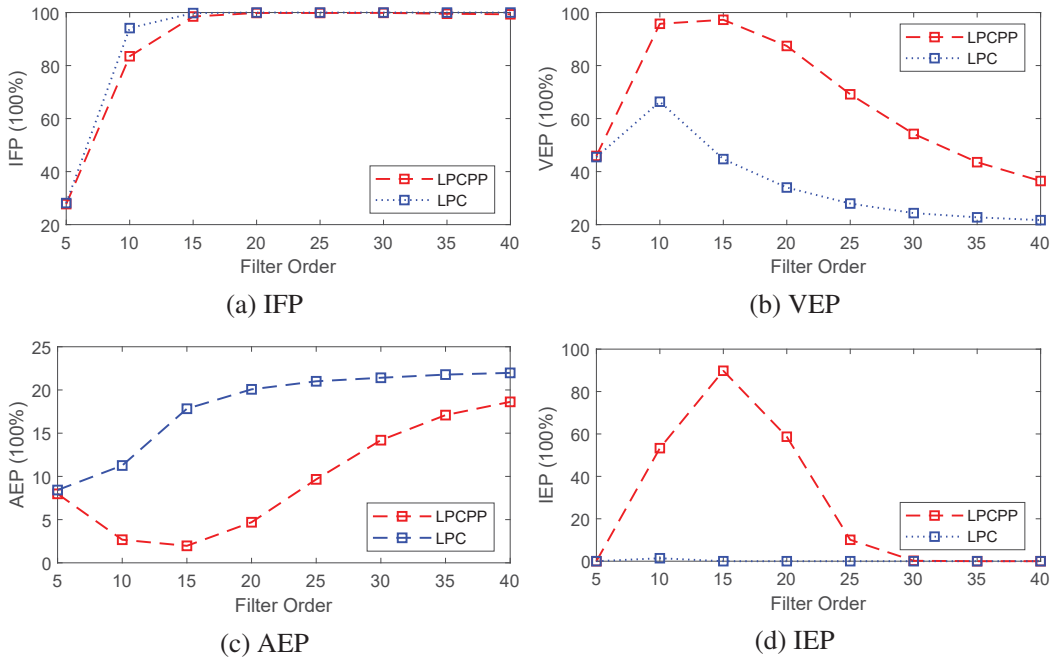

(a) IFP (b) VEP

(c) AEP (d) IEP

Fig. 4.3 Performance for multiple-component PRVF signals for different filter orders.

The second experiment shows the performance of both LPC-based methods on the multiple-component PRVF signal which has three frequency components. The parameters of the LPCPP method are $\beta = 0.7$ and $\lambda = 10$ Hz. Since the PRVF signal here is the multiple-component signal, the β value is increased in order to identify more dominant frequencies. As shown in Fig. 4.3, the IFP value of the LPCPP method is slightly lower than that of

the LPC method when the filter order is less than 15 and the IFP values of the two LPC-based methods show little difference when the filter order is greater than 15. Even the IFP value of the LPCPP method is slightly lower than the LPC method when the filter order is 15, a slight sacrifice in IFP is worthwhile to get a better performance to estimate the frequencies and this feature of the LPCPP method is particularly attractive for scenarios where the number of frequency components in the signal is unknown. Furthermore, the performance of the LPCPP method still needs to consider the choice of the filter order and β. The LPCPP method can provide higher VEP values and lower AEP values than the LPC method at the different filter orders. Furthermore, the LPCPP method can achieve the highest VEP value, lowest AEP value and highest IEP value when the filter order is 15 and β is 0.7. In short, the LPCPP method is still good at identifying the dominant frequency for the multiple-component PRVF signals under the different filter orders.

In this section, the single-component and multiple-component PRVF signals are used to analyse the effect of the filter order on the LPCPP method. For both PRVF signals, the LPCPP method can significantly improve the VEP values and reduce the AEP compared to the LPC method under the different filter orders. In other words, the LPCPP method can provide more valid frequency estimates and can provide more accurate frequency estimates. These are useful for frequency estimation of signals whose frequency components are unknown. Furthermore, the LPCPP method can significantly improve the IEP value compared to the LPC method within a certain filter order interval. The range of this filter order interval depends on the number of frequency components in the signal and the choice of parameters β. In conclusion, the LPCPP method can provide better perfor-

mance to identify the dominant frequencies in the unknown signal compared to the LPC method.

4.1.3 Signal Noise Analysis of LPCPP

This section will analyse the performance of the LPCPP method under different SNRs. It is still divided into two parts for the experimental analysis: single-component PRVF signal analysis and multiple-component PRVF signal analysis. The SNR is expressed in dB from 0 to 18 and is increased in steps of 3 dB. The filter order for the two LPC-based methods is $P = 20$ and all other experimental parameters are the same as those above.

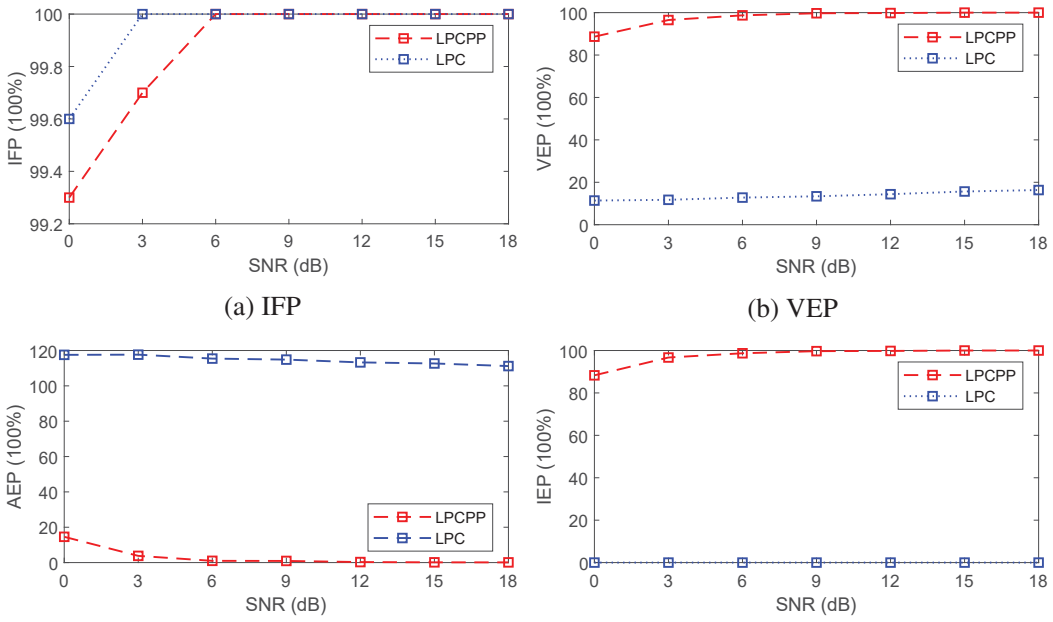

(a) IFP (b) VEP

(c) AEP (d) IEP

Fig. 4.4 Performance analysis for single-component PRVF signals under various SNRs.

The first experiment of this section demonstrates the performance of the LPCPP method and the LPC method on the single-component PRVF signals under the different SNRs. The parameters of the LPCPP method are $\beta = 0.3$ and $\lambda = 10$ Hz. In Fig. 4.4, the

IFP values of both LPC-based methods are greater than 99.3% and both methods can identify all dominant frequencies after SNR is greater than 6 dB. Furthermore, the VEP values of both LPC-based methods increase with the increase of SNR and the VEP value of LPCPP is up to 86.3% higher than that of the LPC method which indicates that the LPCPP method improves the validity of the frequency estimates. The AEP values of both methods decrease with the increase of SNR and the AEP value of the LPCPP method is significantly lower than that of the LPC method. Furthermore, the IEP values of the LPC method are 0 and the LPCPP method can effectively improve the IEP values which are at least higher than 85% at the different SNRs. In other words, the LPCPP method can identify the dominant frequency in the single-component signal under the different SNRs.

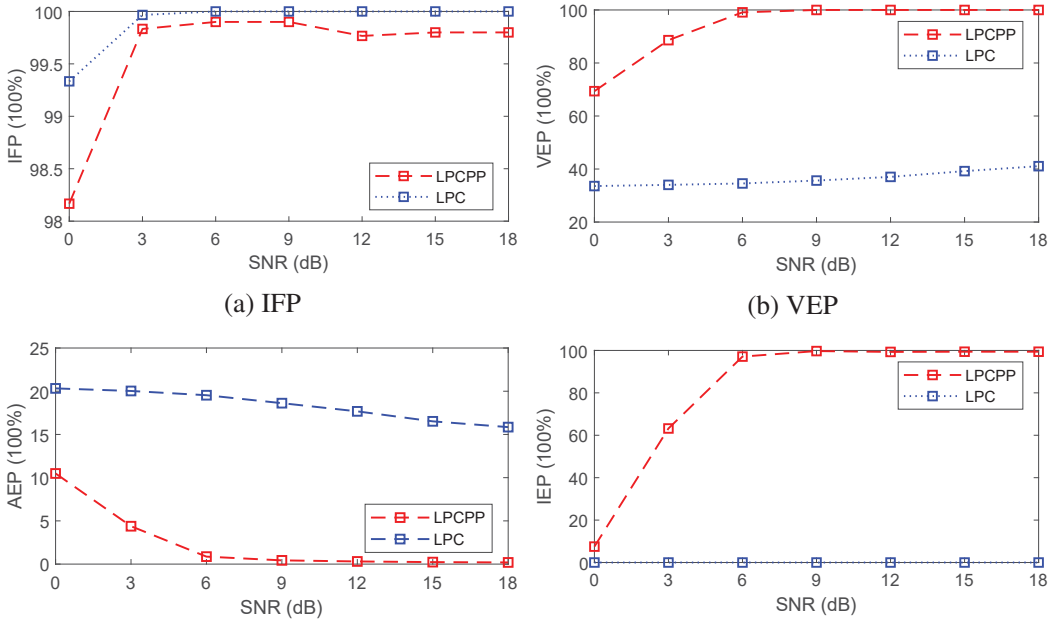

(a) IFP (b) VEP

(c) AEP (d) IEP

Fig. 4.5 Performance analysis for multiple-component PRVF signals under various SNRs.

The second experiment shows the performance of the LPCPP method and the LPC methods on the multiple-component signal for the different SNRs. The parameters of the LPCPP

method are $\beta = 0.7$ and $\lambda = 10$ Hz. Fig. 4.5 shows the four results. As can be seen, the IFP values of the LPCPP method are slightly lower than those of the LPC method under the different SNRs. However, the IFP values of the LPCPP method are still higher than 98.2% which means the LPCPP method still can identify most of the signal frequencies. In addition, the LPCPP method can get much higher VEP values and much lower AEP values than the LPC method under the different SNRs. The LPCPP method can significantly improve the IEP value of the LPC method after the SNR is greater than 3 dB. In short, the LPCPP still can identify most of the dominant signal frequencies and provide more valid and more accurate frequency estimates under this multi-component signal.

This section analysed the performance of both LPC-based methods to identify the dominant frequency under the different SNRs. Although the LPCPP method has a slight loss in IFP value, its significant advantage over the LPC method in terms of the VEP, AEP and IEP values is attractive for frequency estimation of unknown signals. The signal noise is detrimental to the frequency estimation performance of both LPC-based methods and both LPC-based methods have better performance in frequency identification as SNR increases. In conclusion, the LPCPP method exhibits a stronger tolerance to noise than the LPC method and it can provide better performance in the VEP, AEP and IEP at the different SNR scenarios.

4.1.4 LPCPP Parameters Analysis

This section will present the analysis of the parameters of the LPCPP method on frequency identification. The first part is to analyse the impact of the β value which is used to identify the dominant pole(s) for the LPCPP method. In the analysis of the β value, there

is an optimal point (β_{opt}) that can make the IEP achieve the maximum value. This is useful for signals whose spectral information is unknown. Finally, the impact of the λ value is analysed and the λ value is used to identify the associated pole(s) for each dominant pole.

Analysis of the parameter β value

In order to analyse the parameter β, there are two PRVF signals used for analysis: single-component PRVF signal and multi-component PRVF signal. The sampling frequency is $f_s = 100$ Hz and the duration of the signal for each Monte Carlo trial is $t = 1$ s. Furthermore, each PRVF signal is corrupted by 3 dB AWGN and the filter order of both LPC-based methods is 20. The β value is increased from 0.1 to 1 in steps of 0.1. The value of β is not set to 0 because when β is 0 this means that no poles are selected as the dominant poles. Moreover, when the $\beta = 1.0$ all of the poles will be selected as the dominant poles.

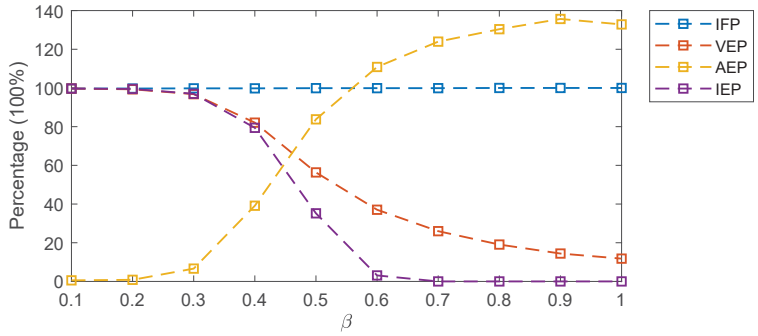

Fig. 4.6 The analysis of β for LPCPP method on the single-component PRVF signals.

The first experiment shows the analysis of the parameter β for the LPCPP method on the single-component signals and the results are shown in Fig. 4.6. As can be seen, the IFP values are always 100% for all values of β. The reason is that the signal here has only one frequency component and there is always a dominant pole corresponding to this frequency component. Furthermore, the values of VEP and IEP decrease as the value of β increases.

The reason is that when the β value increases, the number of dominant poles will also increase which will lead to an increase in the number of invalid estimates in the LPCPP results. Finally, the value of AEP increases with the value of β. When the β increases, the number of invalid estimates increases and the error between the signal frequency and the frequency estimate also increases. Therefore, under the single-component signal, when the value of β is smaller, the LPCPP method can obtain a better performance to identify the dominant frequency (a larger VEP and IEP value and a smaller AEP value) and the change of β value has a negligible effect on IFP.

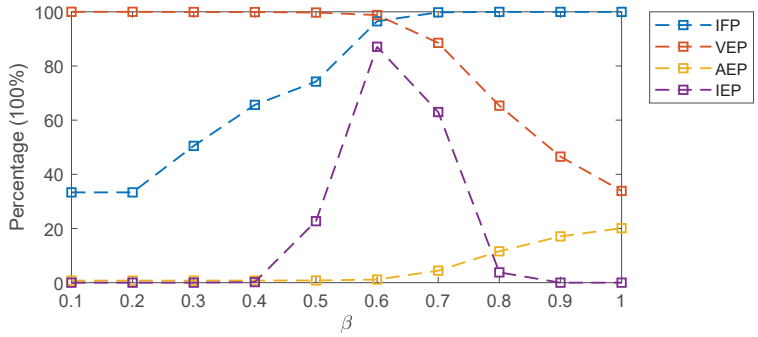

Fig. 4.7 The analysis of β for LPCPP method on the multi-component PRVF signals.

In addition, the multi-component PRVF signals are analysed and it contains three frequency components. Fig. 4.7 shows the results of the analysis of β. It can be seen that there is a trade-off between the IFP and the VEP here. The β value is used to achieve an acceptable trade-off between the two metrics. Furthermore, the AEP value increases as the value of β increases. The IEP value has a maximum at the intersection of the IFP and VEP curves when β is 0.6. The β value corresponding to the intersection point of the IFP and VEP curves is optimal for LPCPP in order to produce the maximum number of ideal experiments with all-valid estimates (i.e. a max IEP value). The β value with the highest IEP value is called the β_{opt}. It should be observed that the β_{opt} is only applicable to the

multi-component PRVF signal analysis. Furthermore, the β_{opt} value of 0.6 here is only applicable under the current parameters (i.e. 3 frequencies components, 3 dB AWGN and the LPCPP method filter order is 20). Therefore, the next experiment will further analyse the β_{opt} value under different parameters.

The LPCPP method has an β_{opt} value which has the highest IEP value under the multi-component PRVF signal analysis. However, the multi-component PRVF signal above contains three frequency components. In order to see the effect of multi-component PRVF signals with the different number of frequencies on the LPCPP method, here the multi-component PRVF signals are divided into two-frequency, three-frequency and four-frequency PRVF signals, they are represented as PRVF-2, PRVF-3 and PRVF-4 in Fig. 4.8. The other parameters of those PRVF signals are the same as in the above experiment.

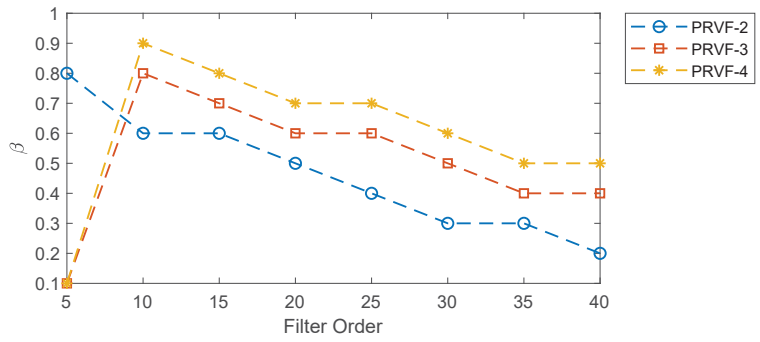

Fig. 4.8 The analysis of β for LPCPP method on the multi-component PRVF signals.

The experiment in Fig. 4.8 shows the relationship between the β_{opt} and the filter order. The SNR is 3 dB and the λ of the LPCPP is 10 Hz. It can be seen that except for the case where the filter order is 5, the greater β value is required when the number of frequency components of the PRVF signal is increased under the same filter order. When the filter order is 5, the number of the LPC poles is not sufficient for LPCPP to classify the poles into dominant and non-dominant poles to further identify the dominant frequencies of the

PRVF-3 and PRVF-4 signals. And the LPCPP method fails to identify the dominant pole when the filter order is too small for the number of frequencies that need to be identified (typically, the value of filter order should be greater than twice the number of frequencies that need to be identified). As a result, the β_{opt} values cannot be found under the PRVF-3 and PRVF-4 signals. However, the β_{opt} is 0.8 under the PRVF-2 signal. Furthermore, when the filter order is greater than 5, there is a trade-off between the filter order and the β_{opt} value. When the filter order is greater than twice the number of signal frequencies, the smaller β value is required when the filter order increases.

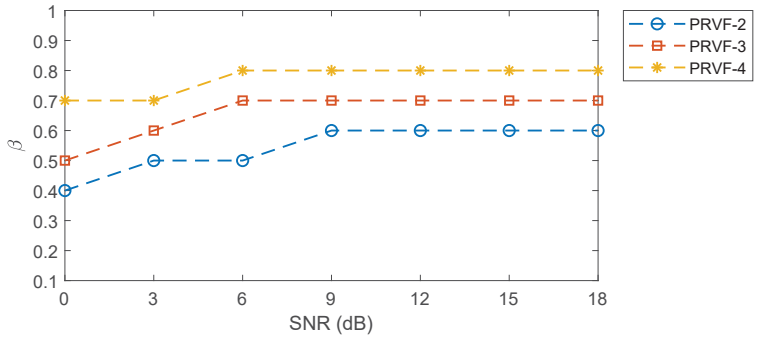

Fig. 4.9 The analysis of β for LPCPP method on the multi-component PRVF signals.

The second experiment in Fig. 4.9 shows the relationship between the β_{opt} and the SNR value. The filter order of the LPCPP method is 20 and the λ is 10 Hz. As can be seen, the β_{opt} value is increased when the number of the frequencies of the PRVF signal is increased under the same SNR value. Furthermore, the β_{opt} value increases with increasing SNR. The reason is that when the SNR value increases, the higher β value is required to find more dominant poles.

Most of the signals in the real world whose frequency components will be unknown. Therefore, it is useful to find the β_{opt} value for the frequency estimation of the signals. It can give us the maximum IEP value which means the maximum number of ideal exper-

iments in all Monte Carlo iterations. The choice of the β value is a challenge because the number of dominant frequencies in the signal cannot be known in advance. Therefore, through the simulation experiments in this part, it can be observed that when the filter order is greater than twice the number of signal frequencies, the selection of the β_{opt} value decreases with the increase of the filter order and there is a trade-off relationship. Furthermore, the greater the intensity of the noise, the smaller the value of β required to filter out the non-dominant poles by the noise and identify the dominant poles.

Analysis of the parameter λ value

The value of λ is used to find the associated poles for each dominant pole and the unit of the λ is Hz. In this part, there are two kinds of PRVF signals (i.e. single-component PRVF signal and multi-component PRVF signal) that are analysed to investigate the effect of the λ value on the LPCPP method. The sampling frequency of the PRVF signal is $f_s = 100$ Hz and the duration of the PRVF signal for each Monte Carlo trial is $t = 1$ s. The PRVF signals here are corrupted by 3 dB AWGN and the filter order of the LPCPP method is $P = 20$. The β value is 0.3 in single-component PRVF signal analysis and 0.7 in the multi-component PRVF signal analysis. The λ value is increased from 5 to 25 Hz in steps of 5 Hz.

It can be seen that Fig. 4.10 and Fig. 4.11 show the four metrics of the LPCPP method on the single-component PRVF signal analysis and the multi-component PRVF signal analysis respectively. When the value of λ is greater than 10 Hz, the values of IFP, VEP and AEP decrease with the increase of λ in both single-frequency and multi-component signals. In addition, the value of AEP increases with the increase of λ when the value of

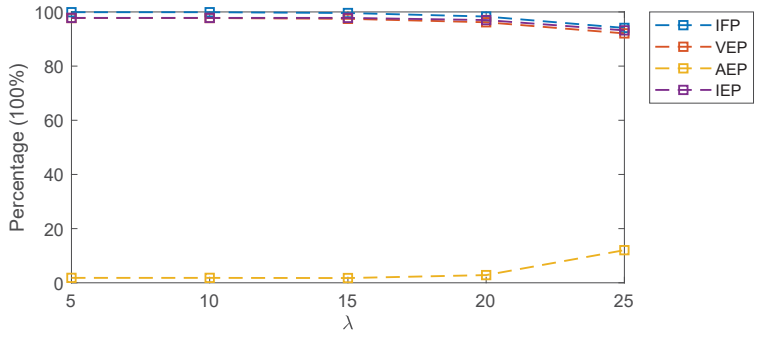

Fig. 4.10 The analysis of λ for LPCPP method on the single-component PRVF signals.

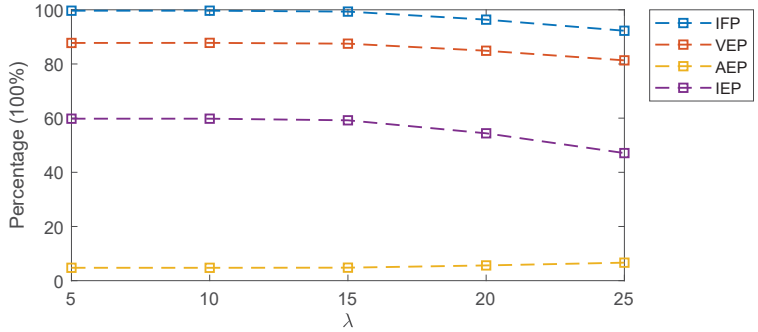

Fig. 4.11 The analysis of λ for LPCPP method on the multi-component PRVF signals.

λ is greater than 10 Hz. The reason is that when the value of λ increases, the frequency separation of the selected associated pole from the corresponding dominant pole also increases. This will cause a larger error between the peak of the reduced-order filter and the real signal frequency. However, when the λ value is between 5 and 10 Hz, the results of the four metrics of the LPCPP method have little difference between them. Furthermore, in the analysis in Section 3.2.3, the pole(s) near the dominant pole had a greater impact on the reduced-order filter. Therefore, the choice of the λ value is recommended to be between 5 and 10 Hz.

4.1.5 Conclusions

In this section, a series of 10,000 Monte Carlo trials on the single-component and multi-component signals are used to analyse the ability of the LPCPP method to identify the dominant frequencies. The results show that the LPCPP method can significantly improve the values of VEP and IEP and reduce the value of AEP compared to the LPC method at the same filter order. Furthermore, the LPCPP method has a high noise tolerance for frequency identification. In addition, the parameters β and λ of the LPCPP method are analysed. There is a β_{opt} value where the LPCPP method can obtain the maximum IEP value. The choice of the β_{opt} value is related to the filter order and the SNR value. There is a trade-off relationship between the β_{opt} and the filter order. Furthermore, the choice of β_{opt} value increases with the increase of SNR. Therefore, the choice of β value will be selected according to the actual situation of the application scenario. Moreover, increasing the value of λ will degrade the performance of the LPCPP method and it is recommended to be chosen in the range of 5 to 10 Hz. In summary, the LPCPP method outperforms the LPC method by accurately identifying the dominant frequency components in a high noise environment and it is a useful tool for spectral analysis of signals of unknown frequency.

4.2 Dominant Frequency Tracking of LPCPP

In this section, the ability of the LPCPP method to track the dominant frequency changes in real-time is further analysed. The term "real-time" in this section means that the LPC-based methods can estimate the frequency at every sampling instant. Linear Chirped Frequency Modulation (LCFM) signals are used to simulate signals with different frequency

change rates. Furthermore, a new definition is given on how to determine whether the LPCPP frequency estimate is valid or invalid in an LCFM signal at each sampling instant.

4.2.1 Experimental Metrics

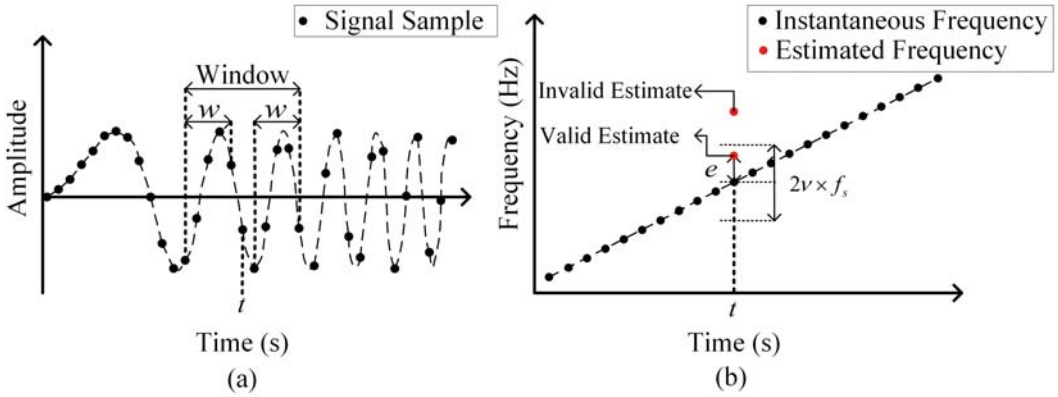

Fig. 4.12 The sampling window and the frequency estimation acceptance criterion.

Linear Chirped Frequency Modulation (LCFM) signals are used to facilitate the analysis of the frequency tracking performance of the LPCPP method under different rates of frequency change. The LCFM signal has an instantaneous frequency sweep $f(t)$ given by

$$f(t) = f(0) + \kappa t \tag{4.5}$$

The coefficient $\kappa = \Delta f / \Delta t$ represents the rate of the frequency change where Δf represents the frequency change over the interval Δt. The frequency of the LCFM signal increases linearly with time. Since the LCFM signal is a time-varying signal, the instantaneous frequency at a time t is estimated from a narrow sample window of the signal which is composed of w samples on either side of the instant t and the window size for each instantaneous frequency estimation is $(2w+1)$ samples. A diagram of the sample

window is shown in Fig. 4.12(a). As the instantaneous frequency $f(t)$ of the LCFM signal is known, the frequency error e between the instantaneous frequency and the estimated frequency of the LPC-based method can be calculated. When the frequency error e is less than $\nu \times f_s$, the frequency estimate is considered to be valid and the signal frequency is considered to be correctly identified as shown in Fig. 4.12(b). Furthermore, the four metrics (i.e. AEP, IFP, VEP and IEP) are used to analyse the ability of frequency tracking of the LPCPP method.

4.2.2 Frequency Change Rate Analysis

Table 4.2 The four metrics for LPC and LPCPP methods.

Method	IFP(100%)	VEP(100%)	AEP(100%)	IEP(100%)
LPC	81.9	9.28	0.19	0
LPCPP	85.53	78.47	0.18	78.54

The first experiment demonstrates the simple scenario of an LCFM signal with an SNR of 10 dB where the frequency of the signal changes from 100 Hz to 400 Hz and the duration of the signal is 2 s (i.e. $\kappa = 150$ Hz/s). The sampling frequency of the LCFM signal is $f_s = 1000$ Hz and the window size is 21 samples (i.e. $w = 10$ samples). The ν value in this section is chosen as 0.1% this mean the frequency threshold is $\nu \times f_s = 1$ Hz. In other words, when the absolute frequency error e is less than 1 Hz, the frequency estimate of the LPC-based methods is considered to be valid and the signal frequency is considered to be correctly identified. The filter order is $P = 5$ for both LPC and LPCPP methods. For the LPCPP method, the parameters are $\beta = 0.5$ and $\lambda = 10$ Hz. The real-time frequency estimation of the LCFM signal by the LPC-based methods is shown in Fig. 4.13 and the values of the four metrics are shown in Table 4.2. As can be seen, the LPCPP method

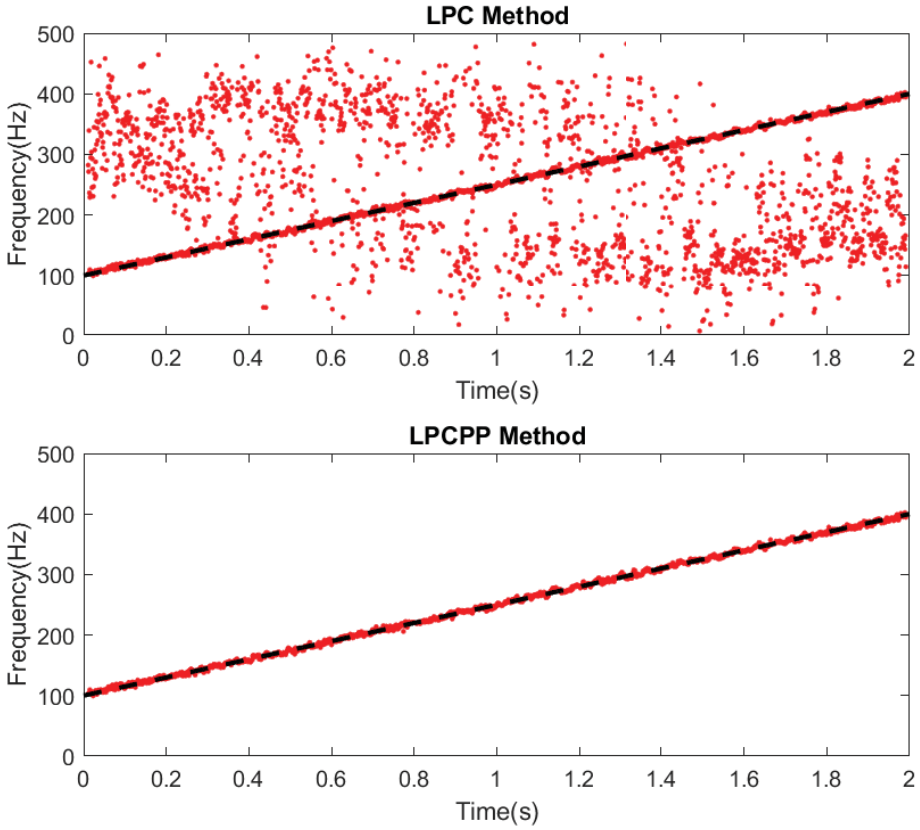

Fig. 4.13 The estimated frequency results from LPC and LPCPP method for a LCFM signal. The red points are the estimates from the LPC method and the black trace is the instantaneous frequency $f(t)$ which is a reference trace.

outperforms the LPC method in all four metrics. Specifically, the VEP and IEP values of the LPCPP method are significantly improved compared to the LPC method. In other words, not all the estimates from the LPC method correspond to the dominant frequency. The LPCPP method can produce more valid dominant frequency estimates over time to achieve real-time tracking of the dominant frequency changes and it can significantly reduce the generation of invalid estimates.

Table 4.3 The starting frequencies of the LCFM signal with different δ.

κ	**50**	**100**	**150**	**200**	**250**
$f(0)$ (Hz)	200	150	100	50	0

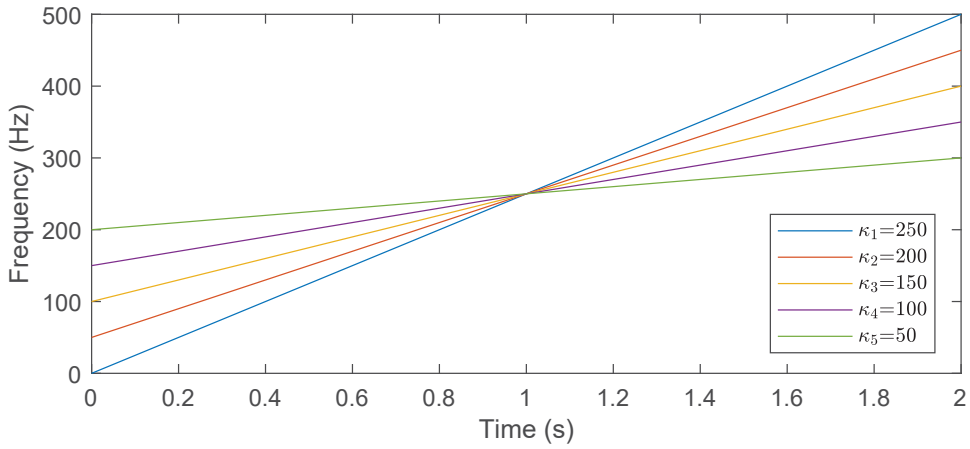

Fig. 4.14 LCFM signals with different frequency change rates in the time-frequency plane.

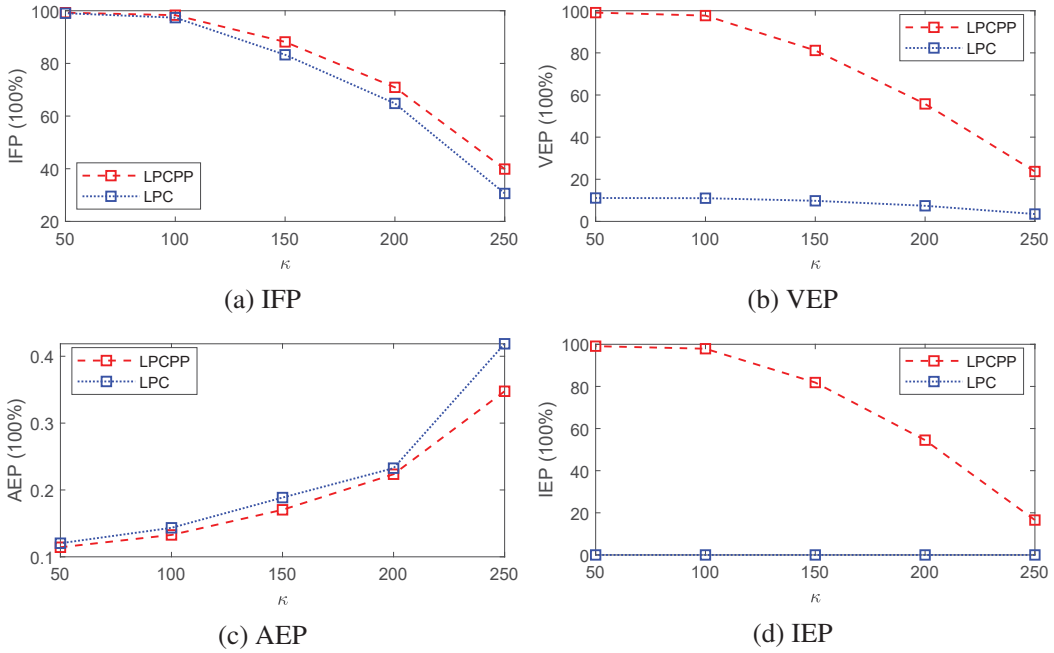

(a) IFP (b) VEP

(c) AEP (d) IEP

Fig. 4.15 Performance analysis of the LPC and LPCPP method for LCFM signals with different rates of frequency change.

The second experiment demonstrates the performance of the LPC and LPCPP methods for LCFM signals with different frequency change rates (i.e. κ values). The duration of all the LCFM signals is 2 s, the sampling frequency is $f_s = 1000$ Hz and the signals are corrupted by AWGN where SNR$=$ 10 dB. The LCFM signals with the different κ values

are shown in Fig. 4.14. The start and end frequencies corresponding to the different rates κ are detailed in Table 4.3. The other experimental parameters are the same as the above experiment. Fig. 4.15 presents the results of the four metrics. In the IFP analysis, the values of the two LPC-based methods decrease with an increase in κ. The IFP value of the LPCPP method is slightly larger than that of the LPC method and this difference increases with the increase of the κ value. Furthermore, the VEP values of both methods still decrease when the rate of frequency changes κ increases. However, the VEP of the LPCPP method is always much higher than that of the LPC method under the same κ value. Specifically, the VEP value of LPCPP is up to 85.9% higher than that of the LPC method which indicates that the LPCPP method significantly improves the validity of estimates. Moreover, the AEP value of the LPCPP method is always slightly smaller than that of the LPC method at the same κ, so the LPCPP method can produce more accurate frequency estimates. Finally, the IEP value of the LPC method is always 0 which means the LPC method always produces invalid frequency estimates in the frequency estimation experiment at every sampling instant. However, the LPCPP method can achieve IEP values up to 96.84%. Although the ability of both LPC-based methods to track the frequency of the LCFM signal decreases as the frequency change rate κ increases, the LPCPP method demonstrates its improvement in the four metrics compared to the LPC method. Specifically, the LPCPP method significantly improves the IFP value and VEP value. In short, the LPCPP method has a greater ability to track the frequency of the LCFM signal than LPC under the different frequency change rates.

4.2.3 Conclusions

This section focused on analysing the ability of the LPCPP method to track the dominant frequency changes of a noisy time-varying LCFM signal in real-time. The results show that the LPCPP method can achieve real-time dominant frequency tracking and it significantly reduces the redundant frequency estimates of LPC. In short, the LPCPP method outperforms the LPC method under fast frequency changes to track real-time changes in frequency.

4.3 Time-bandwidth Product Analysis of LPCPP

Time-frequency methods enable us to study the time-frequency characteristics of signals which exhibit transient oscillatory behavior. One crucial question for the time-frequency method is how accurately one can measure the temporal and spectral events simultaneously. The limit on the accuracy is established by the Heisenberg-Gabor uncertainty principle [71] which shows that there is a trade-off between the time and frequency resolution. There are many different definitions used to measure the time and frequency resolution [78, 119]. However, these definitions are mainly applicable to waveform time-frequency methods (i.e. STFT). The LPCPP method is a parameterised time-frequency method. 10,000 Monte Carlo experiment trials are used to generate an Error Probability Density Function (EPDF) of the error associated with the frequency estimate. The mean and standard deviation of the EPDF are used to define the bias μ and frequency resolution Δf of the LPC-based method. Therefore, a new method to calculate the Time-Bandwidth Product (TBP) of the LPC-based method is proposed here. In this section, the experi-

ments in this section are divided into three parts: The first part gives the definition of TBP and presents the EPDF results of the LPCPP method and the LPC method. The second part analyzes the performance of bias μ and TBP at different time resolutions Δt (i.e. window duration). Finally, the effect of the different frequency ranges on the bias μ and TBP analysis is investigated.

4.3.1 Definition of the Time-bandwidth Product

The probability distribution function is used to describe the probability of a random variable. Here, an EPDF is defined by using the error between the estimation frequency and the real frequency. 10,000 Monte Carlo trials are used to obtain the EPDF for the frequency estimates. The single-component PRVF signal is used for Monte Carlo trials. The sampling frequency is $f_s = 100$ Hz and the SNR value is 3 dB. Since the LPC method is used as a comparison method, only the estimates which have an error of less than 5 Hz are used in order to ensure that the LPC method is not unfairly penalised. A histogram of the frequency errors is generated where the error e range is from -5 Hz to +5 Hz and the bin size $\Delta e = 0.1$ Hz. For each histogram bin, the median value of each bin e is first multiplied and the height of each histogram bin is expressed as a probability $P(e)$ (i.e. to ensure $\sum P(e) = 1$). The bias is defined as

$$\mu = \sum eP(e), \tag{4.6}$$

where μ is the bias of the all estimates.

Furthermore, the standard deviation σ of the EPDF is used to measure the frequency resolution of the LPC-based method. The frequency resolution Δf is defined as

$$\Delta f = \sigma = \sqrt{\Sigma(e-\mu)^2 P(e)} \tag{4.7}$$

The Heisenberg-Gabor uncertainty principle tells us what can be achieved with regard to time-frequency localization for the short-time Fourier transform [71], by referring to the dimensions of the tiles ($\Delta t \times \Delta f$) in the time-frequency plane. Therefore, the Time-Bandwidth Product (TBP) of the parameterised time-frequency method is

$$TBP = \Delta f \times \Delta t \tag{4.8}$$

where Δt represents the time resolution (i.e. the duration of the PRVF signal).

Table 4.4 The details of the EPDFs for the both LPC-based methods.

Method	**Mean**(μ)	**Frequency Resolution**(Δf)	**TBP**
LPCPP	0.0095	0.0769	0.0769
LPC	-0.0338	1.7792	1.7792

The two EPDFs of the LPCPP method and the LPC method are shown in Fig. 4.16. The filter order of both LPC-based methods is $P = 20$ and the $\Delta t = 1$ s. The parameters of the LPCPP method are $\beta = 0.4$ and $\lambda = 10$ Hz. Table 4.4 provides the detailed information of the EDPF. As can be seen, the EPDF of the LPC method is broader than that of the LPCPP method, the reason is that the LPCPP method can produce more accurate frequency estimates and the LPC method produces more invalid frequency estimates (an error greater than 1 Hz). It can be seen that the μ value of the LPCPP method is closer to 0 than that of

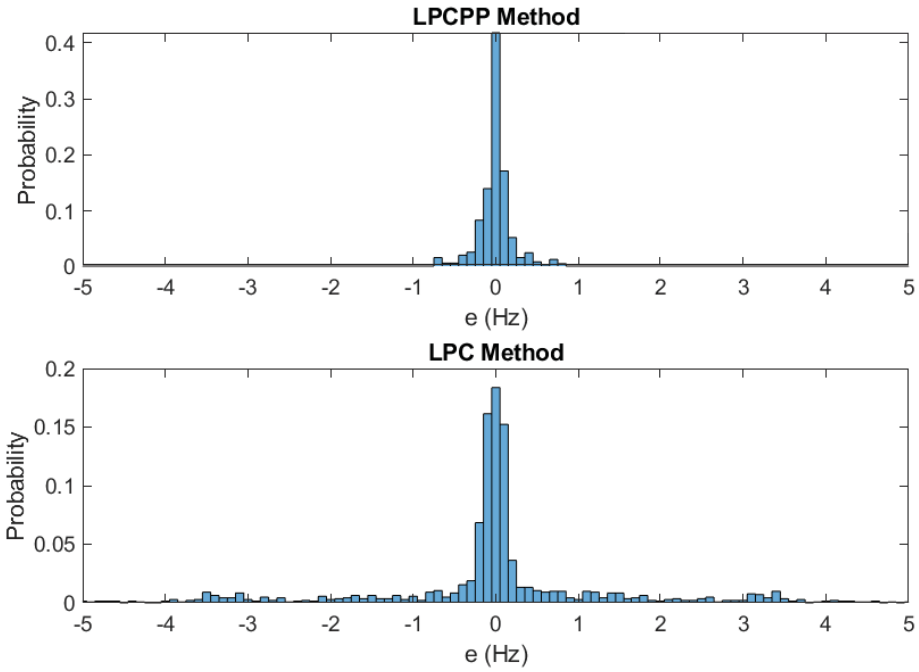

Fig. 4.16 The EPDFs of the both LPC-based methods.

the LPC method which means the LPCPP method can produce more accurate frequency estimates. Furthermore, the TBP of the LPCPP method is much smaller than that of the LPC method. Therefore, the LPCPP method can provide a lower time-bandwidth product and a lower absolute μ than the LPC method. In other words, the LPCPP method can significantly improve spectral resolution and greatly improve the accuracy of the signal frequency estimation.

4.3.2 Time Resolution Analysis

Table 4.5 LPCPP vs LPC: The TBP corresponding to different Δt.

Δt (s)	**0.5**	**1**	**1.5**	**2**	**2.5**	**3**	**3.5**	**4**
LPCPP	0.0880	0.0949	0.1047	0.1318	0.1410	0.1565	0.1638	0.1735
LPC	1.0263	1.7700	1.9117	2.0731	1.8615	1.9800	1.3417	1.3231

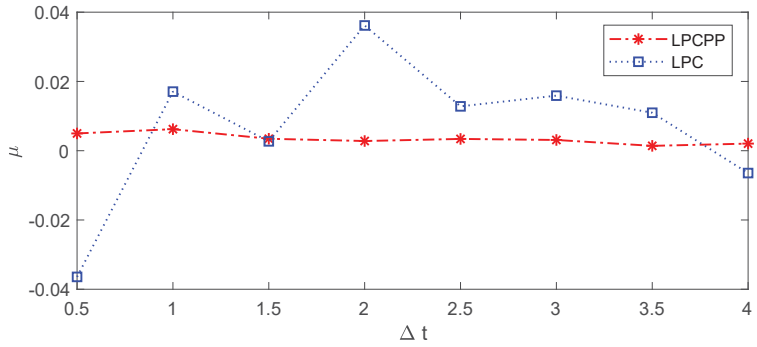

Fig. 4.17 The μ value analysis of EPDF for different Δt.

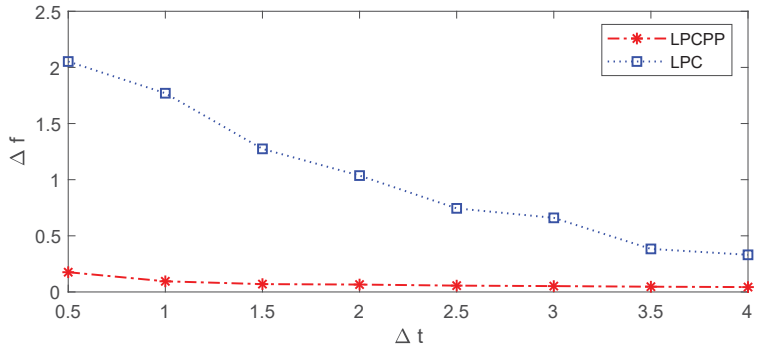

Fig. 4.18 The Δf value analysis for different Δt.

These experiments show the μ and Δf values under the different values of Δt. The Δt is increased from 0.5 s to 4 s as an independent variable and the step size is 0.5 s. This is still a Monte Carlo experiment where 1,000 experiments were run for each Δt. Other experimental parameters are the same as in the first experiment. Fig. 4.17 shows the μ analysis and Fig. 4.18 shows the Δf analysis. Furthermore, the calculation results of TBP are provided in Table 4.5. In Fig. 4.17, the μ value of the LPCPP method shows little change under the different Δt and they are all around 0. However, the μ value of the LPC method varies greatly and the absolute value of μ is greater than that of the LPCPP method under the same Δt. This shows that the LPCPP method has a robust performance to estimate the signal frequency and it can produce more accurate frequency estimates. In Fig. 4.18, it can be seen that the Δf values of both the LPC-based methods decrease with

the increase of Δt. Therefore, the time resolution Δt and the frequency resolution Δf of the LPC-based method is a trade-off relationship. Furthermore, the LPCPP method can provide a smaller frequency resolution than the LPC method at the same time resolution. In Table 4.5, it can be seen that the TBP value of LPCPP is much smaller than that of the LPC method for the same Δt. They all indicate that the LPCPP method can provide a finer spectral resolution than that of the LPC method.

4.3.3 Frequency Interval Analysis

Table 4.6 The frequency range of different frequency intervals.

Label	**B1**	**B2**	**B3**	**B4**	**B5**
Frequency Range (Hz)	0-10	10-20	20-30	30-40	40-50

The frequencies of the PRVF signal used in the above experiments are uniformly distributed over the entire frequency domain in the range 0 to $f_s/2$. Therefore, a question is considered here, whether the signals from different frequency ranges in the frequency domain will have an impact on the performance of the LPCPP method. Therefore, the single-component PRVF signal is used to analyse the performance of the LPCPP method in different frequency intervals and their frequencies are uniformly distributed for each frequency interval. Specifically, the sampling frequency of the PRVF signal is $f_s = 100$ Hz and the frequency domain is equally divided into 5 frequency bands (i.e. B1, B2, B3, B4 and B5). The details of the frequency bands are shown in Table 4.6. It should be noted that the frequency interval classification here is not related to the frequency bands (i.e. Delta, Theta, Alpha, Beta and Gamma, etc.) of EEG. This frequency interval classification is only used for the simulation of PRVF signals and is used to analyse the

effect of different frequency intervals on the frequency estimation performance of the LPCPP method. Specifically, frequency interval B1 corresponds to low frequencies and frequency interval B5 corresponds to high frequencies. The frequency intervals B2, B3 and B4 correspond to middle frequencies. There are 10,000 Monte Carlo trials in each frequency interval. In addition, the PRVF signal is corrupted by 3 dB AWGN and the duration of the PRVF signal for each Monte Carlo trial is 1 s. Other parameters are the same as the above experiment.

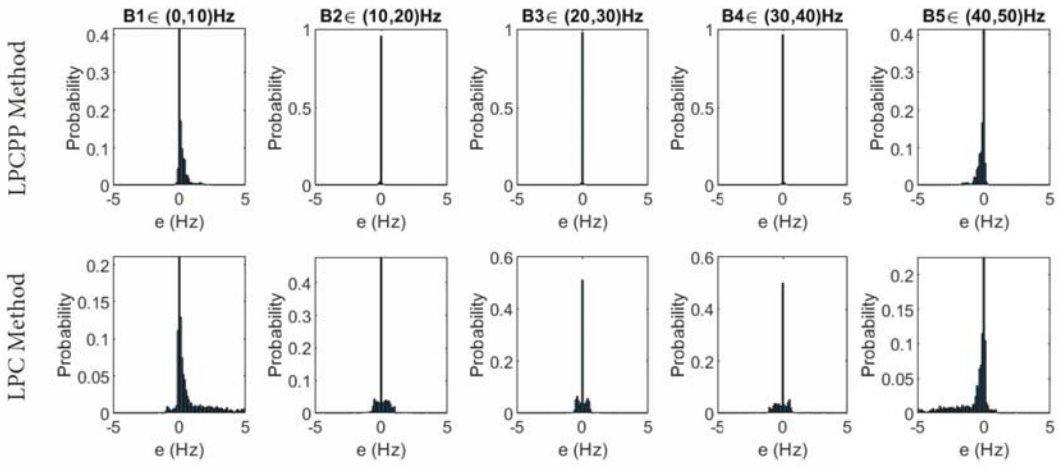

Fig. 4.19 The EPDFs of both LPC-based methods for the different frequency intervals.

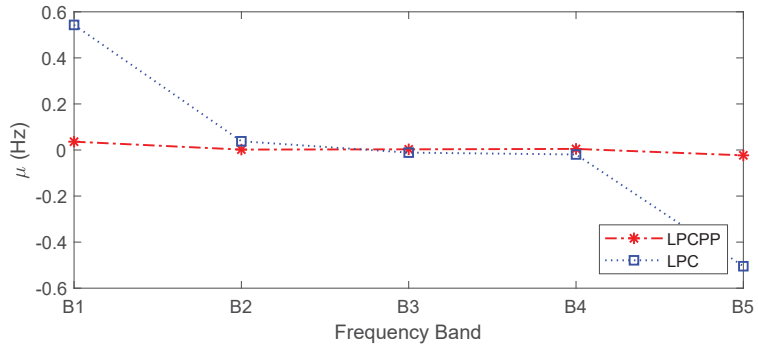

Fig. 4.20 The bias of both LPC-based methods for the different frequency intervals.

The EPDFs of the LPCPP method and the LPC method in the different frequency intervals are shown in Fig. 4.19. It can be seen that the spread of EPDF of the LPC method is

greater than that of the LPCPP method within each frequency interval. For the μ analysis in Fig. 4.20, the μ of the LPC method is greater than 0 in the low-frequency interval (i.e. B1) and is less than 0 in the high-frequency interval (i.e. B5). This indicates that the LPC method overestimates the frequency in the low-frequency interval and underestimates the frequency in the high-frequency interval. The reason is that the EPDF of the LPC method is biased toward a positive error in the low-frequency interval (i.e. B1), i.e. some of the LPC estimates are too large. Similarly, the error is biased toward negative error in the high-frequency interval, i.e. some of the LPC estimates are too small. However, the LPCPP method can significantly reduce this bias of the LPC method.

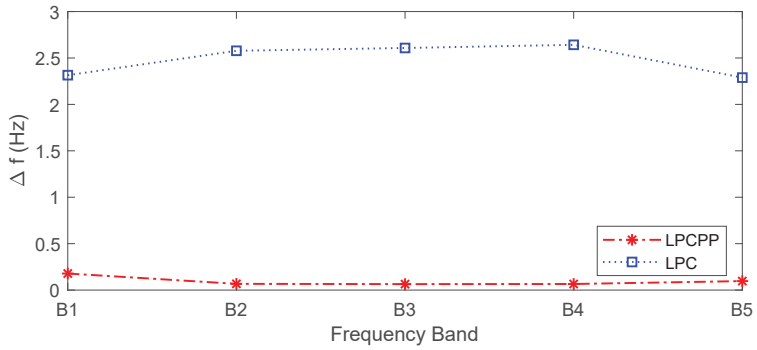

Fig. 4.21 The frequency resolution of both LPC-based methods for the different frequency intervals.

Table 4.7 LPCPP vs LPC: The TBP for the different frequency intervals.

Frequency Interval	B1	B2	B3	B4	B5
LPCPP	0.1783	0.0672	0.0642	0.0655	0.0968
LPC	2.3148	2.5775	2.6077	2.6418	2.2886

For the frequency resolution analysis in Fig. 4.21, the LPC method has a lower value of Δf in the low and high-frequency intervals. The reason is that the estimates of the LPC method in the high-frequency interval and the low-frequency interval are always biased to one side, while the EPDFs in the middle frequency intervals (i.e. B2, B3 and B4)

have little bias (distributed on both sides), thus causing the Δf in the middle frequency interval is higher than other frequency intervals (i.e. B1 and B5). This result is consistent with that observed in Fig. 4.20. For the LPCPP method, the values of Δf in low and high-frequency intervals are slightly higher than that of other frequency intervals. This is because the LPCPP method further processes the LPC pole where the associated pole is combined with the dominant pole to determine the final frequency estimate. In the low-frequency interval or high-frequency interval, the associated poles of the LPCPP method are close to the middle frequency. Therefore, the LPCPP method has slightly higher values of Δf in the low and high-frequency intervals. However, the different reasons cause the performance of the two methods to be different in different frequency intervals, but the Δf of the LPCPP method is always much smaller than that of the LPC method in each frequency interval. In other words, the LPCPP method can provide a higher frequency resolution than that of the LPC method at different frequency intervals. In addition, the details of TBP are shown in Table 4.7. Since Δt is fixed in this experiment, the TBP value of the LPCPP method is much lower than that of the LPC method at the same frequency interval. In short, the LPCPP method can significantly reduce the bias of the LPC method in the low-frequency interval and high-frequency interval. Furthermore, the LPCPP method still can provide finer spectral resolution than that of the LPC method under the different frequency intervals.

4.3.4 Filter Order Analysis for TBP

In this experiment, the effect of the filter order on the bias μ and frequency resolution Δf of both LPC-based methods (i.e. LPCPP and LPC) is analysed. The filter order P is

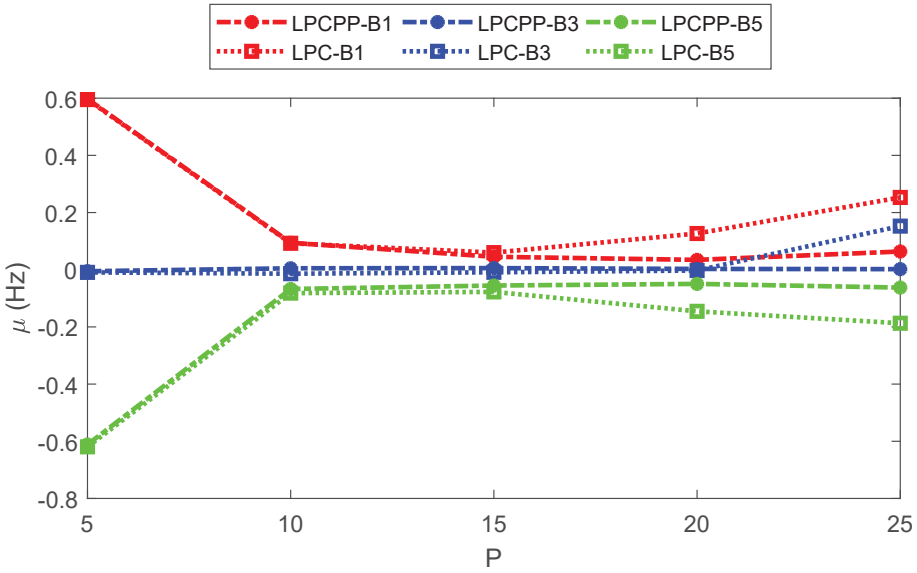

Fig. 4.22 The bias of the LPCPP and the LPC methods for different filter orders.

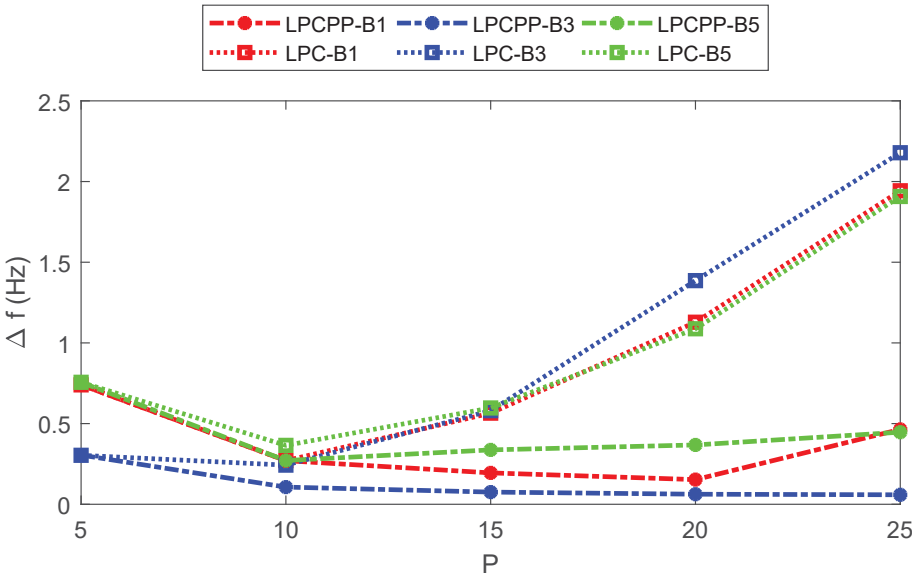

Fig. 4.23 The frequency resolution of the LPCPP and LPC methods for different filter orders.

changed from 5 to 25 and the step size is 5. The single-component PRVF signal is still used for 10,000 Monte Carlo trials and the time duration of each PRVF signal is Δt =1 s. The SNR value is 3 dB and other parameters are the same as in the above experiment. Furthermore, it will focus on selecting three representative frequency bands for detailed

Table 4.8 LPCPP vs LPC: The TBP for different filter orders.

Filter Order		5	10	15	20	25
B1(TBP)	**LPCPP**	0.7398	0.2702	0.1945	0.1529	0.4639
	LPC	0.7399	0.2707	0.5647	1.1282	1.9428
B3(TBP)	**LPCPP**	0.3036	0.1065	0.0756	0.0624	0.0588
	LPC	0.3049	0.2426	0.5803	1.3860	2.1785
B5(TBP)	**LPCPP**	0.7558	0.2712	0.3370	0.3677	0.4467
	LPC	0.7559	0.3650	0.5968	1.0877	1.9075

analysis, namely, B1 represents the high-frequency interval, B3 represents the middle-frequency interval and B5 represents the high-frequency interval. Fig. 4.22 and Fig. 4.23 show the bias analysis and the frequency resolution of LPCPP and LPC for different filter orders. In Fig. 4.22, the bias μ of the LPC method in the low-frequency interval is greater than 0 and in the high-frequency interval is less than 0. This indicates the LPC method has a larger bias in the low and high-frequency intervals than in the middle frequency interval. The bias μ (Fig. 4.22) and the Δf (Fig. 4.23) of the LPC method first decrease and then increase with the increase of filter order. The LPC method has the smallest bias value at $P = 15$ and it has the smallest Δf at $P = 10$. These results indicate the performance of the LPC method is dependent on the filter order. For the LPCPP method, it can provide a smaller bias than the LPC method after P is greater than 10. The reason is that the filter order is too low to provide sufficient spectral information when $P = 5$. In Fig. 4.23, the LPCPP method has a high-frequency resolution under different filter orders and is not much affected by the filter order. So the performance of the LPCPP method is less sensitive to the filter order than that of the LPC method. Table 4.8 shows the TBP results of this experiment in which the LPCPP values are less than the LPC for all cases.

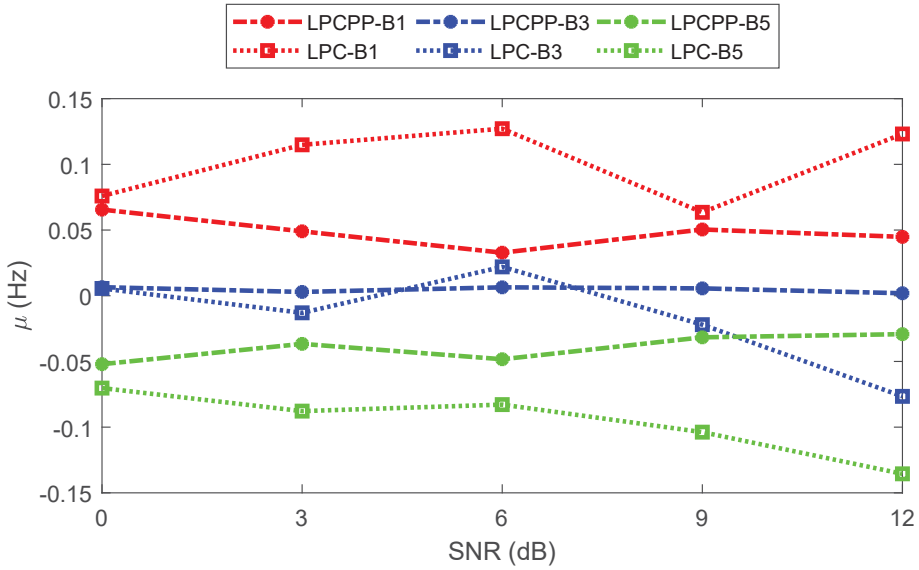

Fig. 4.24 The bias of the LPCPP and LPC methods under different SNRs.

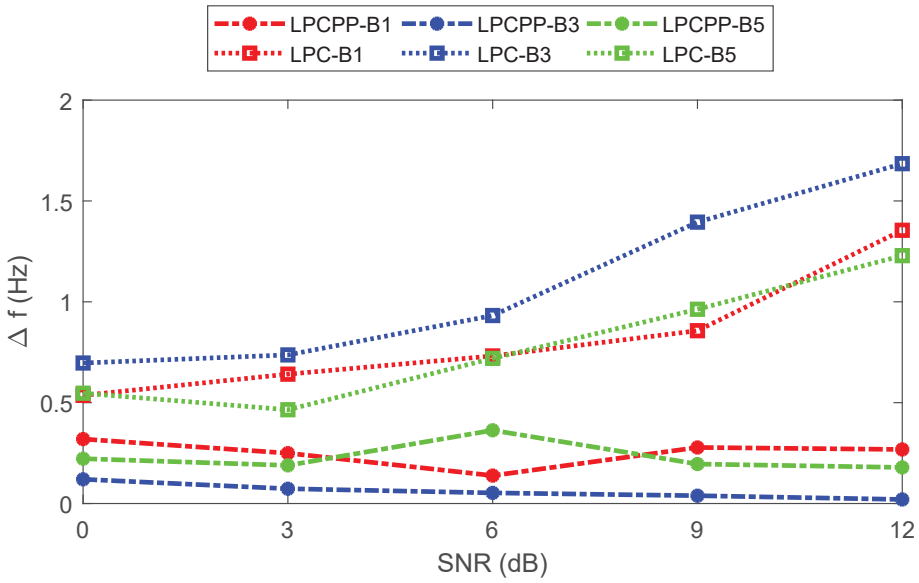

Fig. 4.25 The frequency resolution of the LPCPP and LPC methods under different SNRs.

4.3.5 Signal Noise Analysis for TBP

In this experiment, the effect of different SNRs on the two methods is analysed. The filter order $P = 15$ and the time duration of each PRVF signal is $\Delta t = 1$ s. Other experimental parameters are the same as the above experiment. Fig. 4.24 and Fig. 4.25 demonstrate the

bias μ and Δf of LPCPP and LPC under different SNRs. It can be seen that the LPCPP method has a smaller μ than the LPC method under the same SNR and the LPCPP method can provide a higher frequency resolution than that of LPC for the same SNR. In Fig. 4.25, the Δf of the LPC method becomes larger as the SNR is increased. The reason is that the range of EPDF only analyses frequency errors less than 5 Hz. But the error of estimates of the LPC method is over 5 Hz when the signal has a low SNR. So only the errors between the -5 and 5 Hz are counted which is why the μ and Δf of the LPC method become greater as the SNR increases. Fig. 4.26 and Fig. 4.27 show the results when

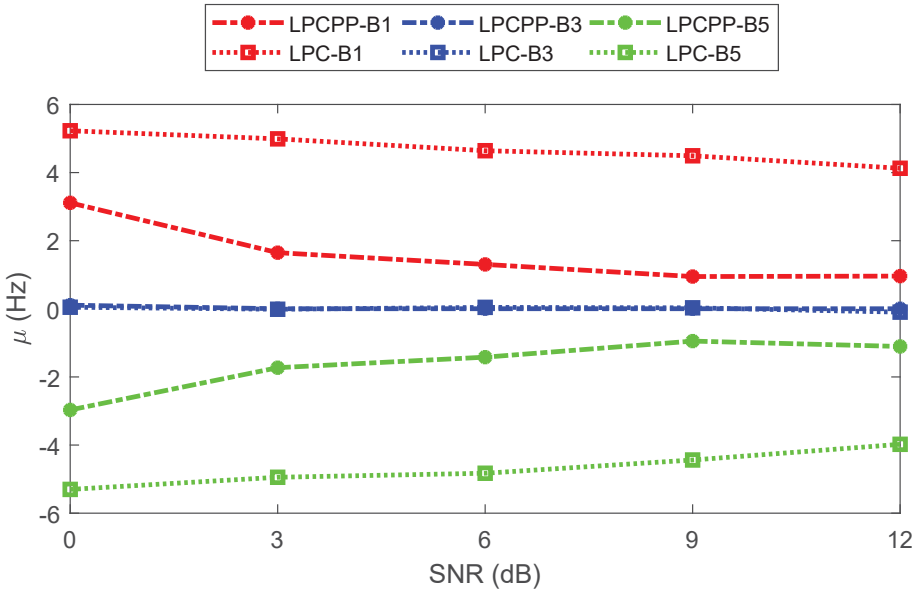

Fig. 4.26 The bias of the LPCPP and LPC methods under different SNRs where the error range extends from -15 to 15 Hz.

the error range extends from -15 to 15 Hz. Fig. 4.26 shows that the bias of both methods is decreased as the SNR increases and Fig. 4.27 shows that the Δf of both methods is decreased as the SNR increases. The bias of the LPCPP method still is much lower than that of LPC and the frequency resolution is much lower than that of LPC at B3. These results show that the LPCPP method has a higher tolerance to noise than LPC. Table 4.9

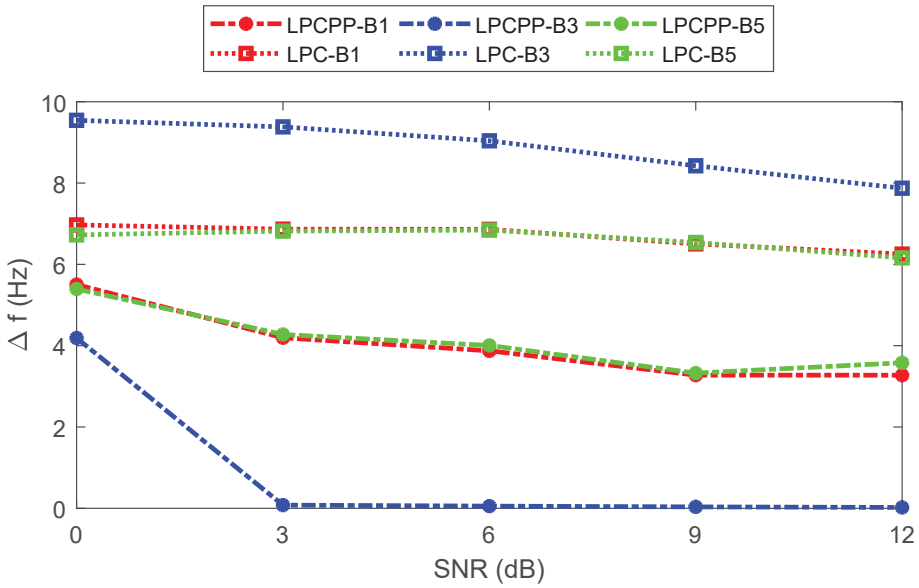

Fig. 4.27 The frequency resolution of the LPCPP and LPC methods under different SNRs where the error range extends from -15 to 15 Hz.

shows the TBP values of LPC and LPCPP where the error range of EPDF is from -5 to 5 Hz. In short, the TBP value of LPCPP is lower than the LPC method for the different SNRs.

Table 4.9 LPCPP vs LPC: The TBP under different SNR levels.

SNR(dB)		**0**	**3**	**6**	**9**	**12**
B1(TBP)	**LPCPP**	0.3195	0.2497	0.1385	0.2779	0.2681
	LPC	0.5363	0.6414	0.7316	0.8568	1.3547
B3(TBP)	**LPCPP**	0.1200	0.0734	0.0527	0.0388	0.0202
	LPC	0.6966	0.7367	0.9320	1.3950	1.6848
B5(TBP)	**LPCPP**	0.2223	0.1892	0.3631	0.1957	0.1790
	LPC	0.5469	0.4649	0.7195	0.9631	1.2289

4.3.6 Conclusions

In this section, the time-bandwidth product for the parameterised time-frequency method was analysed. Specifically, a new method for measuring the frequency resolution of parametric time-frequency methods was presented. The TBP value of the EPDF was used

to analyse the performance of the LPCPP method. Furthermore, the μ value was used to measure the bias of the frequency estimates and the Δf value was used to represent the frequency resolution of the LPC-based method. The experiment of the TBP analysis shows that the LPCPP method can significantly improve the spectral resolution compared to the LPC method. Furthermore, the μ value of the LPCPP method is closer to 0 than that of the LPC method which means the LPCPP method can provide more accurate frequency estimates. In addition, the performance of the LPCPP method and the LPC method in different frequency intervals is also analysed. It can be found that the LPCPP method can significantly reduce the bias of the LPC method in the low and high-frequency intervals. It can provide a higher frequency resolution than LPC in different frequency intervals. Furthermore, the LPCPP method is less sensitive to the filter order and has a higher tolerance of noise than LPC. In short, the LPCPP method has a much smaller TBP value than the LPC method under the same experimental conditions.

4.4 Chapter Summary

This chapter presented some representative simulation analyses of the LPCPP method and the results show that it is particularly suited for EEG signal processing. The first section presented the LPCPP method can realise the enhancement of frequency estimation and it has a high noise tolerance. Furthermore, the results showed that the LPCPP method is particularly useful for the dominant frequency estimation of an unknown signal. The second section demonstrated that the LPCPP method can realise the real-time dominant frequency tacking and it can significantly reduce the invalid frequency estimates of the

LPC method. Moreover, the LPCPP method outperforms the LPC method under fast frequency changes. The third section presented the TPB analysis of the LPCPP method, the results showed that the LPCPP method can significantly improve the spectral resolution compared to the LPC method. Furthermore, the LPCPP method can reduce the bias of the LPC method for the frequency estimation in the low and high-frequency intervals. In short, the LPCPP method is well suited for processing poor signal-to-noise ratio, time-varying, intermittent and multi-component signals (i.e. EEG signals). In conclusion, the LPCPP method has obvious advantages in frequency identification and frequency tracking compared with the LPC method and the LPCPP method is well suited to the analysis of EEG signals. It is believed that the LPCPP method has the potential to be a useful tool in the field of signal processing.

Chapter 5

EEG Spectra Activity Analysis Framework

In this chapter, an EEG spectral analysis framework involving the LPCPP method will be presented and it can realise two benefits for EEG spectra analysis: The first one is the framework that can realise real-time tracking of the dominant frequencies of EEG signals. The second is to propose a number of EEG centre frequencies to describe the dominant EEG spectral activity which respectively corresponds to different EEG waves (i.e. Delta, Theta, Alpha, Beta and Gamma). This chapter has five sections: The first section gives the introduction to the proposed EEG spectral framework. The second section cleans the EEG dataset using the autocorrelation method. The third section presents an example of real-time tracking of EEG dominant frequencies using the LPCPP method. The fourth section presents the spectral analysis results of the proposed framework on three different EEG datasets. The last section is the summary of the chapter.

5.1 Introduction to the EEG Spectra Analysis Framework

From the previous analysis, it can be seen that the LPCPP method is a parameterised time-frequency method that has a high noise tolerance and can provide a lower time-bandwidth product than the LPC method. The LPCPP method is excellent at processing multi-component signals and has the ability to track the instantaneous-frequency change in the form of numerical estimates. Moreover, the EEG signal is a high noise, time-varying, intermittent signal which contains multiple frequency components. The LPCPP method is particularly suited to EEG processing.

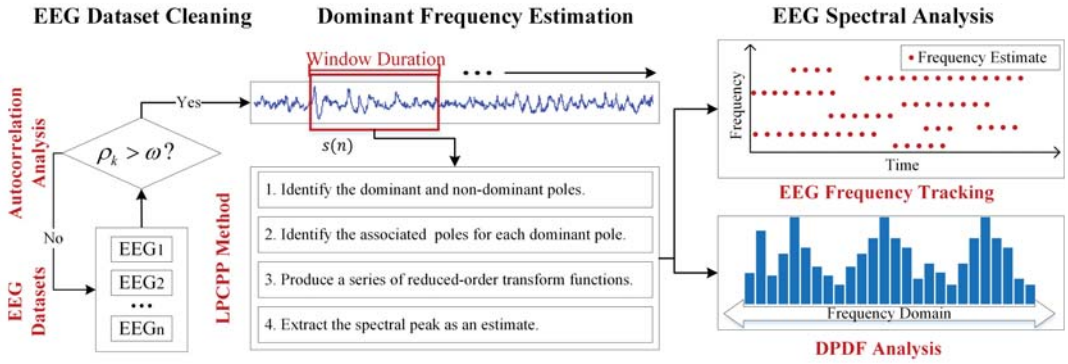

Fig. 5.1 The overview of the EEG spectra analysis framework.

EEG acquisition usually has many different electrode positions to record electrical signals simultaneously. However, not all electrical signals can genuinely correspond to human brain activity. Some failed collections may come from poor electrode contact or some other collected EEG may come from the brain cortex areas with no brain activity at a given time. Poor grounding of the EEG electrodes can cause a significant 50 Hz or 60 Hz artifact which depends on the local power system's frequency. Whether the artifacts are caused by biological or environmental noise, the required EEG signal should contain rich spectral information and not be heavily corrupted by artifacts, i.e. the collected EEG

signal should capture genuine brain spectral activity rather than random noise information. Therefore, EEG datasets need to be cleaned up using autocorrelation methods in order to find correlated EEG signals within a given time. These correlated EEG signals should contain richer spectral information. The LPCPP method provides a numerical estimate of the dominant frequency that can be used to realise EEG dominant frequency tracking. Furthermore, the LPCPP method can generate a histogram that is a distribution of the dominant frequencies in the frequency domain, namely a Discrete Probability Density Function (DPDF). The peaks of the DPDF will be considered as the centre frequency of the EEG activity to describe the dominant EEG spectral activity instead of these fixed frequency boundaries. The overview of the EEG spectra analysis framework is shown in Fig. 5.1. It can be seen that the first step is to clean up the EEG datasets using autocorrelation methods. The second step is to slide a window duration over the EEG signal samples and apply the LPCPP method to each window duration EEG signal to estimate the dominant frequency. For the last step of this EEG spectral framework, there are two objectives to achieve. One is to realise real-time tracking of the dominant frequency of EEG signals. The term 'real-time' is the same as the previous definition for LCFM signal analysis in Section 4.2 which means the LPCPP method can achieve the dominant frequency estimation for each sampling instant. The other is to propose a series of new centre frequencies to describe the EEG spectra activity by analysing EPDF. The following will provide a detailed analysis of each step of the proposed EEG spectral framework.

Table 5.1 Interpretation of the correlation coefficient.

ω	Interpretation
0.9 to 1.0	Very high correlation
0.7 to 0.9	High correlation
0.5 to 0.7	Moderate correlation
0.3 to 0.5	Low correlation
0.0 to 0.3	Negligible correlation

5.2 EEG Dataset Cleanup Analysis

The autocorrelation method is used here first to select EEG signals and to reject EEG signals that are excessively noisy. In statistics, the correlation coefficient measures the strength and direction of a linear relationship between two variables [120]. One of the basic assumptions in the linear regression model is that the random error components or disturbances are identically and independently distributed. For a time series s_i, the autocorrelation for lag k is given by

$$y_k = \frac{c_k}{c_0}, \quad k = 1, 2, \cdots \tag{5.1}$$

where

$$c_k = \frac{1}{N} \sum_{i=1}^{N-k} (s_i - \bar{s})(s_{i+k} - \bar{s}) \tag{5.2}$$

The N represents the effective sample size of s and c_0 is the sample variance of the time series. Autocorrelation is a correlation coefficient that can be used for finding correlated EEG signals at a lag time. Time-frequency analysis of EEG signals usually has a duration of seconds. For example, Xu, Shanzhi et al. used an adaptive graph spectral analysis method to extract features of the EEG signals and they used an EEG window duration

is 2 s [121]. Kim, Hyun-Ji et al. evaluated a hybrid BCI system by comparing features from spatial, spectral and temporal domains and the EEG window duration they used is 3 s [122]. Amin, Md Shahedul et al. performed a spectral analysis of human sleep EEG signals with a window duration of 1 s [123]. In this thesis, the window duration of the EEG signal was chosen to be 1 s, i.e. the autocorrelation coefficient of the EEG signal at a lag time of 1 s is analysed here. Furthermore, the autocorrelation coefficients of the EEG signal whose magnitude should be greater than a threshold value ω at a lag time indicate that the EEG signal is considered which has rich spectral activity information.

$$r_k > \omega \tag{5.3}$$

where the interpretation of the threshold value ω in the Table 5.1 [124]. The autocorrelation method is used here to detect non-randomness in EEG and find the EEG signals with high autocorrelation at a lag time of 1 s. In other words, the correlation coefficient of the EEG signal at a lag time of 1 s should be greater than $\omega = 0.7$.

Table 5.2 The details of the EEG datasets.

Dataset	Subjects	Fs (Hz)	Channels	Times	Number of Signals	Year
BCI109	109	160	64	14	97,664	2004
MI52	52	512	64	5	16,640	2017
GAL12	12	500	32	8	3,072	2014

Table 5.3 The EEG datasets with autocorrelation coefficients greater than 0.7 at 1 s lag time.

Dataset	BCI109	MI52)	GAL12
Percentage (100%)	19.98	93.99	25.42
Number of signals	19,513	15,640	781

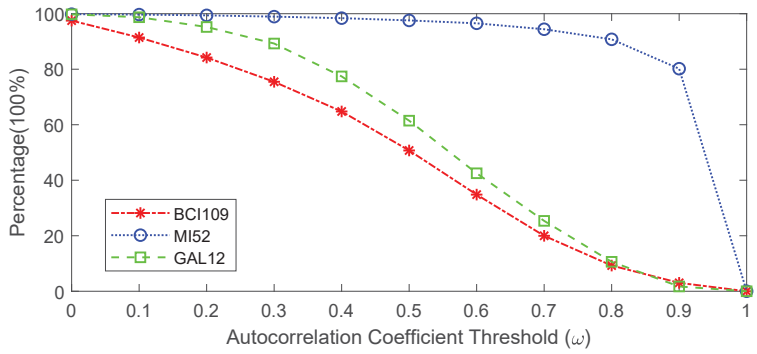

Fig. 5.2 Autocorrelation coefficient analysis of different EEG datasets at lag time 1 s.

Three public EEG datasets are used here, they are BCI109 [2], MI52 [27] and GAL12 [58]. The details of the three datasets are introduced in Chapter 2.1.4. These three datasets were chosen for several factors:

1. They are all open source datasets that are publicly available and easily accessible.

2. They use the same EEG topographic standard (i.e. the international 10-10 system).

3. They all use a non-invasive approach to EEG signals acquisition and they all use the BCI2000 system [2] to collect and store EEG signals.

Table 5.2 summarises the three datasets. It can be seen that BCI109 has the largest number of EEG signals and the earliest acquisition year. Fig. 5.2 shows the results of the analysis of the autocorrelation coefficients for the three EEG datasets. The x-axis represents the threshold of the autocorrelation coefficient and the y-axis represents the percentage of the number of EEG signals that has a correlation coefficient greater than the corresponding x-axis threshold ω at lag time 1 s. It can be seen that as the threshold of the correlation coefficient increases, the number of eligible EEG signals for all three datasets decreases. Furthermore, the percentage of the BCI109 dataset is lower than the percentage of the other two datasets (i.e. MI52 and GAL12) under different ω. The reason is that with

the progress of EEG acquisition equipment over time, the acquisition equipment of the other two datasets can obtain the EEG signals with higher autocorrelation coefficients at the same lag time. In other words, the acquisition equipment of the other two datasets can collect EEG signals containing more non-random information and richer spectrum information. In addition, when the autocorrelation coefficient of the signal is greater than 0.7, the signal has a high correlation at its corresponding lag time [124]. The details of EEG signals with high correlation at a lag time of 1 s in the three datasets are shown in Table 5.3. These selected EEG signals will be used in the following experiments.

5.3 EEG Dominant Frequency Tracking

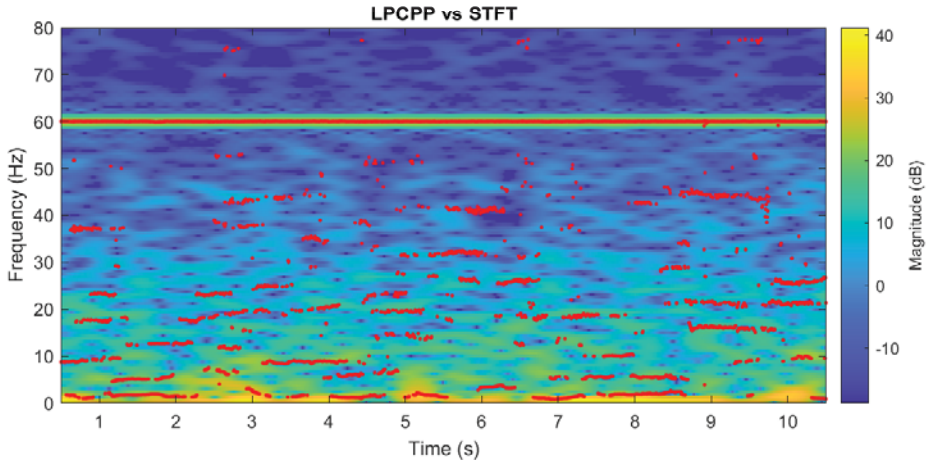

Fig. 5.3 The time-frequency analysis of the LPCPP method and the STFT method for an EEG signal.

An example is presented to achieve real-time tracking of dominant frequencies in an EEG signal by using the proposed EEG spectral analysis framework. Fig. 5.3 shows the time-frequency analysis of a 10 s EEG signal. This EEG signal is from the 104th subject in the dataset BCI109. The sampling frequency of the BCI109 is 160 Hz, the duration

of the window signal is 1 s and the step size is 1 sample (i.e. the length of overlap is 159 samples). The LPCPP method and the STFT method are used in this example. The parameters of the LPCPP method are $P = 40$, $\beta = 0.4$ and $\lambda = 5$ Hz. In Fig. 5.3, the red dots represent the frequency estimates of the LPCPP method at each sampling instant. For the STFT method, the window function is the Hanning window and the number of DFT (Discrete Fourier Transform) points is 256. It can be seen that the LPCPP method can directly give the dominant frequency estimations at each sample instant. In addition, since the frequency estimations of the LPCPP method are in numerical form, the LPCPP method is ideally suited to observe the EEG dominant frequency change in real-time. The STFT method is an example of a waveform time-frequency method that can indicate how the energy of the signal is distributed over the time-frequency plane. Furthermore, both the LPCPP method and the STFT method can identify the AC power supply frequency of 60 Hz. Moreover, it can be seen that most of the EEG spectrum activity is between 0 and 50 Hz which is also one of the reasons why the analysis of the EEG centre frequency in section 5.4 focuses on the range between 0 and 50 Hz. In short, the LPCPP method is a parameterised time-frequency method that can realise the real-time tracking of the spectrum features of dynamic EEG signals.

5.4 EEG Centre Frequency Analysis

The EEG signal is divided into a number of fixed frequency bands (i.e. Delta, Theta, Alpha, Beta and Gamma). However, different researchers have defined different frequencies for these bands with little consensus between them which has significant conse-

quences for EEG interpretation [45, 46, 47, 48, 49, 50]. Furthermore, the EEG spectral activity should not be limited by fixed frequency boundaries. In this section, a new framework of centre frequencies will be proposed to replace the fixed EEG frequency bands.

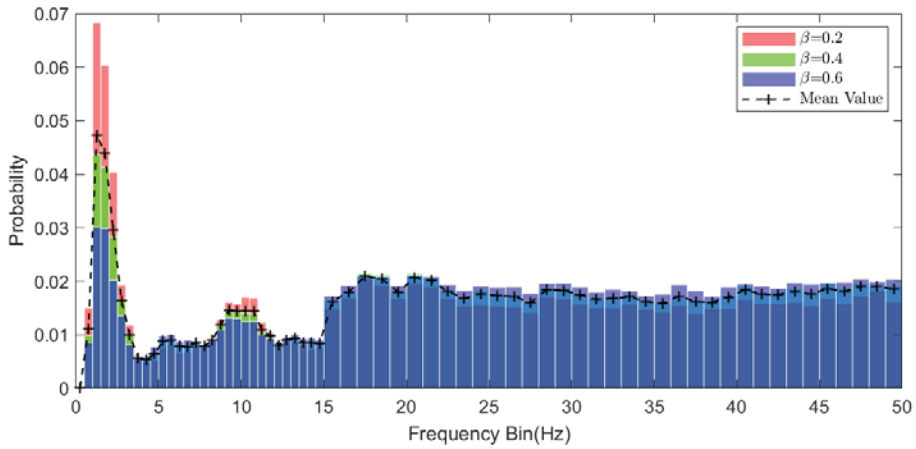

Fig. 5.4 DPDF of the BCI09 dataset at the different β values.

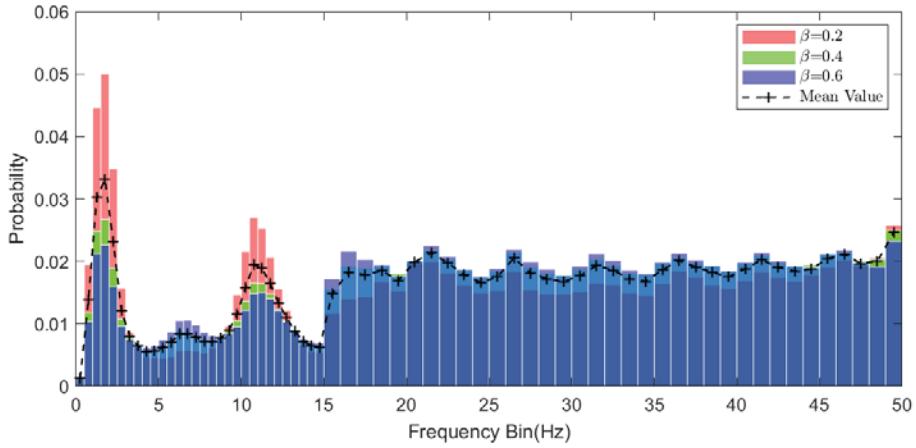

Fig. 5.5 DPDF of the MI52 dataset at the different β values.

Since the LPCPP method is a parameterised time-frequency method that can provide a series of numerical dominant frequency estimates, the method can generate a DPDF (Discrete Probability Density Function) which is a distribution of the dominant frequencies in the frequency domain. The duration of the window is 1 s and the overlap is 0.

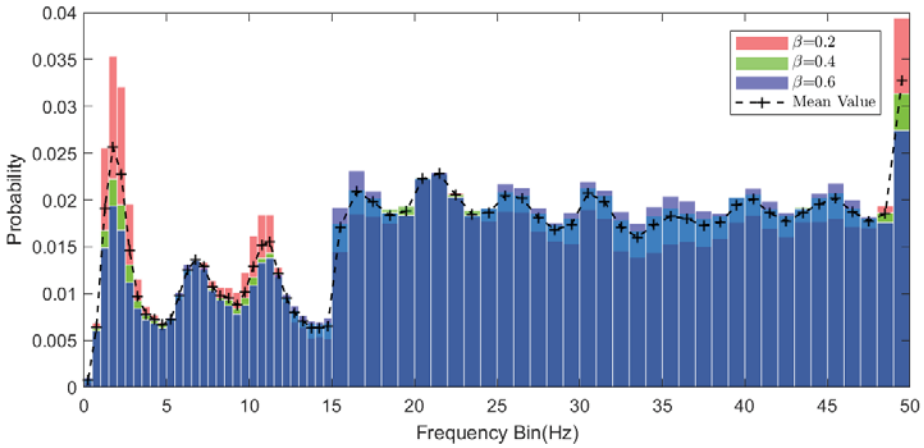

Fig. 5.6 DPDF of the GAL12 dataset at the different β values.

In addition, the three datasets (i.e. CI109, MI52 and GAL12) have different sampling frequencies. Due to the maximum frequency determined by the Nyquist limit, the different EEG datasets have different frequency domain ranges. Furthermore, clinical medicine shows that conventional EEG spectra activity exists between 0.5-30 Hz [39]. Moreover, the experiments in the latter Section 5.3 show that the EEG spectral activity range is mainly between 0 and 50 Hz and this frequency range can also meet the experimental requirements. Therefore, the frequency range of the DPDF of the three EEG datasets is 0-50 Hz. For a more detailed frequency distribution of DPDF from 0 to 15 Hz, the bin size is 0.5 Hz. From 15 to 50 Hz, the bin size is 1 Hz. Moreover, in order to reduce the effect of different sampling frequencies on the LPCPP method, the filter order of the LPCPP method on different datasets is different. The filter order of BCI109 is 40 and the filter order of the other two datasets is 100. Fig. 5.4,Fig. 5.5 and Fig. 5.6 show the DPDF results of the three EEG datasets at different β values (i.e. 0.2, 0.4 and 0.6), respectively. The mean values for different β values for each dataset are calculated and they are represented by black dashed lines. As can be seen, the DPDFs of the three datasets have three

significant peaks between 0 and 15 Hz and the peaks of the mean values are considered as a series of EEG centre frequencies. The median value of the bin corresponding to the three peaks of the mean value is the corresponding centre frequency. For the BCI109 dataset, the first three peaks of the mean values are 1.25 Hz, 5.75 Hz and 10.75 Hz. For the MI52 dataset, the first three peaks are 1.75 Hz, 6.25 Hz and 10.75 Hz. It is particularly noticeable that the DPDFs of the MI52 dataset have a distinct peak at the bin 49-50 Hz. The reason is that the AC power supply frequency of the MI52 dataset is 50 Hz. Furthermore, the first three peaks of the GAL 12 dataset are 1.75 Hz, 6.75 Hz and 10.75 Hz. Although the three peaks in the different datasets are not exactly the same, their third peaks are all at 10.75 Hz. Moreover, the difference between the first peaks of the three datasets and the difference between the second peaks of the three datasets does not exceed the bin size (i.e. 0.5 Hz).

The above experiments independently analyse the DPDFs of the three EEG datasets. Furthermore, Fig. 5.7(a) shows the DPDFs for three EEG dataset. The β value of the LPCPP method for the BCI09 dataset is 0.4 and the β of the other two datasets is selected as 0.2. The reason for choosing these β values is that these β values can produce more significant peaks in the DPDF of the corresponding EEG dataset. Furthermore, the mean value of the DPDFs for the three datasets is calculated. The three peaks for these DPDFs are 1.75 Hz, 6.75 Hz and 10.75 Hz. Fig. 5.7(b) shows the maximum frequency range of different EEG waves (i.e. Delta, Theta, Alpha, Beta and Gamma) from 108 EEG studies [26]. It can be seen that the first peak 1.75 Hz corresponds to the EEG spectral activity in the Delta band, the second peak 6.75 Hz corresponds to the EEG activity in the Theta band and the third peak 10.75 Hz corresponds to the EEG spectral activity in the Alpha

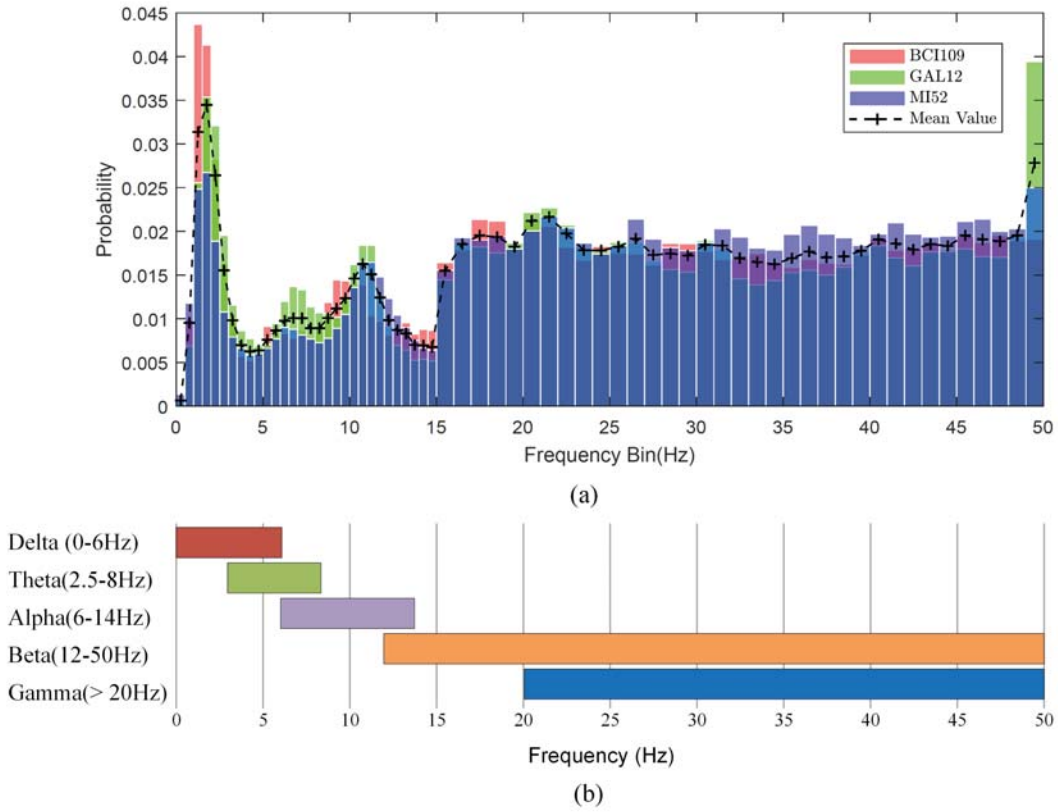

Fig. 5.7 Centre frequency analysis of DPDF for different the EEG datasets.

band. Furthermore, the rest of the frequency bands (i.e. 15 to 50 Hz) in the DPDF analysis without significant peaks correspond to EEG spectral activity in the Beta and Gamma bands.

5.5 Chapter Summary

In this section, a new EEG spectral analysis framework involving the LPCPP method was proposed and three EEG datasets were used for analysis. The first step of this framework is to use the autocorrelation method to eliminate excessively noisy signals from the signal sets. It can be observed that compared with the BCI109 dataset, the latest two

datasets (i.e. MI52 and GAL12) have larger autocorrelation coefficients at the same lag time. Furthermore, EEG signals with autocorrelation coefficients greater than 0.7 at a lag time of 1 s were selected for the further EEG spectra analysis. In addition, this framework presents an example of real-time tracking of EEG dominant frequencies. Compared with the transform-based time-frequency analysis method of STFT, the LPCPP method can provide parameterised frequency estimation and this method can more intuitively observe the dynamic change of the dominant frequency. Furthermore, the dominant spectral activity of the EEG can be found in the range of 0 to 50 Hz. Finally, the DPDFs of the three EEG datasets were analysed separately and three significant peaks between 0 and 15 Hz were found. There is a great deal of variability and difference in opinion as to the specific EEG frequency range that defines each band. The DPDFs of the three datasets can identify three common peaks (i.e. 1.75 Hz, 6.75 Hz and 10.75 Hz) as the three centre frequencies to describe the EEG dominant spectral activity. Furthermore, these three centre frequencies correspond to the EEG activity in the EEG Delta, Theta and Alpha bands, respectively. Compared to fixed EEG bands, EEG centre frequencies can describe the statistical distribution of the wave frequencies. The spectral activity of the EEG depends on the activity being performed by the subject and is not restricted by a series of fixed frequency bands.

Chapter 6

Summary and Future Work

This chapter will summarise the research work of this thesis and propose a series of future research topics. This chapter is organised as follows. The contributions and achievements of this thesis are summarised in the first section. As already discussed, the EEG signal is a high-complexity bioelectric signal, typically characterized by a poor signal-to-noise ratio, whose frequency is time-varying, intermittent and contains multiple frequency components. A robust and time-resolved spectral analysis method for EEG signals is required for its use in BCI systems. The objective of the thesis is to improve the analysis of EEG signals. A new method called Linear Predictive Coding Pole Processing (LPCPP) method was developed which is particularly suited to EEG signal analysis. The LPCPP method can enhance frequency estimation and realise real-time dominant frequency tracking. Furthermore, it has a high noise tolerance and can greatly improve upon spectral resolution of the LPC method. Furthermore, a new EEG spectra analysis framework was proposed using the LPCPP method and this framework has two benefits for EEG spectra analysis. The first one is to observe the dynamic changes in the EEG signal spectra activity in real-time.

The second one is to propose a new spectral analysis framework to describe the dominant spectral activity region of the EEG instead of the fixed EEG frequency bands. In short, this thesis focused on analysing the spectral information of EEG signals and proposed a new parameterised time-frequency analysis LPCPP method which can realise enhanced identification and real-time tracking of the dominant frequencies of the signal. In the second section, some open questions are raised about the LPCPP method and the EEG analysis. The LPCPP method still has some limitations that need to be considered in future work, such as adaptive tuning of the LPCPP parameters (i.e. β and λ). Furthermore, the LPCPP method is ideally suited to its integration into machine learning-based systems and some BCI applications incorporating the LPCPP method can be developed in the future. Finally, details of the publications and other publicly available materials resulting from this work are listed.

6.1 Summary of Contributions and Achievements

The EEG signal can be used to track and record brain wave patterns. It has been widely used in various BCI applications, such as medical rehabilitation, smart home, education and training, etc. However, EEG signals exhibit many of the typical characteristics of biological signals:

- EEG is a high-noise signal. Its acquisition is always accompanied by various kinds of noise, including biological noise and environmental noise.

- EEG is a time-varying signal. EEG signal responds to human brain activity (emotion, cognitive, etc.) and these brain activities depend on the activity of the subject and they vary over time.

- EEG is an intermittent signal. The spectral components of EEG signals are intermittent because the appearance and disappearance of certain brain activities is dynamic.

- EEG is a multi-component signal. EEG signal has been divided into different frequency components (i.e. Delta, Theta, Alpha, Beta and Gamma) to reflect their corresponding brain activities.

Therefore, the ability to track the dominant frequency changes in real-time is important for studying EEG signals to observe the dynamics of brain activities. Time-frequency methods provide a way to analyse the frequency dynamics in EEG signals. Furthermore, there are some requirements for time-frequency analysis methods to analyse EEG signals:

- The method should be a parameterised method. Biomedical researchers are more interested in establishing significant levels of electrical activity across the defined wave bands (i.e. Delta, Theta, Alpha, Beta and Gamma). Many time-frequency methods are spectrum waveform (not parameterised) methods, they can tell whether a certain frequency component exists or not at any given time interval. However, it is still a challenge in analysing multi-component signals to realise the separation of the spectrum components when they are overlapped in the time-frequency plane. The parameterised time-frequency method can produce numerical dominant frequency estimates and it is well suited to multi-components signal processing (i.e. EEG signals).

- The method should provide higher spectral resolution and enable real-time observation of dynamic EEG dominant spectra. The Heisenberg-Gabor Uncertainty Principle indicates that there is a trade-off relationship between time resolution and frequency resolution. When the time-frequency analysis method has a smaller TBP (Time-bandwidth Product) value, it can provide a higher frequency resolution at the same time duration (i.e. time resolution). Similarly, it can provide a higher time resolution at the same frequency resolution. Therefore, the time-frequency analysis methods with a smaller TBP value are required for real-time analysis of dynamic EEG frequencies.

- The method requires a high tolerance for noise. It needs to have a robust performance in high noise environments.

Therefore, in this thesis, a new parameterised time-frequency method called the LPCPP method has been proposed which can be used for identifying and tracking the dominant frequency components of an EEG signal.

In the previous chapters, the ability of the LPCPP method to identify and track the dominant frequency of a signal was analysed in detail. It is well suited to EEG signal processing. Furthermore, a new definition of TBP (Time-bandwidth Product) for the parameterised time-frequency methods was proposed and the results showed that the LPCPP method can provide a higher spectral resolution in signal analysis. In addition, a new EEG spectrum analysis framework including the LPCPP method was proposed. The LPCPP method can realise real-time tracking of the dominant frequencies of EEG signals which helps us to observe the dynamic changes of the EEG spectra over time.

Furthermore, a series of new EEG centre frequencies have been proposed which can more accurately represent the spectral activity of EEG without being restricted to the boundaries of fixed frequency bands. Specifically, the detailed contributions of this thesis are summarised as follows:

1. The LPCPP method can achieve enhanced identification of the dominant frequency. A PRVF (Pseudo-Randomly Varying Frequency) signal was used for the experimental analysis and four metrics (i.e. AEP, IFP, VEP and IEP) were used to analyse the performance of the LPCPP method to identify the dominant frequencies. The results showed that the majority of the frequency estimates of LPCPP are valid and are more accurate than the estimates of LPC. This is particularly useful for applications where it is required to identify the dominant frequencies of an unknown signal (e.g. EEG). Furthermore, the LPCPP method is more robust to noise.

2. The LPCPP method can achieve real-time dominant frequency tracking. An LCFM (Linear Chirped Frequency Modulation) signal was used to simulate signals with different frequency change rates. The results showed that the LPCPP method outperforms LPC under time-varying signals and it significantly reduces the redundant frequency estimates of LPC.

3. The LPCPP method can provide a higher spectra resolution than that of LPC. A series of 10,000 Monte Carlo experiment trials were used to generate an EPDF (Error Probability Density Function) of the error associated with the frequency estimate. The mean and standard deviation of the EPDF were used to define the bias μ and frequency resolution Δf for the parameterised time-frequency method (i.e. LPC

and LPCPP). This resulted in a new definition of TBP (Time-bandwidth Product) for the LPC-based method was proposed. The results showed that the LPCPP method can provide a lower time-bandwidth product than the LPC method and it can significantly reduce the bias of the LPC method in the low and high-frequency intervals.

4. Real-time EEG dominant frequency tracking. Compared with the waveform time-frequency analysis method of STFT, the LPCPP method can provide parameterised frequency estimation and it can directly observe the dynamic change of the dominant frequency.

5. EEG centre frequency analysis. Three public EEG datasets (i.e., BCI109, MI52 and GAL12) collected from 173 subjects with a total EEG acquisition duration of more than 100 hours were used here. The autocorrelation method was used to eliminate excessively noisy signals from the signal sets. Furthermore, a series of new EEG centre frequencies were proposed to describe the concentrated frequency of EEG activity from a statistical point of view. Specifically, the first three centre frequencies 1.75 Hz, 6.75 Hz and 10.75 Hz correspond to EEG spectral activity in the Delta, Theta and Alpha frequency bands, respectively. These EEG frequencies are not confined to a fixed band and they should not be restricted by the classification of frequency bands. The EEG centre frequencies can more accurately describe the spectral activity of EEG and they can highlight the dynamic changes of the dominant spectrum components in the EEG signal.

In the next section, some open problems and the future work for this thesis will be discussed.

6.2 Open Problems and Future Work

The LPCPP method is particularly suited to EEG processing. However, there are still a number of shortcomings associated with the LPCPP method. For example, the parameters (i.e. β and λ) of the LPCPP method need to be manually adjusted which can be time-consuming and can result in ambiguous results. Furthermore, the EEG signal is a dynamic signal whose spectral activity changes with time, an adaptive automatic EEG processing method is required for the BCI application. Therefore, this section introduces some of the research directions which are closely related to the work in this thesis and appear promising for future work.

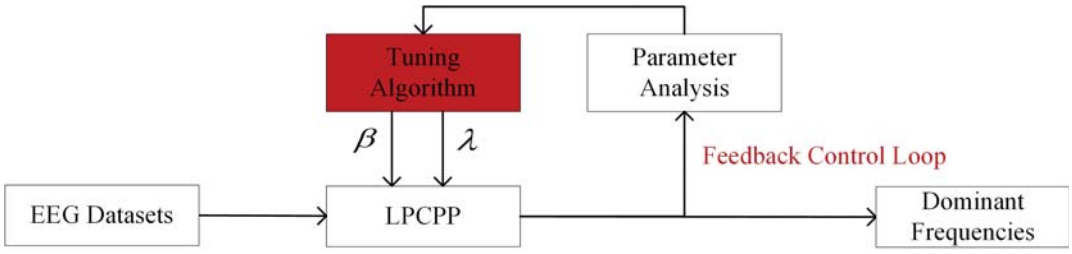

Fig. 6.1 The feedback control loop system for the ELPCPP method.

A. The Enhanced LPCPP (ELPCPP) Method. With the continuous popularity of BCI applications, an automated method is necessary for large-scale EEG data processing, especially automated methods that are more efficient and are less error-prone than manual methods in dealing with big data. The Enhanced LPCPP (ELPCPP) method could be considered in future work to overcome these current limitations to realise the automated setting of these parameters. An algorithm capable of adaptively tuning the LPCPP parameters is required in order to fully automate the settings of these parameters [125, 126]. The ELPCPP method could initially consider using a classic feedback control loop system to

realise the automatic setting of the LPCPP parameters. The diagram of the ELPCPP method is shown in Fig. 6.1. There are two steps in this system: The first step is to analyse the parameters of the LPCPP method (i.e. β and λ). The second step is the tuning algorithm to automatically set the parameters which are indicated by the red box in Fig. 6.1. The choice of the parameters depends on the filter order, the noise level and the application scenarios (e.g. the EEG signals). The behaviors of these parameters are as follows:

- If the value of β is too large, it will cause the number of dominant poles to increase which may cause the LPCPP method to produce too many redundant frequency estimates. Conversely, if the value of β is too small, the number of dominant poles will decrease and the LPCPP method may not be able to identify all of the dominant signal frequencies. This is a trade-off required in the choice of the β parameter value.

- If the value of λ is too large, it will lead to an associated pole whose frequency is too far away from the dominant pole and it will cause a deviation in the frequency estimation. Conversely, if the value of λ is too small, it will cause some non-dominant poles not to be considered in the final frequency estimates and it will cause some loss of spectral information.

In addition, the greater the noise level and the filter order, the smaller the value of β required to filter out the non-dominant poles to identify the dominant poles and the value of λ needs to be increased to avoid loss of spectral information. Similarly, when the number of frequencies that are needed to be identified increases, the value of β needs to

increase to find more dominant poles. The frequency estimates generated by this ELPCPP method could be more consistent and could be generated in a timely manner to enable its use in BCI applications. In summary, the ELPCPP method can be a highly adaptive automatic method that can automatically set the experimental parameters and realise real-time EEG dominant frequency tracking.

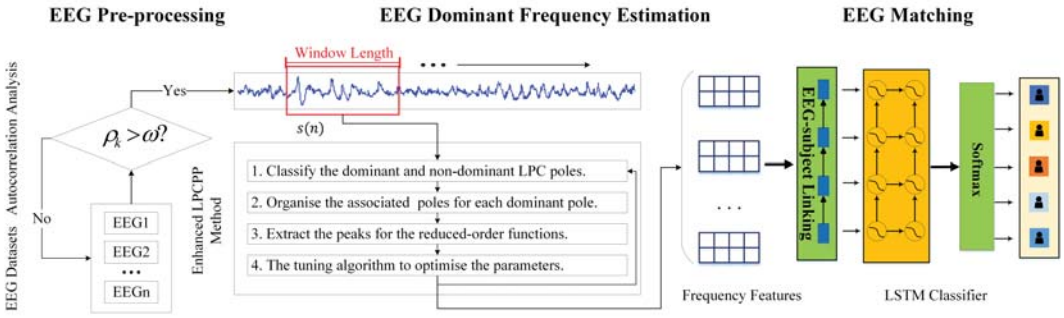

Fig. 6.2 The overview of the EEG applications for EEG-based human activity recognition.

B. Demonstration in EEG Applications. An EEG application involving the LPCPP method can be developed in future work to realise the EEG-based human activity recognition. A real-world EEG application to realise EEG-based human activity recognition that can help in delivering the BCI technique out of the laboratory and into the real world. Fig. 6.2 shows an overview of the framework to achieve EEG-based human activity recognition. There are three steps for this EEG analysis framework: The first step is EEG pre-processing. The autocorrelation method is used to select the EEG signals which contain rich spectral information. The second step is EEG dominant frequency estimation. The raw EEG signal will be separated into a fixed-length window signal and each window signal is processed by the LPCPP method to estimate the dominant frequencies which will be considered as the frequency features of the EEG signals. The last step is to realise

the EEG matching. A deep learning algorithm called Long Short-Term Memory (LSTM) method could be used to achieve EEG-based activity recognition. Machine and deep learning-based algorithms are the emerging approaches to addressing prediction problems in time series. The LSTM algorithm is a special type of Recurrent Neural Networks (RNN) model which is suitable for modeling time-series data [127, 128, 129, 130, 131]. Therefore, the LSTM method could be considered to realise the EEG-based activity recognition. The proposed new LPCPP method can be used for continuous EEG signal monitoring to observe and track changes in EEG signals to support clinical diagnosis. For example, EEG signals can be used for real-time emotion [132] and attention [133, 134] monitoring. The LPCPP method can directly give robust numerical frequency estimates compared to the waveform time-frequency analysis method (e.g. short-time Fourier transform and continuous wavelet transform) and these frequency estimates can be used to monitor changes in the EEG signal to observe its real-time spectral activity. In addition, EEG still has many applications in BCI systems, such as medical rehabilitation [135, 136, 137, 138, 139], smart home [140, 141, 142, 143], education [144, 145, 146, 147] and training [148, 149, 150, 151, 152], etc. It has the potential to become a potentially powerful tool in the field of EEG research and BCI applications.

C. Other Potential Applications for LPCPP. The LPCPP method was proposed for the spectral analysis of EEG and it shows excellent performance in the processing of time-varying, high-noise and multi-component data. Furthermore, spectral features are important for the study of many applications, such as speech analysis [153, 154, 155, 156, 157, 158], mechanical vibration analysis [159, 160, 161, 162], seismographic anal-

ysis [163, 164, 165, 166, 167, 168, 169] and image analysis [170, 171, 172, 173]. The LPCPP method is a parameterised time-frequency method that can provide the numerical dominant spectral features and is therefore ideally suited to its integration into machine learning-based systems. It has the potential to become a useful general tool in the field of signal processing.

Bibliography

[1] G. Pfurtscheller, C. Neuper, C. Guger, W. Harkam, H. Ramoser, A. Schlogl, B. Obermaier, and M. Pregenzer, "Current trends in Graz brain-computer interface (BCI) research," *IEEE Transactions on Rehabilitation Engineering*, vol. 8, no. 2, pp. 216–219, 2000.

[2] G. Schalk, D. J. McFarland, T. Hinterberger, N. Birbaumer, and J. R. Wolpaw, "BCI2000: a general-purpose brain-computer interface (BCI) system," *IEEE Transactions on Biomedical Engineering*, vol. 51, no. 6, pp. 1034–1043, 2004.

[3] E. Buch, C. Weber, L. G. Cohen, C. Braun, M. A. Dimyan, T. Ard, J. Mellinger, A. Caria, S. Soekadar, A. Fourkas, *et al.*, "Think to move: a neuromagnetic brain-computer interface (BCI) system for chronic stroke," *Stroke*, vol. 39, no. 3, pp. 910–917, 2008.

[4] G. Edlinger, B. Z. Allison, and C. Guger, "How many people can use a BCI system?," *Clinical Systems Neuroscience*, pp. 33–66, 2015.

[5] S. Selim, M. M. Tantawi, H. A. Shedeed, and A. Badr, "A CSP\AM-BA-SVM approach for motor imagery BCI system," *IEEE Access*, vol. 6, pp. 49192–49208, 2018.

[6] M. K. Kumar, B. Parameshachari, S. Prabu, and S. liberata Ullo, "Comparative analysis to identify efficient technique for interfacing BCI system," in *IOP Conference Series: Materials Science and Engineering*, vol. 925, p. 012062, IOP Publishing, 2020.

[7] J. W. Britton, L. C. Frey, J. L. Hopp, P. Korb, M. Z. Koubeissi, W. E. Lievens, E. M. Pestana-Knight, and E. L. St, *Electroencephalography (EEG): An Introductory Text and Atlas of Normal and Abnormal Findings in Adults, Children, and Infants*. American Epilepsy Society, Chicago, 2016.

[8] G. Ramantani, L. Maillard, and L. Koessler, "Correlation of invasive EEG and scalp EEG," *Seizure*, vol. 41, pp. 196–200, 2016.

[9] F. A. Azevedo, L. R. Carvalho, L. T. Grinberg, J. M. Farfel, R. E. Ferretti, R. E. Leite, W. J. Filho, R. Lent, and S. Herculano-Houzel, "Equal numbers of neuronal and nonneuronal cells make the human brain an isometrically scaled-up primate brain," *Journal of Comparative Neurology*, vol. 513, no. 5, pp. 532–541, 2009.

[10] L. J. Hirsch, "Continuous EEG monitoring in the intensive care unit: an overview," *Journal of clinical neurophysiology*, vol. 21, no. 5, pp. 332–340, 2004.

[11] H. H. Jasper, "The ten-twenty electrode system of the international federation," *Electroencephalogr. Clin. Neurophysiol.*, vol. 10, pp. 370–375, 1958.

[12] G. Chatrian, E. Lettich, and P. Nelson, "Ten percent electrode system for topographic studies of spontaneous and evoked EEG activities," *American Journal of EEG technology*, vol. 25, no. 2, pp. 83–92, 1985.

[13] R. W. Homan, J. Herman, and P. Purdy, "Cerebral location of international 10–20 system electrode placement," *Electroencephalography and Clinical Neurophysiology*, vol. 66, no. 4, pp. 376–382, 1987.

[14] U. Herwig, P. Satrapi, and C. Schönfeldt-Lecuona, "Using the international 10-20 EEG system for positioning of transcranial magnetic stimulation," *Brain Topography*, vol. 16, no. 2, pp. 95–99, 2003.

[15] R. Oostenveld and P. Praamstra, "The five percent electrode system for high-resolution EEG and ERP measurements," *Clinical Neurophysiology*, vol. 112, no. 4, pp. 713–719, 2001.

[16] V. Jurcak, D. Tsuzuki, and I. Dan, "10/20, 10/10, and 10/5 systems revisited: their validity as relative head-surface-based positioning systems," *Neuroimage*, vol. 34, no. 4, pp. 1600–1611, 2007.

[17] P. Giacometti, K. L. Perdue, and S. G. Diamond, "Algorithm to find high density EEG scalp coordinates and analysis of their correspondence to structural and functional regions of the brain," *Journal of Neuroscience Methods*, vol. 229, pp. 84–96, 2014.

[18] G. Repovs, "Dealing with noise in EEG recording and data analysis," in *Informatica Medica Slovenica*, vol. 15, pp. 18–25, 2010.

[19] W. Zhou and J. Gotman, "Removal of EMG and ECG artifacts from EEG based on wavelet transform and ICA," in *The 26th Annual International Conference of the IEEE Engineering in Medicine and Biology Society*, vol. 1, pp. 392–395, IEEE, 2004.

[20] A. G. Correa, E. Laciar, H. Patiño, and M. Valentinuzzi, "Artifact removal from EEG signals using adaptive filters in cascade," in *Journal of Physics: Conference Series*, vol. 90, p. 012081, IOP Publishing, 2007.

[21] S. P. Fitzgibbon, D. M. Powers, K. J. Pope, and C. R. Clark, "Removal of EEG noise and artifact using blind source separation," *Journal of Clinical Neurophysiology*, vol. 24, no. 3, pp. 232–243, 2007.

[22] C.-Y. Chang, S.-H. Hsu, L. Pion-Tonachini, and T.-P. Jung, "Evaluation of artifact subspace reconstruction for automatic EEG artifact removal," in *2018 40th Annual International Conference of the IEEE Engineering in Medicine and Biology Society (EMBC)*, pp. 1242–1245, IEEE, 2018.

[23] X. Jiang, G.-B. Bian, and Z. Tian, "Removal of artifacts from EEG signals: a review," *Sensors*, vol. 19, no. 5, p. 987, 2019.

[24] A. Delorme, T. Sejnowski, and S. Makeig, "Enhanced detection of artifacts in EEG data using higher-order statistics and independent component analysis," *Neuroimage*, vol. 34, no. 4, pp. 1443–1449, 2007.

[25] M. R. N. Kousarrizi, A. A. Ghanbari, M. Teshnehlab, M. A. Shorehdeli, and A. Gharaviri, "Feature extraction and classification of EEG signals using Wavelet transform, SVM and artificial neural networks for brain computer interfaces," in *2009 International Joint Conference on Bioinformatics, Systems Biology and Intelligent Computing*, pp. 352–355, IEEE, 2009.

[26] J. J. Newson and T. C. Thiagarajan, "EEG frequency bands in psychiatric disorders: a review of resting state studies," *Frontiers in Human Neuroscience*, vol. 12, p. 521, 2019.

[27] H. Cho, M. Ahn, S. Ahn, M. Kwon, and S. C. Jun, "EEG datasets for motor imagery brain–computer interface," *GigaScience*, vol. 6, no. 7, p. gix034, 2017.

[28] C. A. Majmudar, R. Mahajan, and B. I. Morshed, "Real-time hybrid ocular artifact detection and removal for single channel EEG," in *2015 IEEE International Conference on Electro/Information Technology (EIT)*, pp. 330–334, IEEE, 2015.

[29] K. Asaduzzaman, M. Reaz, F. Mohd-Yasin, K. Sim, and M. Hussain, "A study on discrete wavelet-based noise removal from EEG signals," in *Advances in Computational Biology*, pp. 593–599, Springer, 2010.

[30] M. Rohál'ová, P. Sykacek, M. Koskaand, and G. Dorffner, "Detection of the EEG Artifacts by the Means of the (Extended) Kalman Filter," *Meas. Sci. Rev*, vol. 1, no. 1, pp. 59–62, 2001.

[31] F. Amzica and M. Steriade, "Electrophysiological correlates of sleep delta waves," *Electroencephalography and Clinical Neurophysiology*, vol. 107, no. 2, pp. 69–83, 1998.

[32] G. Tinguely, L. A. Finelli, H.-P. Landolt, A. A. Borbély, and P. Achermann, "Functional EEG topography in sleep and waking: state-dependent and state-independent features," *Neuroimage*, vol. 32, no. 1, pp. 283–292, 2006.

[33] C. J. Davis, J. M. Clinton, K. A. Jewett, M. R. Zielinski, and J. M. Krueger, "Delta wave power: an independent sleep phenotype or epiphenomenon?," *Journal of Clinical Sleep Medicine*, vol. 7, no. 5 Suppl, pp. S16–S18, 2011.

[34] D. L. Schacter, "EEG theta waves and psychological phenomena: A review and analysis," *Biological Psychology*, vol. 5, no. 1, pp. 47–82, 1977.

[35] M. Grunwald, T. Weiss, W. Krause, L. Beyer, R. Rost, I. Gutberlet, and H.-J. Gertz, "Power of theta waves in the EEG of human subjects increases during recall of haptic information," *Neuroscience Letters*, vol. 260, no. 3, pp. 189–192, 1999.

[36] W. Klimesch, "EEG alpha and theta oscillations reflect cognitive and memory performance: a review and analysis," *Brain Research Reviews*, vol. 29, no. 2-3, pp. 169–195, 1999.

[37] M. Teplan *et al.*, "Fundamentals of EEG measurement," *Measurement Science Review*, vol. 2, no. 2, pp. 1–11, 2002.

[38] O. Bazanova and D. Vernon, "Interpreting EEG alpha activity," *Neuroscience & Biobehavioral Reviews*, vol. 44, pp. 94–110, 2014.

[39] C. S. Nayak and A. C. Anilkumar, *EEG Normal Waveforms*. StatPearls Publishing, Treasure Island (FL), 2021.

[40] J. Holz, H. Piosczyk, B. Feige, K. Spiegelhalder, C. Baglioni, D. Riemann, and C. Nissen, "EEG sigma and slow-wave activity during NREM sleep correlate with overnight declarative and procedural memory consolidation," *Journal of Sleep Research*, vol. 21, no. 6, pp. 612–619, 2012.

[41] M. Gola, M. Magnuski, I. Szumska, and A. Wróbel, "EEG beta band activity is related to attention and attentional deficits in the visual performance of elderly subjects," *International Journal of Psychophysiology*, vol. 89, no. 3, pp. 334–341, 2013.

[42] M. Host'oveckỳ and B. Babušiak, "Brain activity: beta wave analysis of 2D and 3D serious games using EEG," *Journal of Applied Mathematics, Statistics and Informatics*, vol. 13, no. 2, pp. 39–53, 2017.

[43] N. S. Kort, P. Cuesta, J. F. Houde, and S. S. Nagarajan, "Bihemispheric network dynamics coordinating vocal feedback control," *Human Brain Mapping*, vol. 37, no. 4, pp. 1474–1485, 2016.

[44] M. Li and B.-L. Lu, "Emotion classification based on gamma-band EEG," in *2009 Annual International Conference of the IEEE Engineering in Medicine and Biology Society*, pp. 1223–1226, IEEE, 2009.

[45] G. Deuschl, "Recommendations for the practice of clinical neurophysiology," *Guidelines of the International Federation of Clinical Neurophysiology*, 1999.

[46] H. Adeli, S. Ghosh-Dastidar, and N. Dadmehr, "A wavelet-chaos methodology for analysis of EEGs and EEG subbands to detect seizure and epilepsy," *IEEE Transactions on Biomedical Engineering*, vol. 54, no. 2, pp. 205–211, 2007.

[47] R. Ferri, F. Rundo, O. Bruni, M. G. Terzano, and C. J. Stam, "The functional connectivity of different EEG bands moves towards small-world network organization during sleep," *Clinical Neurophysiology*, vol. 119, no. 9, pp. 2026–2036, 2008.

[48] J. C. de Munck, S. I. Gonçalves, R. Mammoliti, R. M. Heethaar, and F. L. Da Silva, "Interactions between different EEG frequency bands and their effect on alpha–fMRI correlations," *Neuroimage*, vol. 47, no. 1, pp. 69–76, 2009.

[49] W.-L. Zheng and B.-L. Lu, "Investigating critical frequency bands and channels for EEG-based emotion recognition with deep neural networks," *IEEE Transactions on Autonomous Mental Development*, vol. 7, no. 3, pp. 162–175, 2015.

[50] M. Abo-Zahhad, S. M. Ahmed, and S. N. Abbas, "A new EEG acquisition protocol for biometric identification using eye blinking signals," *International Journal of Intelligent Systems and Applications*, vol. 7, no. 6, p. 48, 2015.

[51] R. J. Riding, A. Glass, S. R. Butler, and C. W. Pleydell-Pearce, "Cognitive style and individual differences in EEG alpha during information processing," *Educational Psychology*, vol. 17, no. 1-2, pp. 219–234, 1997.

[52] S. N. A. Seha and D. Hatzinakos, "EEG-based human recognition using steady-state aeps and subject-unique spatial filters," *IEEE Transactions on Information Forensics and Security*, vol. 15, pp. 3901–3910, 2020.

[53] X. Huang, S. Altahat, D. Tran, and D. Sharma, "Human identification with electroencephalogram (EEG) signal processing," in *2012 International symposium on communications and information technologies (ISCIT)*, pp. 1021–1026, IEEE, 2012.

[54] A. R. Clarke, R. J. Barry, R. McCarthy, and M. Selikowitz, "Age and sex effects in the EEG: development of the normal child," *Clinical neurophysiology*, vol. 112, no. 5, pp. 806–814, 2001.

[55] O. Vysata, J. Kukal, A. Prochazka, L. Pazdera, J. Simko, and M. Valis, "Age-related changes in EEG coherence," *Neurologia i neurochirurgia polska*, vol. 48, no. 1, pp. 35–38, 2014.

[56] P. J. Marshall, Y. Bar-Haim, and N. A. Fox, "Development of the EEG from 5 months to 4 years of age," *Clinical neurophysiology*, vol. 113, no. 8, pp. 1199–1208, 2002.

[57] A. L. Goldberger, L. A. Amaral, L. Glass, J. M. Hausdorff, P. C. Ivanov, R. G. Mark, J. E. Mietus, G. B. Moody, C.-K. Peng, and H. E. Stanley, "Physiobank, physiotoolkit, and physionet: components of a new research resource for complex physiologic signals," *Circulation*, vol. 101, no. 23, pp. e215–e220, 2000.

[58] M. D. Luciw, E. Jarocka, and B. B. Edin, "Multi-channel EEG recordings during 3,936 grasp and lift trials with varying weight and friction," *Scientific Data*, vol. 1, no. 1, pp. 1–11, 2014.

[59] M. Akin, "Comparison of wavelet transform and FFT methods in the analysis of EEG signals," *Journal of Medical Systems*, vol. 26, no. 3, pp. 241–247, 2002.

[60] M. M. Shaker, "EEG waves classifier using wavelet transform and Fourier transform," *Brain*, vol. 2, no. 3, 2006.

[61] O. Rosso, M. Martin, A. Figliola, K. Keller, and A. Plastino, "EEG analysis using wavelet-based information tools," *Journal of Neuroscience Methods*, vol. 153, no. 2, pp. 163–182, 2006.

[62] K. Polat and S. Güneş, "Classification of epileptiform EEG using a hybrid system based on decision tree classifier and fast Fourier transform," *Applied Mathematics and Computation*, vol. 187, no. 2, pp. 1017–1026, 2007.

[63] B. Xu, L. Zhang, A. Song, C. Wu, W. Li, D. Zhang, G. Xu, H. Li, and H. Zeng, "Wavelet transform time-frequency image and convolutional network-based motor imagery EEG classification," *IEEE Access*, vol. 7, pp. 6084–6093, 2018.

[64] S. Madhavan, R. K. Tripathy, and R. B. Pachori, "Time-frequency domain deep convolutional neural network for the classification of focal and non-focal EEG signals," *IEEE Sensors Journal*, vol. 20, no. 6, pp. 3078–3086, 2019.

[65] M. Portnoff, "Time-frequency representation of digital signals and systems based on short-time Fourier analysis," *IEEE Transactions on Acoustics, Speech, and Signal Processing*, vol. 28, no. 1, pp. 55–69, 1980.

[66] D. Griffin and J. Lim, "Signal estimation from modified short-time Fourier transform," *IEEE Transactions on Acoustics, Speech, and Signal Processing*, vol. 32, no. 2, pp. 236–243, 1984.

[67] P. S. Wright, "Short-time Fourier transforms and Wigner-Ville distributions applied to the calibration of power frequency harmonic analyzers," *IEEE Transactions on Instrumentation and Measurement*, vol. 48, no. 2, pp. 475–478, 1999.

[68] L. Durak and O. Arikan, "Short-time Fourier transform: two fundamental properties and an optimal implementation," *IEEE Transactions on Signal Processing*, vol. 51, no. 5, pp. 1231–1242, 2003.

[69] C. Zhao, M. He, and X. Zhao, "Analysis of transient waveform based on combined short time Fourier transform and wavelet transform," in *2004 International Conference on Power System Technology, 2004. PowerCon 2004.*, vol. 2, pp. 1122–1126, IEEE, 2004.

[70] A. K. U. Malikov, Y. Cho, Y. H. Kim, J. Kim, J. Park, and J.-H. Yi, "Ultrasonic assessment of thickness and bonding quality of coating layer based on short-time Fourier transform and convolutional neural networks," *Coatings*, vol. 11, no. 8, p. 909, 2021.

[71] D. Gabor, "Theory of communication. part 1: The analysis of information," *Journal of the Institution of Electrical Engineers-Part III: Radio and Communication Engineering*, vol. 93, no. 26, pp. 429–441, 1946.

[72] P. M. Oliveira and V. Barroso, "Uncertainty in the time-frequency plane," in *Proceedings of the Tenth IEEE Workshop on Statistical Signal and Array Processing (Cat. No. 00TH8496)*, pp. 607–611, IEEE, 2000.

[73] C. Manders and S. Mann, "Digital camera resolution: An improved Heisenberg-Gabor testing method," in *Eighth IEEE International Symposium on Multimedia (ISM'06)*, pp. 16–23, IEEE, 2006.

[74] N. Patin and M. L. Vinals, "Toward an optimal Heisenberg's closed-loop gate drive for power mosfets," in *IECON 2012-38th Annual Conference on IEEE Industrial Electronics Society*, pp. 828–833, IEEE, 2012.

[75] Y. Yao, Y. Lu, X. Zhang, F. Wang, and R. Wang, "Reducing trade-off between spatial resolution and frequency accuracy in BOTDR using Cohen's class signal processing method," *IEEE Photonics Technology Letters*, vol. 24, no. 15, pp. 1337–1339, 2012.

[76] V. V. Moca, H. Bârzan, A. Nagy-Dăbâcan, and R. C. Muresan, "Time-frequency super-resolution with superlets," *Nature Communications*, vol. 12, no. 1, pp. 1–18, 2021.

[77] I. Daubechies, "The wavelet transform, time-frequency localization and signal analysis," *IEEE Transactions on Information Theory*, vol. 36, no. 5, pp. 961–1005, 1990.

[78] O. Rioul and M. Vetterli, "Wavelets and signal processing," *IEEE Signal Processing Magazine*, vol. 8, no. 4, pp. 14–38, 1991.

[79] D. M. Green, J. A. Swets, *et al.*, *Signal Detection Theory and Psychophysics*, vol. 1. Wiley New York, 1966.

[80] K. Mikolajczyk and C. Schmid, "A performance evaluation of local descriptors," *IEEE Transactions on Pattern Analysis and Machine Intelligence*, vol. 27, no. 10, pp. 1615–1630, 2005.

[81] N. Sen and T. Basu, "A new Nyquist window with near optimal time-bandwidth product," in *2009 Annual IEEE India Conference*, pp. 1–4, IEEE, 2009.

[82] D. P. Allen and C. D. MacKinnon, "Time–frequency analysis of movement-related spectral power in EEG during repetitive movements: A comparison of methods," *Journal of Neuroscience Methods*, vol. 186, no. 1, pp. 107–115, 2010.

[83] D. Magill and C.-K. Un, "Residual excited linear predictive coder," *The Journal of the Acoustical Society of America*, vol. 55, no. S1, pp. S81–S81, 1974.

[84] T. E. Tremain, "The government standard linear predictive coding algorithm: LPC-10," *Speech Technology*, pp. 40–49, 1982.

[85] M. Schroeder and B. Atal, "Code-excited linear prediction (CELP): High-quality speech at very low bit rates," in *ICASSP'85. IEEE International Conference on Acoustics, Speech, and Signal Processing*, vol. 10, pp. 937–940, IEEE, 1985.

[86] L. Madour, *A Low-Delay Code Excited Linear Prediction Speech Coder at 8 Kbit/s*. McGill University, 1994.

[87] A. V. McCree and T. P. Barnwell, "A mixed excitation LPC vocoder model for low bit rate speech coding," *IEEE Transactions on Speech and Audio Processing*, vol. 3, no. 4, pp. 242–250, 1995.

[88] J. Bradbury, "Linear predictive coding," *Mc G. Hill*, 2000.

[89] J. Hai and E. M. Joo, "Improved linear predictive coding method for speech recognition," in *Fourth International Conference on Information, Communications and Signal Processing, 2003 and the Fourth Pacific Rim Conference on Multimedia. Proceedings of the 2003 joint*, vol. 3, pp. 1614–1618, IEEE, 2003.

[90] A. R. Madane, Z. Shah, R. Shah, and S. Thakur, "Speech compression using linear predictive coding," in *proceedings International Workshop on Machine Intelligence Research MIR Labs*, pp. 119–122, 2009.

[91] R. de Fréin, "Power-weighted LPC formant estimation," *IEEE Transactions on Circuits and Systems II: Express Briefs*, vol. 68, no. 6, pp. 2207–2211, 2020.

[92] A. Harma, "Linear predictive coding with modified filter structures," *IEEE Transactions on Speech and Audio Processing*, vol. 9, no. 8, pp. 769–777, 2001.

[93] Y. Yang, S. Feng, W. Ye, and X. Ji, "A transmission scheme for encrypted speech over GSM network," in *2008 International Symposium on Computer Science and Computational Technology*, vol. 2, pp. 805–808, IEEE, 2008.

[94] C.-H. Min and A. H. Tewfik, "Automatic characterization and detection of behavioral patterns using linear predictive coding of accelerometer sensor data," in *2010 Annual International Conference of the IEEE Engineering in Medicine and Biology*, pp. 220–223, IEEE, 2010.

[95] R. J. Javier and Y. Kim, "Application of linear predictive coding for human activity classification based on micro-doppler signatures," *IEEE Geoscience and Remote Sensing Letters*, vol. 11, no. 10, pp. 1831–1834, 2014.

[96] M. F. Anjum, S. Dasgupta, R. Mudumbai, A. Singh, J. F. Cavanagh, and N. S. Narayanan, "Linear predictive coding distinguishes spectral EEG features of parkinson's disease," *Parkinsonism & Related Disorders*, vol. 79, pp. 79–85, 2020.

[97] G. Antoniol, V. F. Rollo, and G. Venturi, "Linear predictive coding and cepstrum coefficients for mining time variant information from software repositories," in *Proceedings of the 2005 International Workshop on Mining Software Repositories*, pp. 1–5, 2005.

[98] O. K. Hamid, "Speech sound coding using linear predictive coding (LPC)," *Signal*, vol. 1, p. 5, 2017.

[99] P. B. Patil, "Linear predictive codes for speech recognition system at 121bps," *International Journal of Hybrid Information Technology*, vol. 13, no. 1, pp. 33–40, 2020.

[100] G. K. Vallabha and B. Tuller, "Systematic errors in the formant analysis of steady-state vowels," *Speech Communication*, vol. 38, no. 1-2, pp. 141–160, 2002.

[101] T. W. Parsons, *Voice and Speech Processing*. McGraw-Hill Book Company, 1986.

[102] R. C. Snell and F. Milinazzo, "Formant location from LPC analysis data," *IEEE Transactions on Speech and Audio Processing*, vol. 1, no. 2, pp. 129–134, 1993.

[103] T. P. Barnwell III, K. Nayebi, and C. H. Richardson, *Speech Coding: A Computer Laboratory Textbook*. John Wiley & Sons, Inc., 1995.

[104] S. Rao and W. A. Pearlman, "Analysis of linear prediction, coding, and spectral estimation from subbands," *IEEE Transactions on Information Theory*, vol. 42, no. 4, pp. 1160–1178, 1996.

[105] M. Owren and R. Bernacki, "Applying linear predictive coding (LPC) to frequency-spectrum analysis of animal acoustic signals," in *Animal Acoustic Communication*, pp. 129–162, Springer, 1998.

[106] G. Duncan and M. Jack, "Formant estimation algorithm based on pole focusing offering improved noise tolerance and feature resolution," in *IEE Proceedings F (Communications, Radar and Signal Processing)*, vol. 135, pp. 18–32, IET, 1988.

[107] E. S. Carotti, J. C. De Martin, D. Farina, and R. Merletti, "Linear predictive coding of myoelectric signals," in *Proceedings.(ICASSP'05). IEEE International Conference on Acoustics, Speech, and Signal Processing, 2005.*, vol. 5, pp. v–629, IEEE, 2005.

[108] P. Liu, S. Li, and H. Wang, "Steganography integrated into linear predictive coding for low bit-rate speech codec," *Multimedia Tools and Applications*, vol. 76, no. 2, pp. 2837–2859, 2017.

[109] L. Jackson, D. Tufts, F. Soong, and R. Rao, "Frequency estimation by linear prediction," in *ICASSP'78. IEEE International Conference on Acoustics, Speech, and Signal Processing*, vol. 3, pp. 352–356, IEEE, 1978.

[110] S. Kay, "The effects of noise on the autoregressive spectral estimator," *IEEE Transactions on Acoustics, Speech, and Signal Processing*, vol. 27, no. 5, pp. 478–485, 1979.

[111] J. Tierney, "A study of LPC analysis of speech in additive noise," *IEEE Transactions on Acoustics, Speech, and Signal Processing*, vol. 28, no. 4, pp. 389–397, 1980.

[112] T. Shimamura, N. Kunieda, and J. Suzuki, "A robust linear prediction method for noisy speech," in *ISCAS'98. Proceedings of the 1998 IEEE International Symposium on Circuits and Systems (Cat. No. 98CH36187)*, vol. 4, pp. 257–260, IEEE, 1998.

[113] S. V. Andersen, W. B. Kleijn, R. Hagen, J. Linden, M. Murthi, and J. Skoglund, "iLBC-a linear predictive coder with robustness to packet losses," in *Speech Coding, 2002, IEEE Workshop Proceedings.*, pp. 23–25, IEEE, 2002.

[114] L. Liu and T. Shimamura, "A noise compensation LPC method based on pitch synchronous analysis for speech," *Journal of Signal Processing*, vol. 17, no. 6, pp. 283–292, 2013.

[115] J. Xu, M. Davis, and R. de Fréin, "New robust LPC-based method for time-resolved morphology of high-noise multiple frequency signals," in *2020 31st Irish Signals and Systems Conference (ISSC)*, pp. 1–6, IEEE, 2020.

[116] J. Xu, M. Davis, and R. de Fréin, "An LPC pole processing method for enhancing the identification of dominant spectral features," *Electronics Letters*, vol. 57, no. 18, pp. 708–710, 2021.

[117] J. Xu, M. Davis, and R. de Fréin, "A linear predictive coding filtering method for the time-resolved morphology of EEG activity," in *2021 32nd Irish Signals and Systems Conference (ISSC)*, pp. 1–6, IEEE, 2021.

[118] J. Xu, M. Davis, and R. de Fréin, "Dominant frequency component tracking of noisy time-varying signals using the linear predictive coding pole processing method," *Electronics Letters*, vol. 58, no. 2, pp. 79–81, 2022.

[119] S. Nam, "An uncertainty principle for discrete signals," *arXiv preprint arXiv:1307.6321*, 2013.

[120] G. E. Box, G. M. Jenkins, G. C. Reinsel, and G. M. Ljung, *Time Series Analysis: Forecasting and Control*. John Wiley & Sons, 2015.

[121] S. Xu, H. Hu, L. Ji, and P. Wang, "An adaptive graph spectral analysis method for feature extraction of an EEG signal," *IEEE Sensors Journal*, vol. 19, no. 5, pp. 1884–1896, 2018.

[122] H.-J. Kim, I.-N. Wang, Y.-T. Kim, H. Kim, and D.-J. Kim, "Comparative analysis of NIRS-EEG motor imagery data using features from spatial, spectral and temporal domain," in *2020 8th International Winter Conference on Brain-Computer Interface (BCI)*, pp. 1–4, IEEE, 2020.

[123] M. S. Amin, M. R. Azim, T. Latif, M. A. Hoque, and F. M. Hasan, "Spectral analysis of human sleep EEG signal," in *2010 2nd International Conference on Signal Processing Systems*, vol. 3, pp. V3–106, IEEE, 2010.

[124] M. M. Mukaka, "A guide to appropriate use of correlation coefficient in medical research," *Malawi Medical Journal*, vol. 24, no. 3, pp. 69–71, 2012.

[125] S. K. Smit and A. E. Eiben, "Comparing parameter tuning methods for evolutionary algorithms," in *2009 IEEE Congress on Evolutionary Computation*, pp. 399–406, IEEE, 2009.

[126] X.-S. Yang, S. Deb, M. Loomes, and M. Karamanoglu, "A framework for self-tuning optimization algorithm," *Neural Computing and Applications*, vol. 23, no. 7, pp. 2051–2057, 2013.

[127] S. Alhagry, A. A. Fahmy, and R. A. El-Khoribi, "Emotion recognition based on EEG using LSTM recurrent neural network," *Emotion*, vol. 8, no. 10, pp. 355–358, 2017.

[128] P. Wang, A. Jiang, X. Liu, J. Shang, and L. Zhang, "LSTM-based EEG classification in motor imagery tasks," *IEEE Transactions on Neural Systems and Rehabilitation Engineering*, vol. 26, no. 11, pp. 2086–2095, 2018.

[129] S. Siami-Namini, N. Tavakoli, and A. S. Namin, "The performance of LSTM and BiLSTM in forecasting time series," in *2019 IEEE International Conference on Big Data (Big Data)*, pp. 3285–3292, IEEE, 2019.

[130] Y. Hua, Z. Zhao, R. Li, X. Chen, Z. Liu, and H. Zhang, "Deep learning with long short-term memory for time series prediction," *IEEE Communications Magazine*, vol. 57, no. 6, pp. 114–119, 2019.

[131] X. Xing, Z. Li, T. Xu, L. Shu, B. Hu, and X. Xu, "SAE+LSTM: A new framework for emotion recognition from multi-channel EEG," *Frontiers in Neurorobotics*, vol. 13, p. 37, 2019.

[132] Z. Lan, O. Sourina, L. Wang, and Y. Liu, "Real-time EEG-based emotion monitoring using stable features," *The Visual Computer*, vol. 32, no. 3, pp. 347–358, 2016.

[133] G. Zhong, "Analysis of healthy people's attention based on EEG spectrum," in *2015 International Conference on Mechatronics, Electronic, Industrial and Control Engineering (MEIC-15)*, pp. 922–925, Atlantis Press, 2015.

[134] S. Markovska-Simoska and N. Pop-Jordanova, "Quantitative EEG in children and adults with attention deficit hyperactivity disorder: comparison of absolute and relative power spectra and theta/beta ratio," *Clinical EEG and neuroscience*, vol. 48, no. 1, pp. 20–32, 2017.

[135] P. C. Petrantonakis and L. J. Hadjileontiadis, "Emotion recognition from EEG using higher order crossings," *IEEE Transactions on Information Technology in Biomedicine*, vol. 14, no. 2, pp. 186–197, 2009.

[136] W. Min and G. Luo, "Medical applications of EEG wave classification," *Chance*, vol. 22, no. 4, pp. 14–20, 2009.

[137] Y.-P. Lin, C.-H. Wang, T.-P. Jung, T.-L. Wu, S.-K. Jeng, J.-R. Duann, and J.-H. Chen, "EEG-based emotion recognition in music listening," *IEEE Transactions on Biomedical Engineering*, vol. 57, no. 7, pp. 1798–1806, 2010.

[138] Q. Wang, O. Sourina, and M. K. Nguyen, "EEG-based" serious" games design for medical applications," in *2010 International Conference on Cyberworlds*, pp. 270–276, IEEE, 2010.

[139] M. Soufineyestani, D. Dowling, and A. Khan, "Electroencephalography (EEG) technology applications and available devices," *Applied Sciences*, vol. 10, no. 21, p. 7453, 2020.

[140] W. T. Lee, H. Nisar, A. S. Malik, and K. H. Yeap, "A brain computer interface for smart home control," in *2013 IEEE International Symposium on Consumer Electronics (ISCE)*, pp. 35–36, IEEE, 2013.

[141] U. R. Acharya, S. V. Sree, G. Swapna, R. J. Martis, and J. S. Suri, "Automated EEG analysis of epilepsy: a review," *Knowledge-Based Systems*, vol. 45, pp. 147–165, 2013.

[142] H. Sun, Y. Fu, X. Xiong, J. Yang, C. Liu, and Z. Yu, "Identification of EEG induced by motor imagery based on Hilbert-Huang transform," *Acta Automatica Sinica*, vol. 41, no. 9, pp. 1686–1692, 2015.

[143] Z.-K. Gao, C.-Y. Liu, Y.-X. Yang, Q. Cai, W.-D. Dang, X.-L. Du, and H.-X. Jia, "Multivariate weighted recurrence network analysis of EEG signals from ERP-based smart home system," *Chaos: An Interdisciplinary Journal of Nonlinear Science*, vol. 28, no. 8, p. 085713, 2018.

[144] E. Altenmüller, W. Gruhn, D. Parlitz, and G. Liebert, "The impact of music education on brain networks: evidence from EEG-studies," *International Journal of Music Education*, no. 1, pp. 47–53, 2000.

[145] M. Bensalem-Owen, D. F. Chau, S. C. Sardam, and B. G. Fahy, "Education research: evaluating the use of podcasting for residents during EEG instruction: a pilot study," *Neurology*, vol. 77, no. 8, pp. e42–e44, 2011.

[146] T. Prauzner, "Analysis of the results of the pedagogical research and EEG in the aspect of effective modern teaching aids in the technical education," in *SOCIETY. INTEGRATION. EDUCATION. Proceedings of the International Scientific Conference*, vol. 4, pp. 480–489, 2015.

[147] F. A. Nascimento, A. Maheshwari, J. Chu, and J. R. Gavvala, "EEG education in neurology residency: background knowledge and focal challenges," *Epileptic Disorders*, vol. 22, no. 6, pp. 769–774, 2020.

[148] S. Bodda, H. Chandranpillai, P. Viswam, S. Krishna, B. Nair, and S. Diwakar, "Categorizing imagined right and left motor imagery BCI tasks for low-cost robotic neuroprosthesis," in *2016 International Conference on Electrical, Electronics, and Optimization Techniques (ICEEOT)*, pp. 3670–3673, IEEE, 2016.

[149] A. Das, S. Suresh, and N. Sundararajan, "A discriminative subject-specific spatio-spectral filter selection approach for EEG based motor-imagery task classification," *Expert Systems with Applications*, vol. 64, pp. 375–384, 2016.

[150] N. Shaari, M. Syafiq, M. Amin, and O. Mikami, "Electroencephalography (EEG) application in neuromarketing-exploring the subconscious mind," *Journal of Advanced Manufacturing Technology (JAMT)*, vol. 13, no. 2 (2), 2019.

[151] J. Lee and J. H. Yang, "Analysis of driver's EEG given take-over alarm in SAE level 3 automated driving in a simulated environment," *International Journal of Automotive Technology*, vol. 21, no. 3, pp. 719–728, 2020.

[152] T. Hecht, A. Feldhütter, J. Radlmayr, Y. Nakano, Y. Miki, C. Henle, and K. Bengler, "A review of driver state monitoring systems in the context of automated driving," in *Congress of the International Ergonomics Association*, pp. 398–408, Springer, 2018.

[153] J. I. Makhoul and J. J. Wolf, "Linear prediction and the spectral analysis of speech," tech. rep., BOLT BERANEK AND NEWMAN INC CAMBRIDGE MA, 1972.

[154] J. Makhoul, "Spectral analysis of speech by linear prediction," *IEEE Transactions on Audio and Electroacoustics*, vol. 21, no. 3, pp. 140–148, 1973.

[155] K. Tokuda, T. Kobayashi, T. Masuko, and S. Imai, "Mel-generalized cepstral analysis-a unified approach to speech spectral estimation," in *ICSLP*, vol. 94, pp. 18–22, Citeseer, 1994.

[156] M. Nasrolahzadeh, Z. Mohammadpoory, and J. Haddadnia, "Higher-order spectral analysis of spontaneous speech signals in alzheimer's disease," *Cognitive Neurodynamics*, vol. 12, no. 6, pp. 583–596, 2018.

[157] G. Korvel, P. Treigys, G. Tamulevicus, J. Bernataviciene, and B. Kostek, "Analysis of 2D feature spaces for deep learning-based speech recognition," *Journal of the Audio Engineering Society*, vol. 66, no. 12, pp. 1072–1081, 2018.

[158] S. Koval and S. Krynov, "Practice of usage of spectral analysis for forensic speaker identification," in *RLA2C 1998-Speaker Recognition and its Commercial and Forensic Applications*, pp. 136–140, 2020.

[159] I. Popov and L. Veselov, "Mechanical vibration spectrum analysis by means of a speckle method," *Optics Communications*, vol. 105, no. 3-4, pp. 167–170, 1994.

[160] M. Romano, A. Fratini, G. D. Gargiulo, M. Cesarelli, L. Iuppariello, and P. Bifulco, "On the power spectrum of motor unit action potential trains synchronized with mechanical vibration," *IEEE Transactions on Neural Systems and Rehabilitation Engineering*, vol. 26, no. 3, pp. 646–653, 2018.

[161] K. Wang, Z.-J. Xu, Y. Gong, and K.-L. Du, "Mechanical fault prognosis through spectral analysis of vibration signals," *Algorithms*, vol. 15, no. 3, p. 94, 2022.

[162] H. Xu, C. Meng, Q. Huang, C. Luo, J. Zhang, and Z. Liu, "Time-frequency vibration characteristics analysis of disconnectors of GIS equipment with poor contact mechanical defect," in *2021 IEEE 5th International Conference on Condition Assessment Techniques in Electrical Systems (CATCON)*, pp. 215–219, IEEE, 2021.

[163] K. Aki, "Scaling law of seismic spectrum," *Journal of Geophysical Research*, vol. 72, no. 4, pp. 1217–1231, 1967.

[164] A. Berkhout, "Combining full wavefield migration and full waveform inversion, a glance into the future of seismic imaging," *Geophysics*, vol. 77, no. 2, pp. S43–S50, 2012.

[165] A. Berkhout, "An outlook on the future of seismic imaging, part II: Full-wavefield migration," *Geophysical Prospecting*, vol. 62, no. 5, pp. 931–949, 2014.

[166] M. Davydenko and D. Verschuur, "Full-wavefield migration: using surface and internal multiples in imaging," *Geophysical Prospecting*, vol. 65, no. 1, pp. 7–21, 2017.

[167] D. E. McNamara and R. I. Boaz, "Visualization of the seismic ambient noise spectrum," *Seismic Ambient Noise*, pp. 1–29, 2019.

[168] Z. Zhang, Z. Wu, Z. Wei, J. Mei, R. Huang, and P. Wang, "FWI imaging: Full-wavefield imaging through full-waveform inversion," in *SEG Technical Program Expanded Abstracts 2020*, pp. 656–660, Society of Exploration Geophysicists, 2020.

[169] R. Huang, Z. Zhang, Z. Wu, Z. Wei, J. Mei, and P. Wang, "Full-waveform inversion for full-wavefield imaging: Decades in the making," *The Leading Edge*, vol. 40, no. 5, pp. 324–334, 2021.

[170] D. R. Lyzenga, "Numerical simulation of synthetic aperture radar image spectra for ocean waves," *IEEE Transactions on Geoscience and Remote Sensing*, no. 6, pp. 863–872, 1986.

[171] J. Siewerdsen, I. Cunningham, and D. Jaffray, "A framework for noise-power spectrum analysis of multidimensional images," *Medical Physics*, vol. 29, no. 11, pp. 2655–2671, 2002.

[172] L. J. Rodriguez-Aragon and A. Zhigljavsky, "Singular spectrum analysis for image processing," *Statistics and Its Interface*, vol. 3, no. 3, pp. 419–426, 2010.

[173] J.-G. Minonzio, B. Cataldo, R. Olivares, D. Ramiandrisoa, R. Soto, B. Crawford, V. H. C. De Albuquerque, and R. Munoz, "Automatic classifying of patients with non-traumatic fractures based on ultrasonic guided wave spectrum image using a dynamic support vector machine," *IEEE Access*, vol. 8, pp. 194752–194764, 2020.